Application of Optimized High Order Compact Schemes for Aeroacoustics and Turbulence Simulations

KAIST, Duck-Joo Lee

2013.11.11

Taiwan

Introduction

- **What is Sound?**
  Pressure perturbation that propagates to our ears

- **What is Aeroacoutics?**
  A branch of science that is concerned with the sound generated by aerodynamic forces or turbulence.

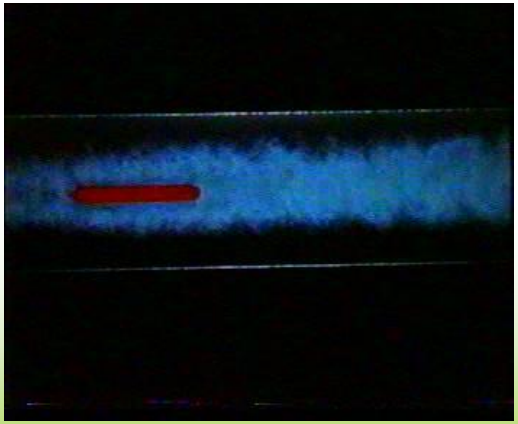

Visualization

- Sphere flying over a perforated plate : M=3.0

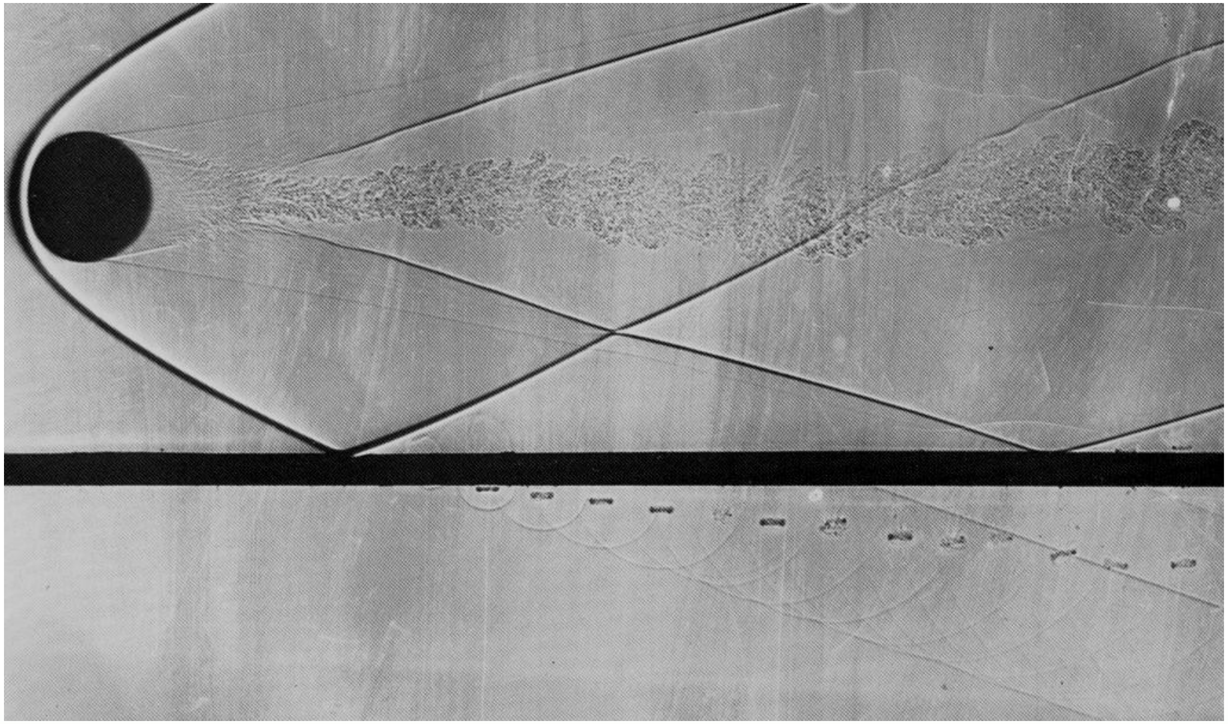

@ An Album of Fluid Motion, Van Dyke

Jet Aeo-acoustics

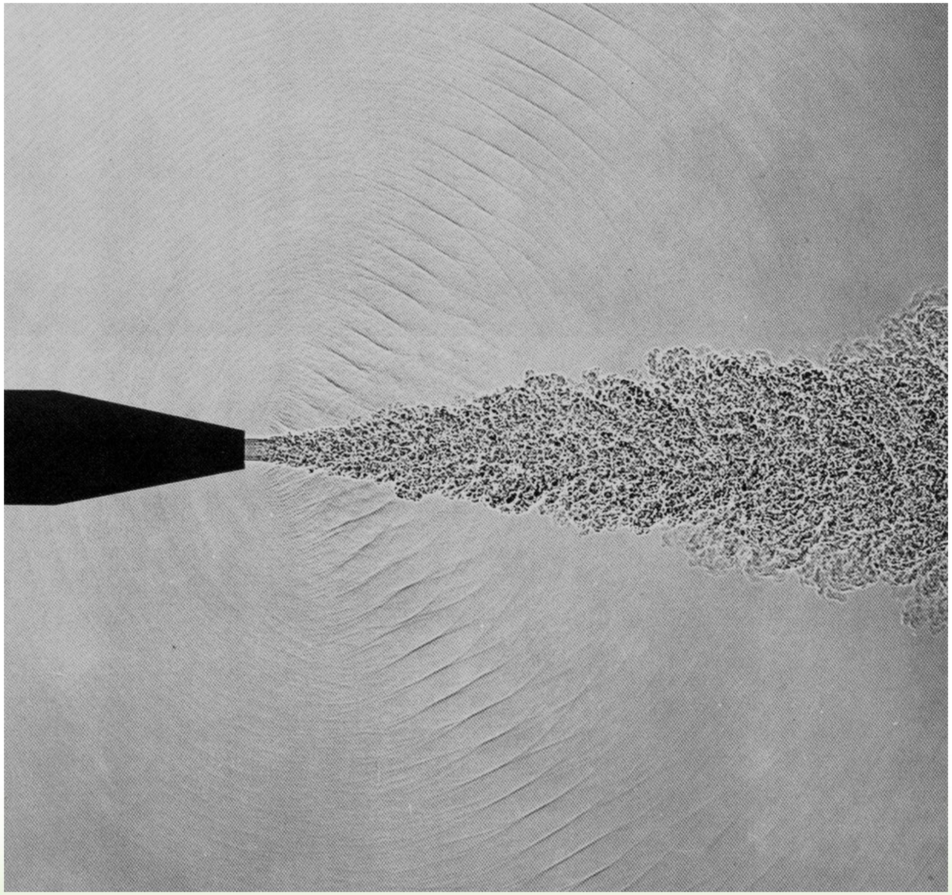

@ An Album of Fluid Motion, Van Dyke

- Periodic waves from a supersonic jet
  - ✓ It radiates weak shock of frequency 85kHz, directed primarily along a cone 60º from the axis

Jet Flow

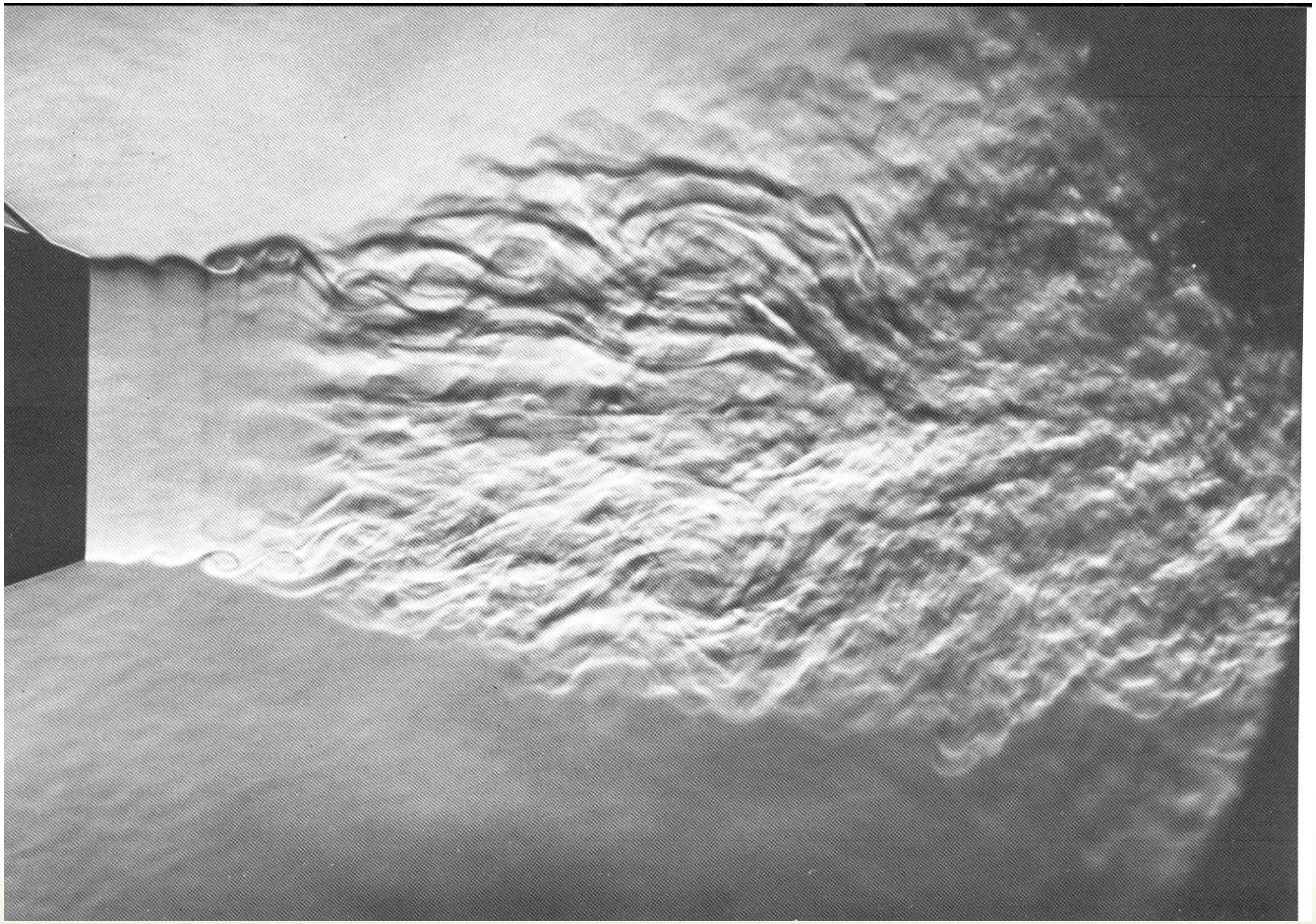

List of Lucasian Professors (University of Cambriedge)

Year appointed	Name	Speciality
1664	Isaac Barrow	Classics and mathematics
1669	Isaac Newton	Mathematics and physics
1702	William Whiston	Mathematics
1711	Nicholas Saunderson	Mathematics
1739	John Colson	Mathematics
1760	Edward Waring	Mathematics
1798	Isaac Milner	Mathematics and chemistry
1820	Robert Woodhouse	Mathematics
1822	Thomas Turton	Mathematics
1826	George Biddell Airy	Astronomy
1828	Charles Babbage	Mathematics and computing
1839	Joshua King	Mathematics
1849	George Gabriel Stokes	Physics and fluid mechanics
1903	Joseph Larmor	Physics
1932	Paul Dirac	Physics
1969	James Lighthill	Fluid mechanics
1979	Stephen Hawking	Theoretical physics
2009	Michael Green	Theoretical physics

← Founder of Aeroacoustics

Aero Acoustics Lab

Flow Induced Noise;Aeroacoustics

- **Lighthill Euqation**

Continuity: $$\frac{\partial \rho}{\partial t} + \nabla \cdot (\rho \vec{V}) = 0 \quad \textbf{(1)}$$

Momentum: $$\frac{\partial}{\partial t}(\rho \vec{V}) + \nabla \cdot (\rho \vec{V}\vec{V} - \vec{\tau} + p\tilde{I}) = 0 \quad \textbf{(2)}$$

$$\frac{\partial}{\partial t}(1) - \nabla \cdot (2) = 0 \qquad \frac{\partial^2 \rho}{\partial t^2} - \frac{\partial^2}{\partial x_i \partial x_j}(\rho v_i v_j - \tau_{ij} + p\delta_{ij}) = 0$$

Addition and Substraction $a_0^2 \frac{\partial^2 \rho}{\partial x_i \partial x_j}$

$$\frac{\partial^2 \rho}{\partial t^2} - a_0^2 \frac{\partial^2 \rho}{\partial x_i \partial x_j} = \frac{\partial^2}{\partial x_i \partial x_j}(\rho v_i v_j - \tau_{ij} + p\delta_{ij} - a_0^2 \rho \delta_{ij})$$

$$T_{ij} = \rho v_i v_j - \tau_{ij} + (p - a_0^2 \rho)\delta_{ij}$$

Lighthill's stress tensor

Assumptions

$\rho = \rho_0 + \rho'$

Inviscid, Isentropic $T_{ij} = \rho v_i v_j$ $\quad \tau_{ij} = 0$ and $p' = a_0^2 \rho'$

$$\frac{\partial^2 \rho}{\partial t^2} - a_0^2 \frac{\partial^2 \rho}{\partial x_i \partial x_j} = \frac{\partial^2}{\partial x_i \partial x_j} \rho v_i v_j$$

Lighthil ‘s Quadrupole source

$$\rho'(\vec{x}, t) = \frac{1}{4\pi a_0^2} \frac{\partial^2}{\partial x_i \partial x_j} \int_{\vec{y}} \left[\frac{\rho v_i v_j}{|\vec{x} - \vec{y}|} \right]_{\tau = t - \frac{r}{a_0}} d\vec{y}$$

AeroAcoustics Lab

Previous Works

Pre-Lighthill	1937	Demming : monopole
	1948	Gutin : dipole
Aeroacoustic Formulation	1952	Lighthill : quadrupole
	1970	Ffowcs Williams Hawkings : moving body
Jet Era	~	Experiment, Flight Test
Computational Aeroacoustics		Spectral-like (Lele, 1992)
		DRP (Tam, 1993)
		OHOC (Kim & Lee, 1995)
CAA Benchmark	1995	Aeroacoustic conference

AeroAcoustics Lab

Computational Aeroacoustics

- Computational Aeroacoustics (CAA)
  - ✓ CAA = Computational Fluid Dynamics + Aerodynamics + Acoustics
  - ✓ High-Order & High-Resolution Numerical Algorithms

Visualization of acoustic wave generated by turbulence & moving body

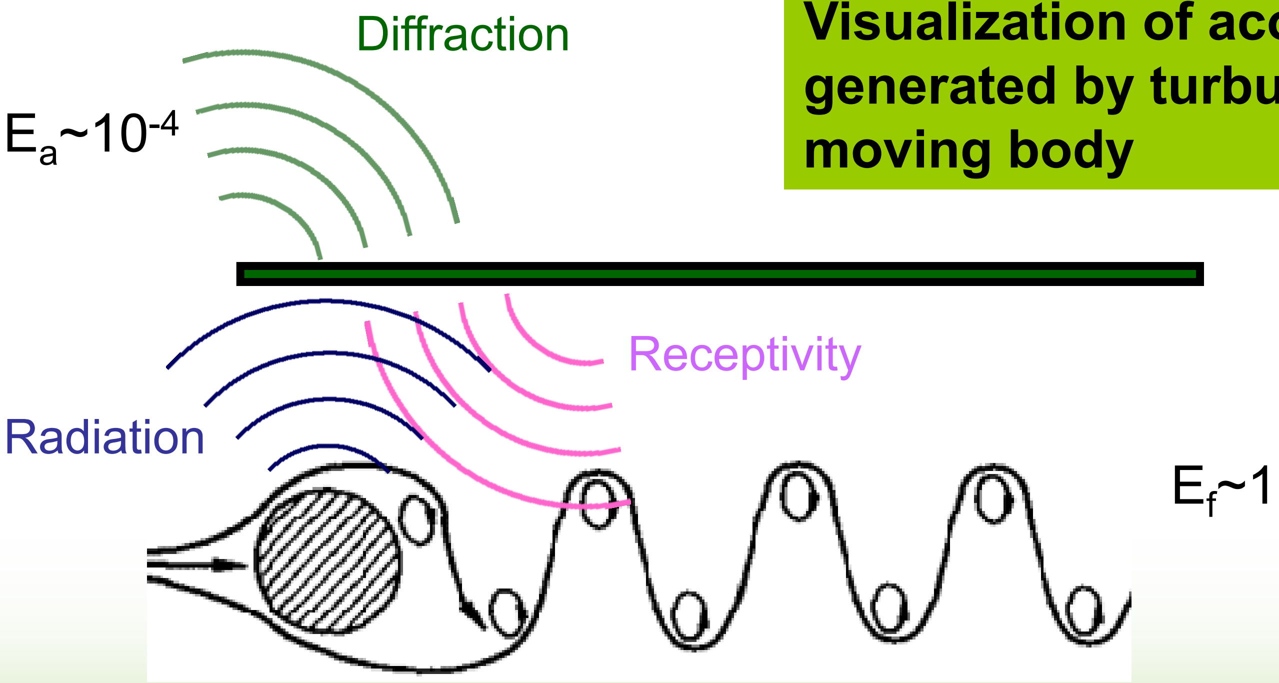

Generation and Radiation

Diffraction

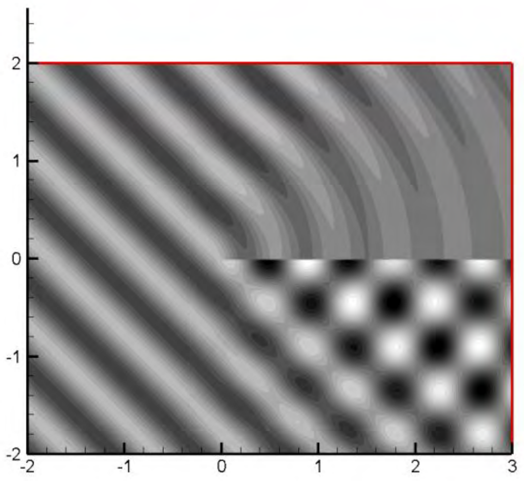

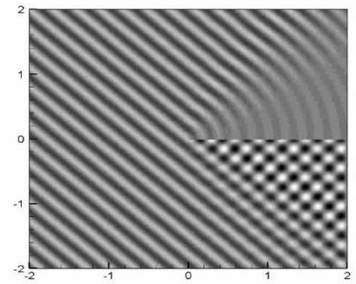

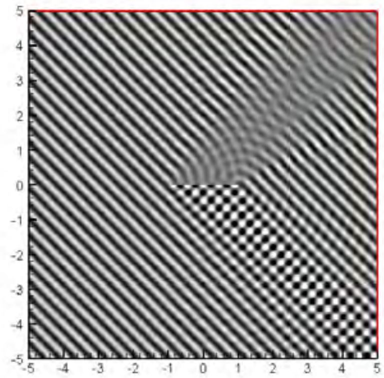

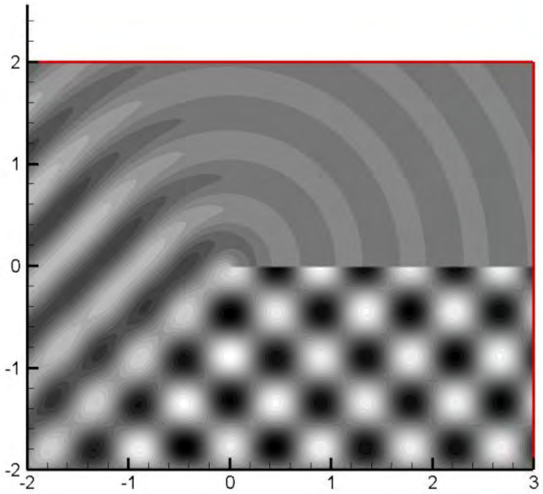

Anechoic Wind Tunnel(KAIST)

- **Anechoic Wind Tunnel**
  - Test Section : 35cm X 35cm
  - Max. Velocity : 62.8m/s

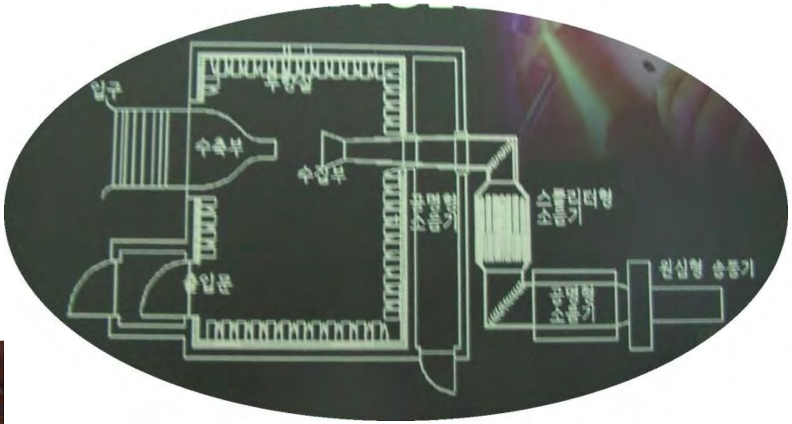

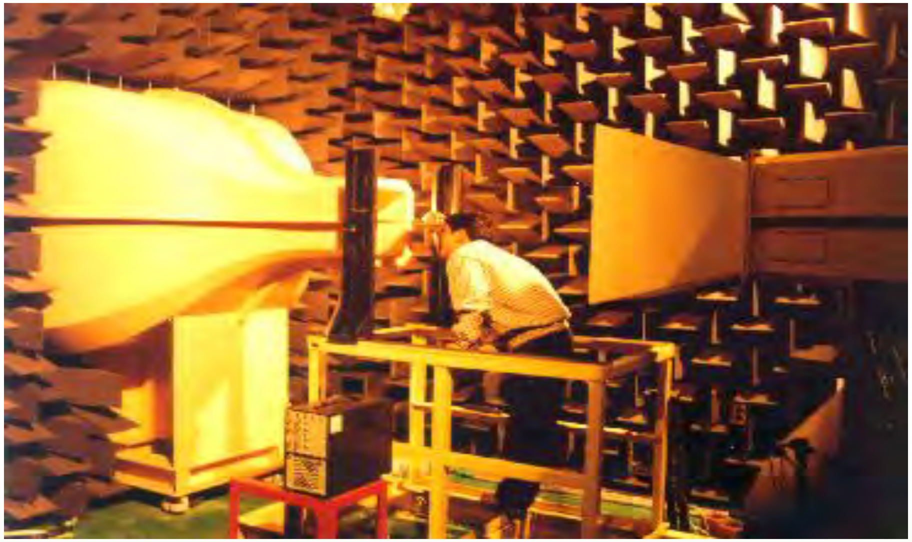

Problems of Concern

- High-order, high-resolution scheme for spatial derivative in nonlinear convection term and for time integration
  - ✓ Dissipation error : Central Scheme or Upwind scheme
  - ✓ Dispersion error : high-resolution
  - ✓ Truncation error : 4th order

    DRP, spectral-like, OHOC,MP,ENO

- Boundary conditions
  - ✓ Non-reflection condition
  - ✓ Inflow condition

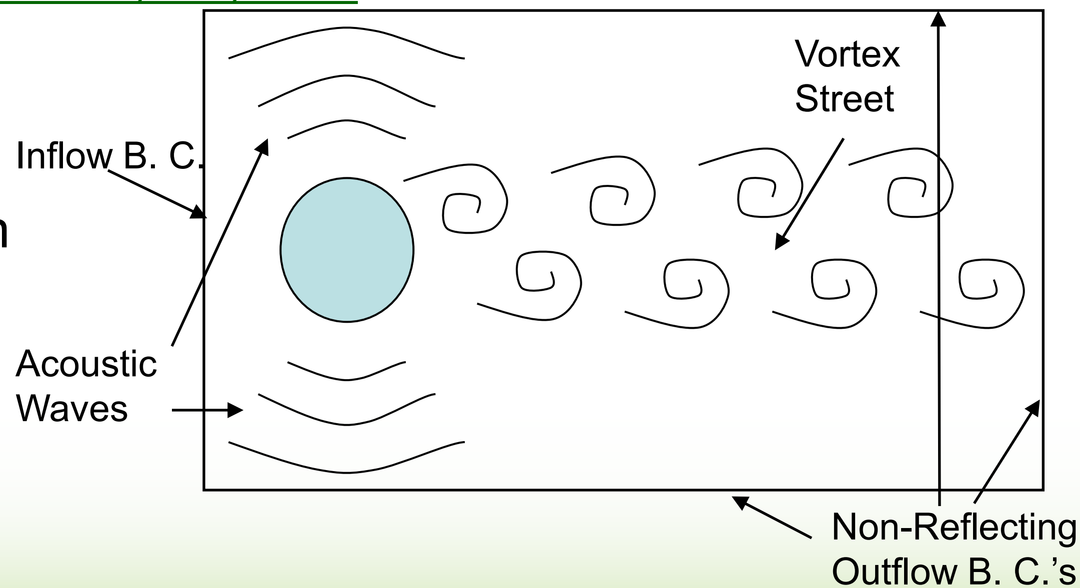

- Artificial dissipation

Special Topics

- Low speed incompressible radiation
  - ✓ Hydrodynamic density + dipole : Hardin, 1992
  - ✓ Non-linear acoustic + quadrupole vortex : Lee & Koo, 1995
  - ✓ Splitting method : Moon, 2003

- Acoustic-flow feedback mechanism
  - ✓ Cavity tone; Compressible feedback; Heo & Lee
  - ✓ Screech tone ;Compressible feedback; Lee & Lee
  - ✓ Incompressible acoustic-flow feedback; Kim & Lee

- Challenges to CAA
  - ✓ 3 dimensional simulation of rotor

Cylinder

- **Pressure Contours**

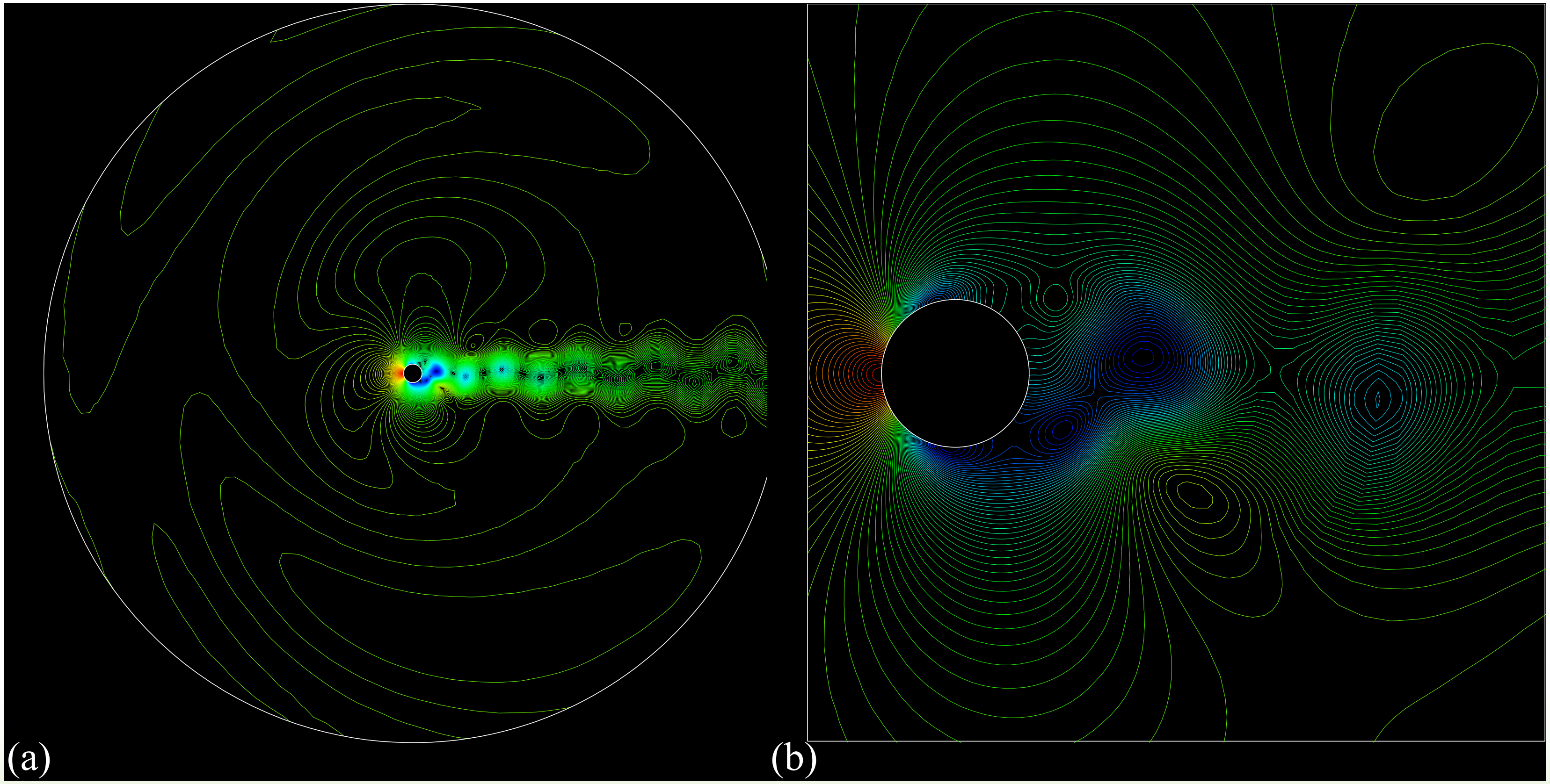

2-D Cylinder Flow with Re = 400 and M = 0.3

Aeolian Tone

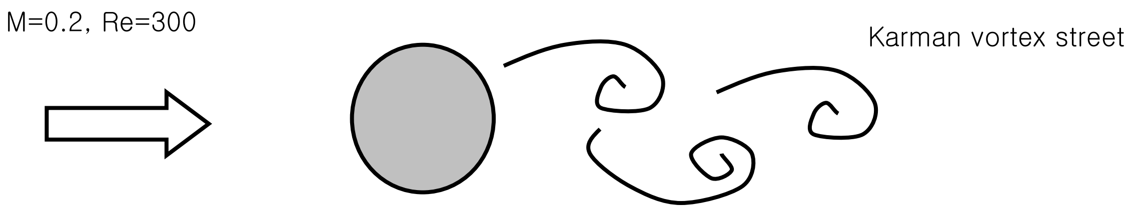

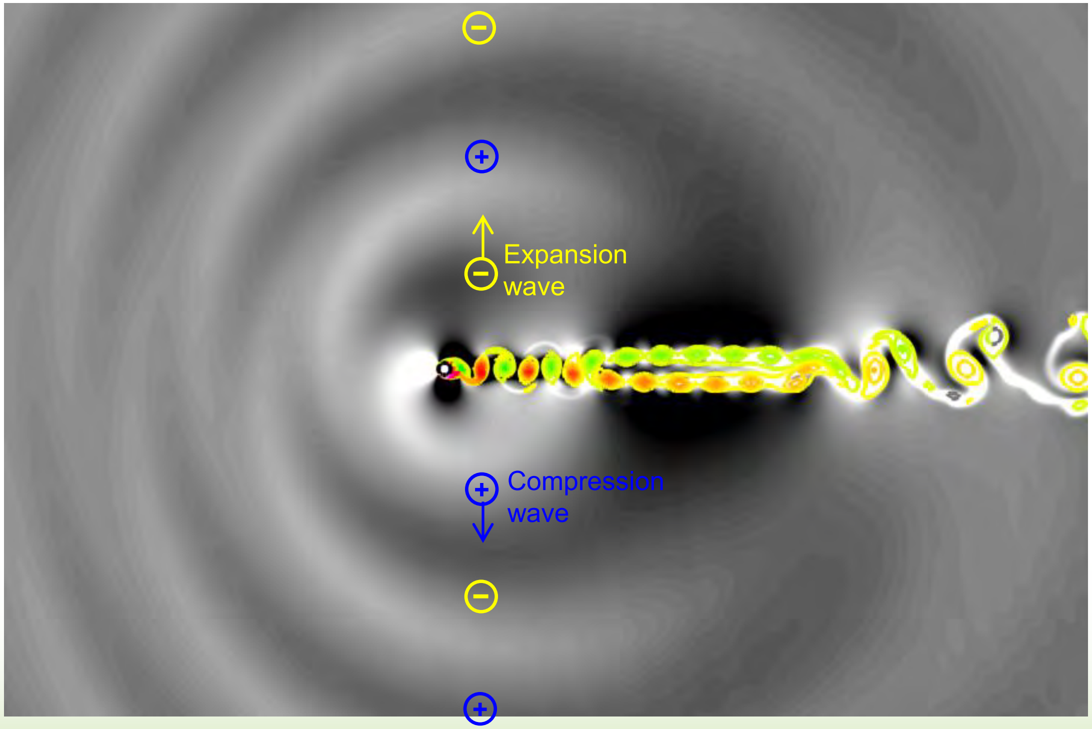

Von Karman Vortex

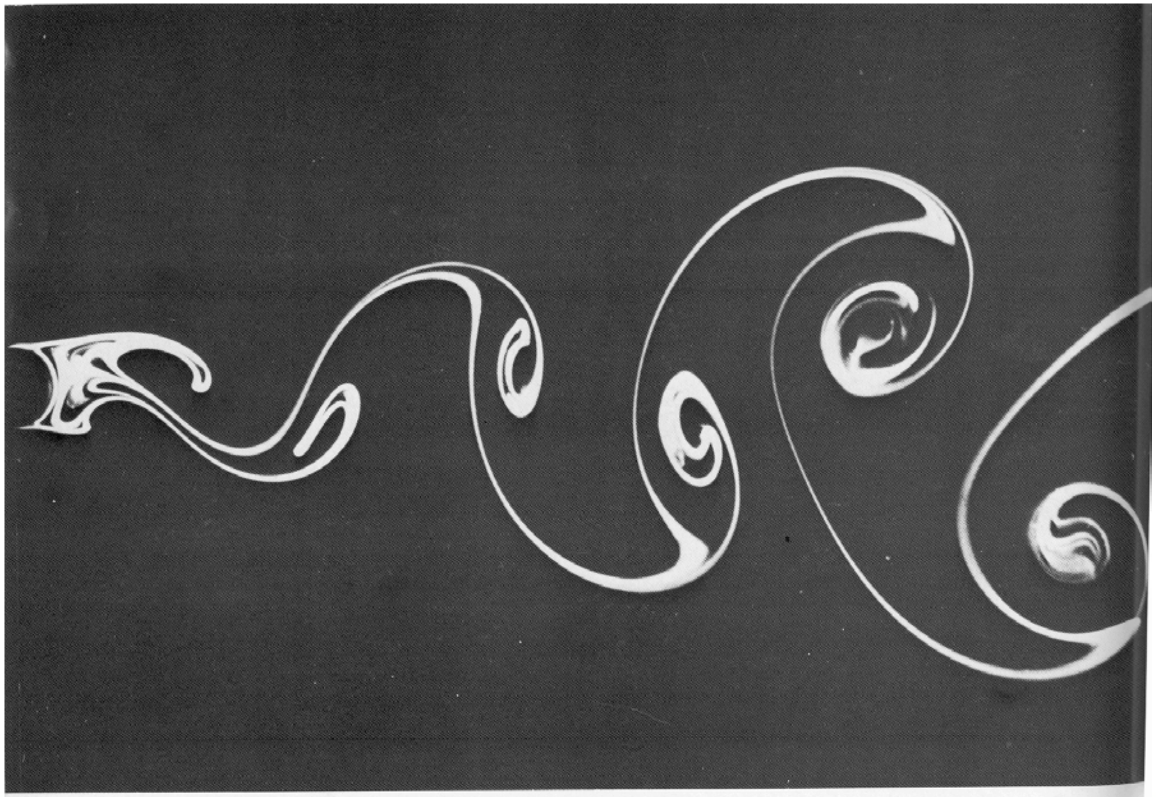

94. Kármán vortex street behind a circular cylinder at $R=140$. Water is flowing at 1.4 cm/s past a cylinder of diameter 1 cm. Integrated streaklines are shown by electrolytic precipitation of a white colloidal smoke, illuminated by a sheet of light. The vortex sheet is seen to grow in width downstream for some diameters. *Photograph by Sadatoshi Taneda*

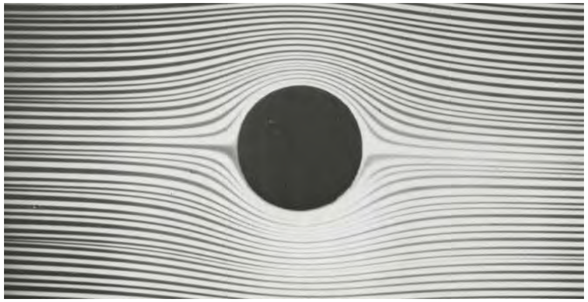

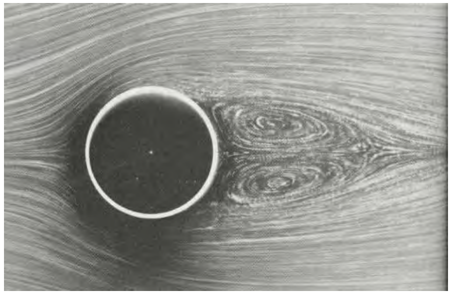

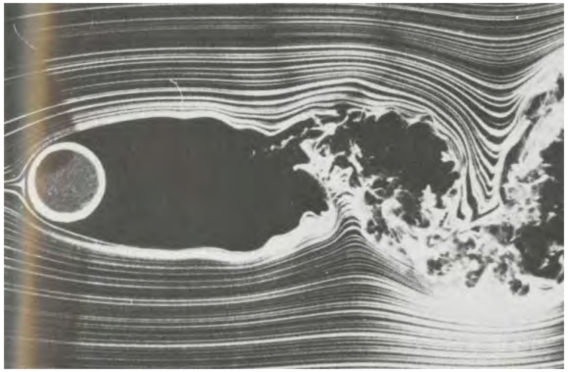

Noise reduction by spiral line

- 나선 송전선에 의한 소음 감쇄 측정

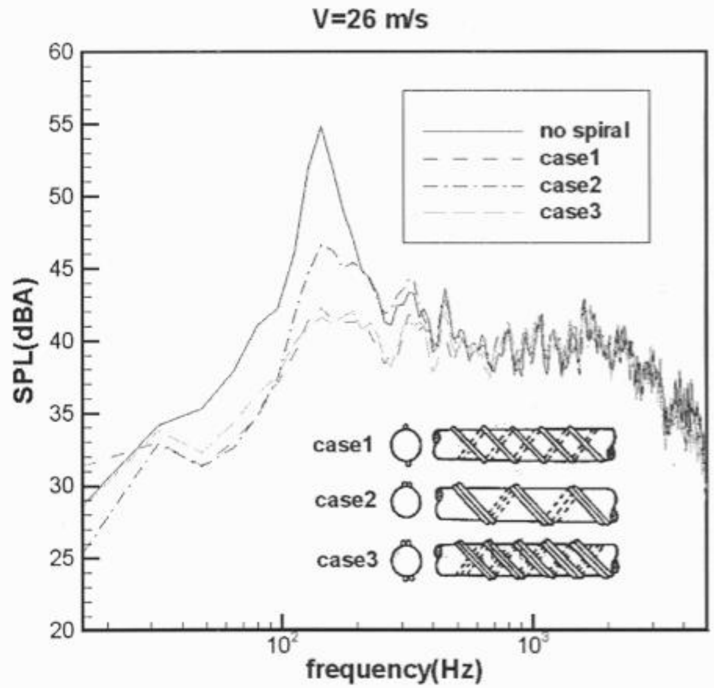

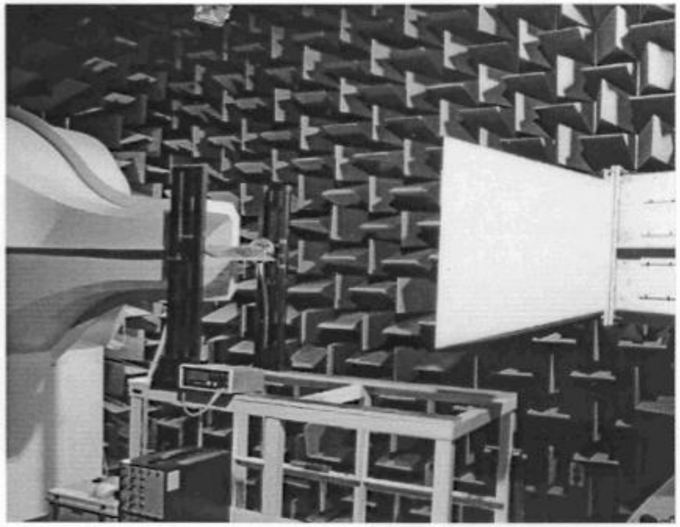

Airframe Noise

- Chaotic wake flow behind a Blunt-Based Body
  - ✓ Airliner
  - ✓ Airplane spoiler

<Airliner>

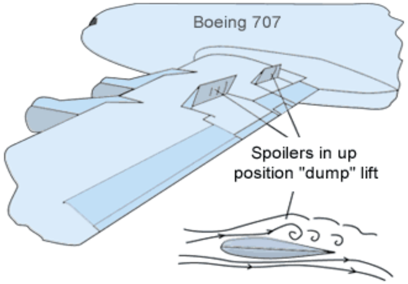

<Spoiler>

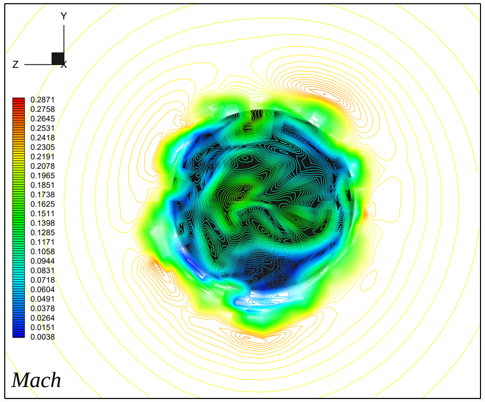

<Mach contour>

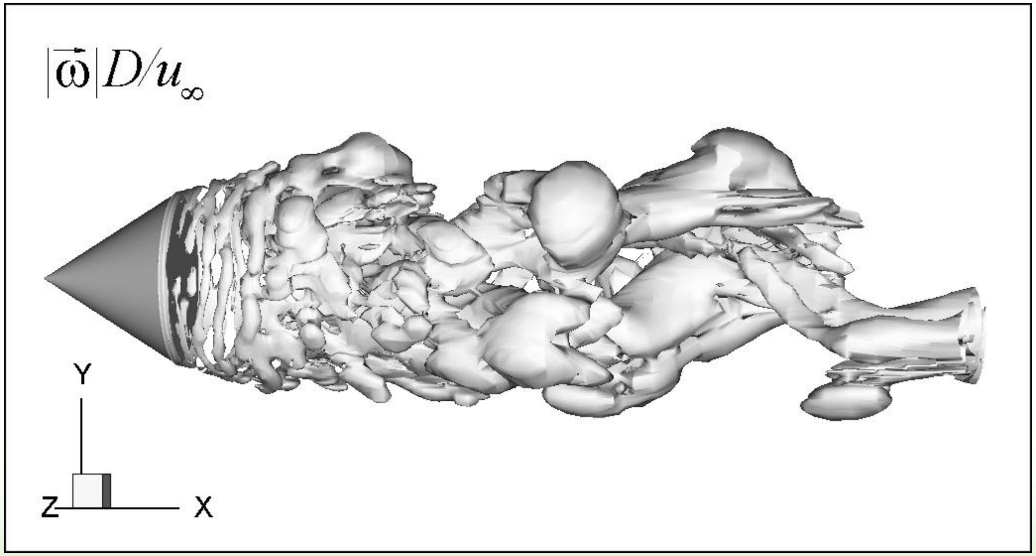

<Vorticity contour>

Aero Acoustics Lab

Cavity Tone

Cavity Tone

<Landing gear>

<Bomber>

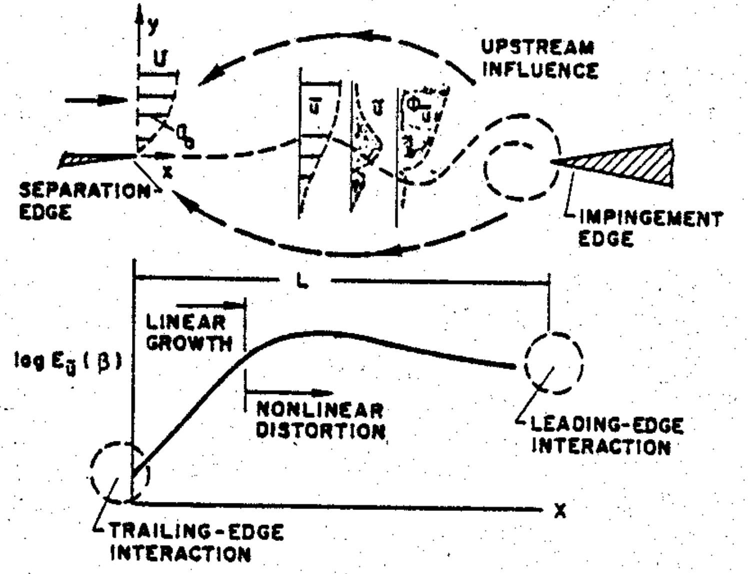

- Rossiter
- Colonius
- Heo & Lee

(e) Schlieren, $M=0.8$

<Schileren photographs of cavity noise (Krishnamurty Karamchetti, 1956)>

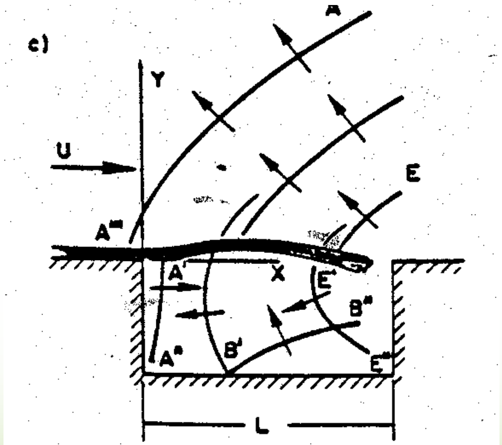

<Generation of cavity tone>

Cavity Tone

- Issues
  - ✓ Flow frequency
    vs. acoustic resonance frequency
  - ✓ Acoustic-vortex interaction

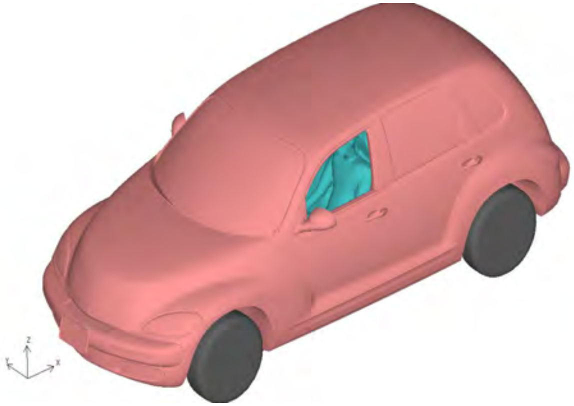

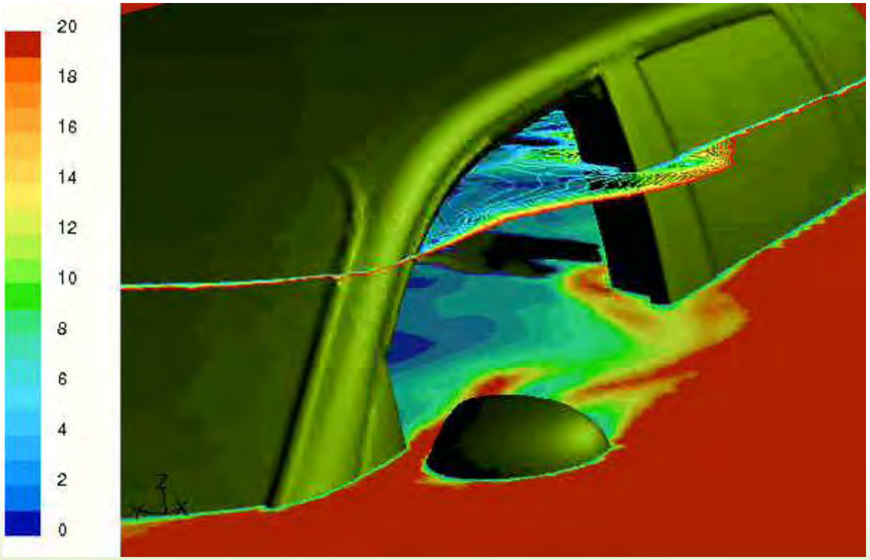

Cavity Tone

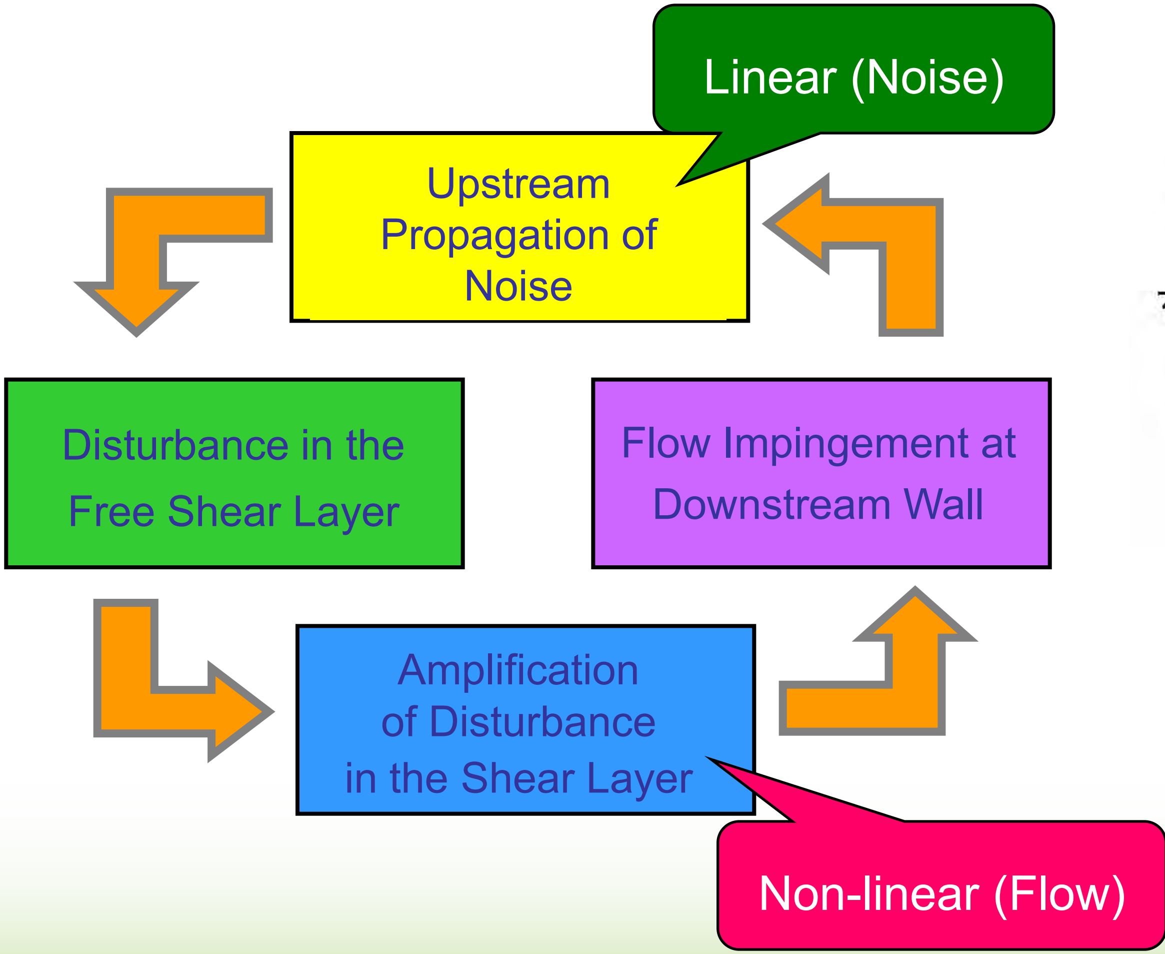
Linear (Noise)
Upstream Propagation of Noise
Disturbance in the Free Shear Layer
Flow Impingement at Downstream Wall
Amplification of Disturbance in the Shear Layer
Non-linear (Flow)

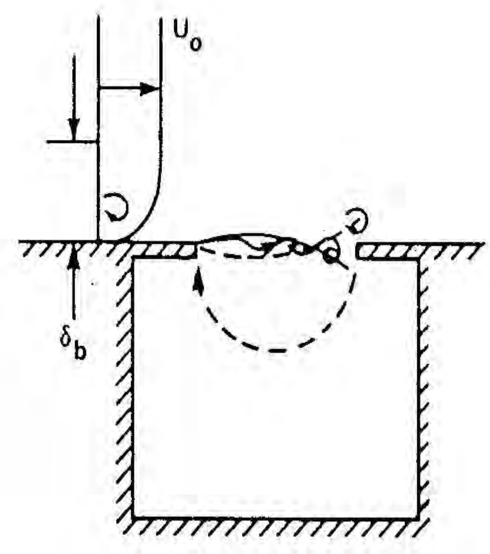
U_o
δ_b

Cavity Tone

- Mode change of rectangular cavity
  - ✓ Mode changes as M, Re_θ, L/D become larger

Steady mode ⇨ **Shear layer mode** ⇨ **Wake mode**

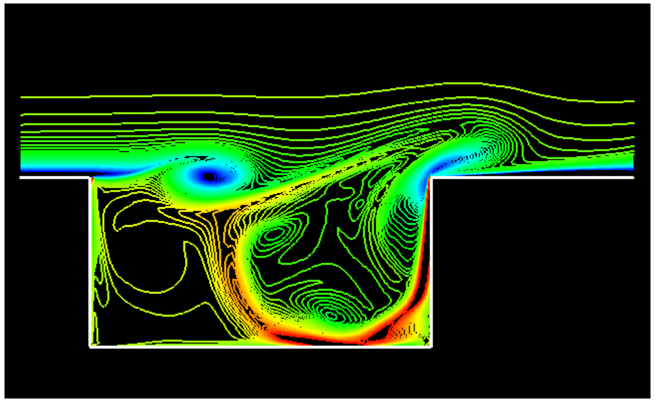

M=0.5, L/D=2, Re_θ=200,θ/D=0.04

<Shear layer mode>

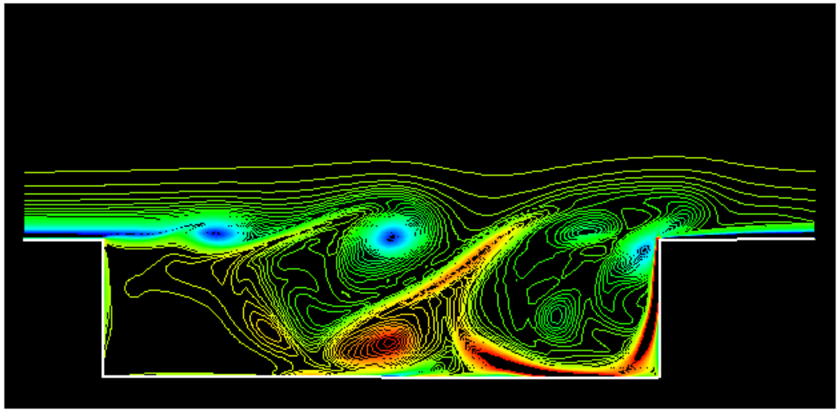

M=0.5, L/D=4, Re_θ=200,θ/D=0.04

<Wake mode>

AeroAcoustics Lab

Cavity Tone

- Rossiter's equation
  - ✓ 1962
  - ✓ Fitting with experiment
  - ✓ Resonance frequency

$$\frac{L}{U_c} + \frac{L}{c_0} = \frac{n-\beta}{f}, \quad n = 1, 2, 3, \cdots$$

$$St_n = \frac{fL}{U} = \frac{n-\beta}{M + 1/k}, \quad n = 1, 2, 3, \cdots$$

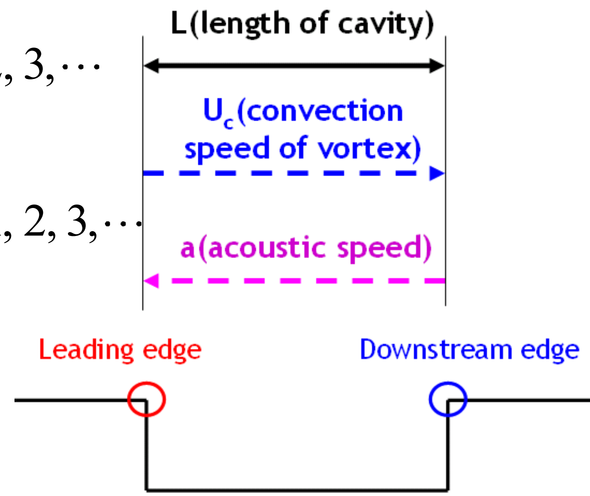

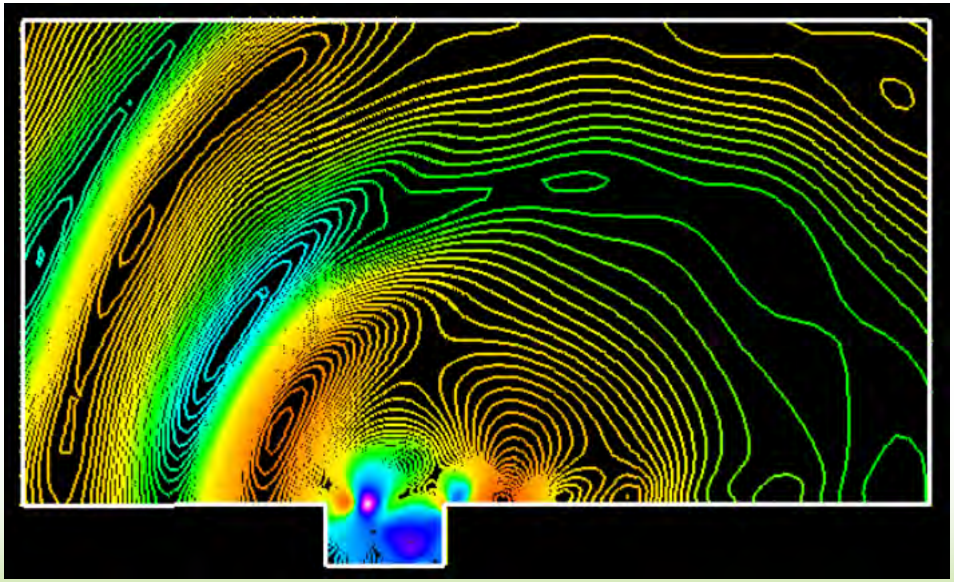

<Shear layer mode>

- Issues
  - ✓ Frequency f
  - ✓ Length L
  - ✓ Phase lag β
  - ✓ Amplitude

AeroAcoustics Lab

Cavity Tone

- Cross correlation

$$R(x_1, x_2, \tau) = E[q(x_1, t)q(x_2, t+\tau)]$$

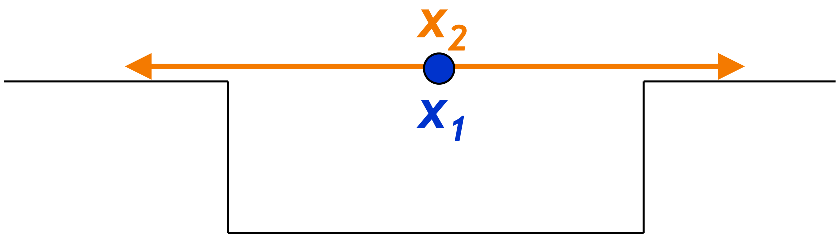

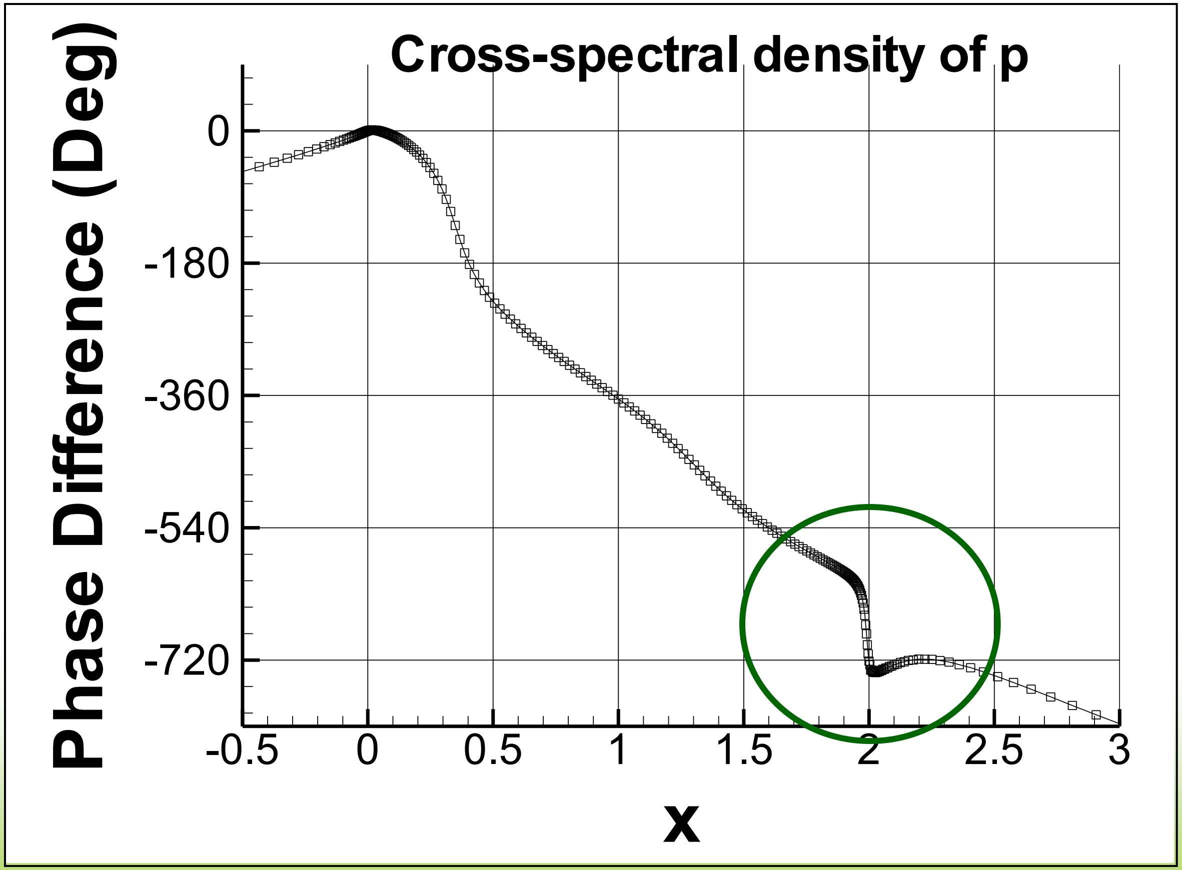

Cavity Tone

- Modified Rossiter's equation
  - ✓ Original Rossiter's eq.: $$\frac{L}{U_c}+\frac{L}{a_\infty}=\frac{n-\beta}{f_n},\quad n=1,2,3,\cdots \qquad \beta=0.25$$
  - ✓ Integral form: $$\int_{VG}^{VC}\left(\frac{1}{u}+\frac{1}{a-u}\right)dl_{\text{(along vortex convection path)}}=\frac{n-\tilde{\beta}}{f_n},\quad n=1,2,3,\cdots$$

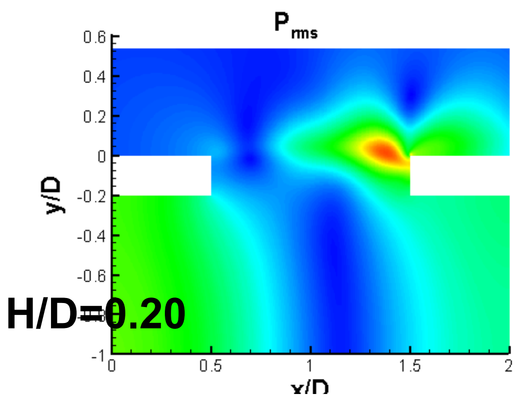

Case	n=2
Integral form & β=0.25	0.47
Integral form & β=0	0.53
Original Rossiter's Eq.	0.77
CAA	0.52

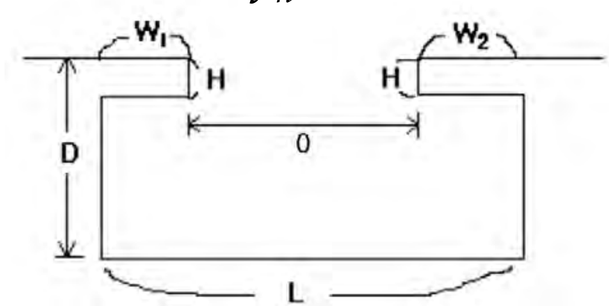

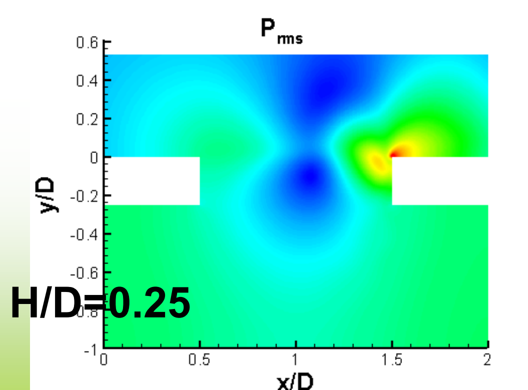

Case	n=1
Integral form β=0.25	0.29
Integral form β=0	0.38
Original Rossiter's Eq.	0.33
CAA	0.30

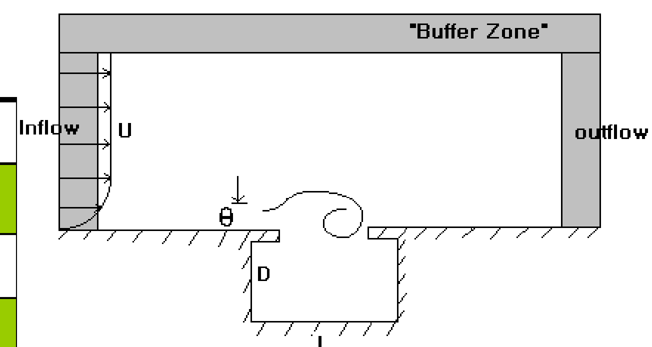

AeroAcoustics Lab

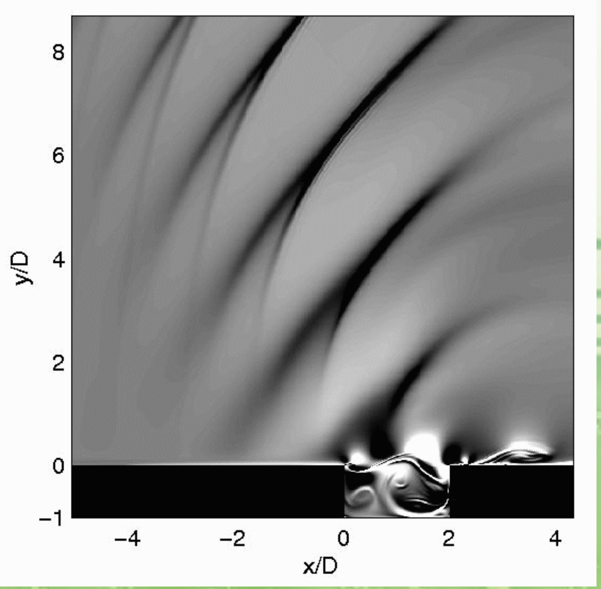

KTX

Jet Screech Tone

Governing Equations
Optimized High Order Compact
Numerical Techniques

Governing Equations

- Unsteady Compressible Euler Equations
  - ✓ Fully conservative form
  - ✓ 3 dimensional formulation

$$\frac{\partial}{\partial t}\begin{pmatrix}\rho\\ \rho u\\ \rho v\\ \rho w\\ \rho e_t\end{pmatrix}+\frac{\partial}{\partial x}\begin{pmatrix}\rho u\\ \rho u^2\\ \rho v u\\ \rho w u\\ (\rho e_t+p)u\end{pmatrix}+\frac{\partial}{\partial y}\begin{pmatrix}\rho v\\ \rho u v\\ \rho v^2\\ \rho w v\\ (\rho e_t+p)v\end{pmatrix}+\frac{\partial}{\partial z}\begin{pmatrix}\rho w\\ \rho u w\\ \rho v w\\ \rho w^2\\ (\rho e_t+p)w\end{pmatrix}=\mathbf{0}$$

  - ✓ Continuity equation in vector form

$$\frac{\partial\rho}{\partial t}+\nabla\cdot\rho\vec{v}=\mathbf{0}$$

$$\frac{D\rho}{Dt}+\rho\nabla\cdot\vec{v}=0 \qquad \therefore\nabla\cdot\vec{v}=S \quad \text{where} \quad S=-\frac{1}{\rho}\frac{D\rho}{Dt}$$

AeroAcoustics Lab

Optimized High Order Compact

- DRP (Dispersion-Relation-Preserving)
  - ✓ Tam (1993)
  - ✓ Analytically optimized central scheme
- Spectral-like scheme
  - ✓ Lele (1992)
  - ✓ Numerically optimized compact scheme
- Optimized High Order Compact :
  - ✓ Kim & Lee (1996)
  - ✓ Analytically optimized compact scheme

$$\beta f'_{i-2} + \alpha f'_{i-1} + f'_i + \alpha f'_{i+1} + \beta f'_{i+2} =$$
$$a\,\frac{f_{i+1} - f_{i-1}}{2\Delta x} + b\,\frac{f_{i+2} - f_{i-2}}{4\Delta x} + c\,\frac{f_{i+3} - f_{i-3}}{6\Delta x}$$

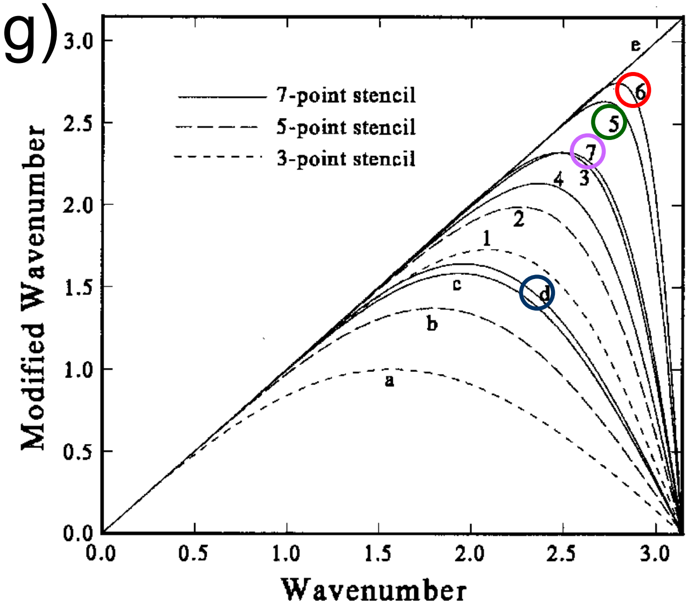

a: second-order central differences
b: fourth-order central differences
c: sixth-order central differences
d: Tam's DRP scheme in space
e: exact differentiation
1: standard Padé scheme
2: sixth-order tridiagonal scheme ($c = 0$)
3: OSOT (optimized sixth-order tridiagonal) scheme
4: eighth-order tridiagonal scheme
5: Lele's fourth-order spectral-like pentadiagonal scheme
6: OFOP (optimized fourth-order pentadiagonal) scheme
7: tenth-order pentadiagonal scheme

$$\beta f'_{i-2} + \alpha f'_{i-1} + f'_i + a f'_{i+1} + \beta f'_{i+2} = a \frac{f_{i+1} - f_{i-1}}{2\Delta x} + b \frac{f_{i+2} - f_{i-2}}{4\Delta x} + c \frac{f_{i+3} - f_{i-3}}{6\Delta x}$$

	α	β	a	b	c
Central scheme (2^{nd} order)	0	0	1	0	0
DRP scheme	0	0	0.726325187522	-0.120619908868	0.003728657553
Original compact scheme (4^{th} order)	1/6	2/3	1	0	0
Spectral-like scheme (4^{th} order)	0.5771439	0.0896406	1.3025166	0.9935500	0.03750245
OHOC (4^{th} order)	0.590010816707	0.097797917674	1.279672797796	1.051191982414	0.0044752688552

➢ Optimized compact difference scheme

$$\beta f'_{i-2} + \alpha f'_{i-1} + f'_i + \alpha f'_{i+1} + \beta f'_{i+2} \cong a\frac{f_{i+1}-f_{i-1}}{2\Delta x} + b\frac{f_{i+2}-f_{i-2}}{4\Delta x} + c\frac{f_{i+3}-f_{i-3}}{6\Delta x}$$

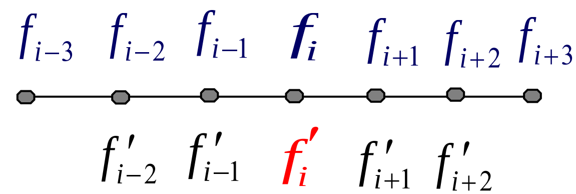

- ✓ Penta-diagonal formulation and 4th-order spatial accuracy
- ✓ Fourier analysis of dispersion errors in the wave-number domain

➢ Maximum resolution characteristics

$$\kappa = k\Delta x = \frac{2\pi}{\lambda}\Delta x$$

$$\kappa = 2.5, \quad \frac{\lambda}{\Delta x} \approx 6.3$$

a. 2nd-order central differences

b. 4th-order central differences

d. DRP scheme

3. OSOT scheme

6. OFOP scheme

e. exact differentiation

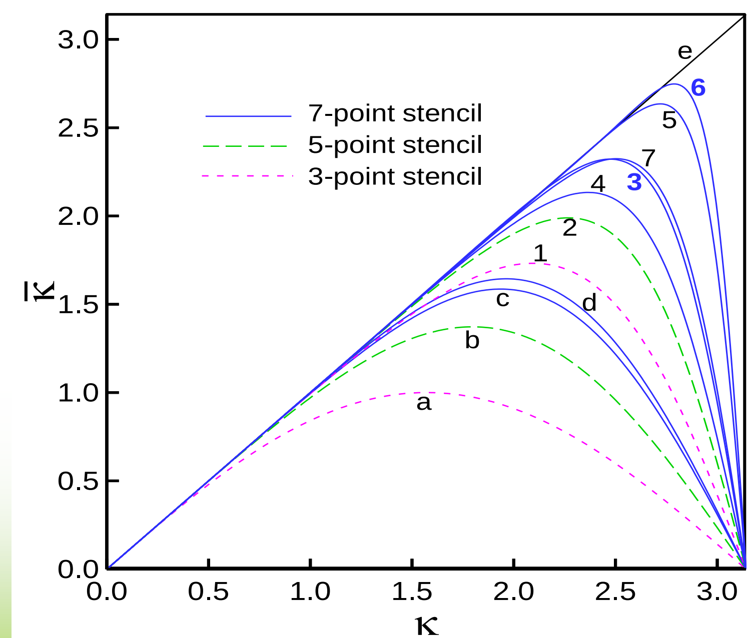

Numerical Techniques

- Optimized high-order compact (OHOC) : Kim & Lee (1996)
- Low dissipation and dispersion Runge-Kutta (LDDRK) : Hu et al. (1996)
- Adaptive nonlinear artificial dissipation (ANAD) : Kim & Lee (2001)
- Generalized characteristic boundary condition (GCBC) : Kim & Lee (2000)

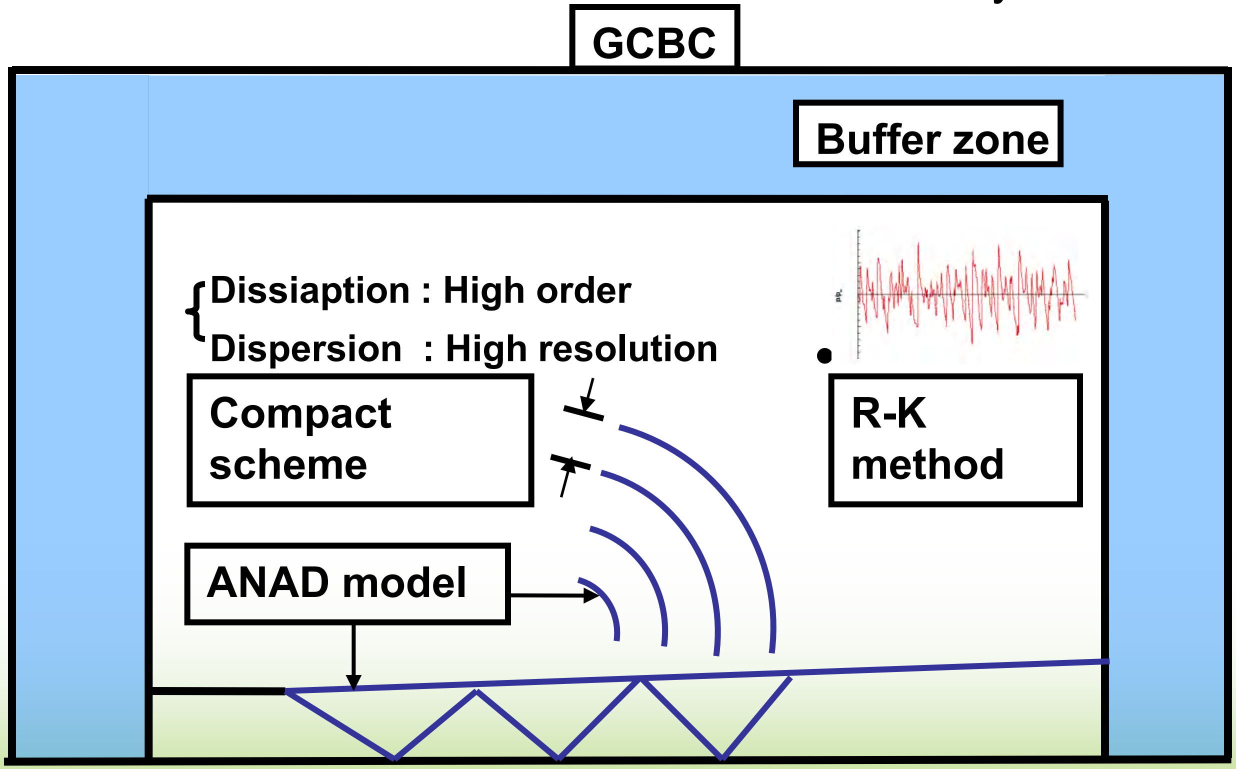

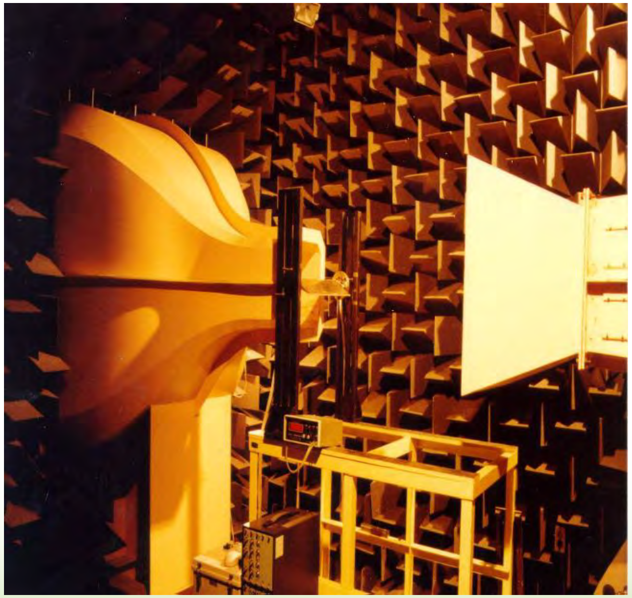

Rocket Noise

- ✓ Ariane 4 : Among 116 launch 3 fail(Noise)
- ✓ Ariane 5 : Among 60 launch 4 fail(Electronic Equipment Operation)
- ✓ Conestoga Rocket : 6 Model (Electronic Equipment due to Noise)

Ariane 5 rocket explosion

Conestoga rocket explosion

Screech Tone

- Screech Tone

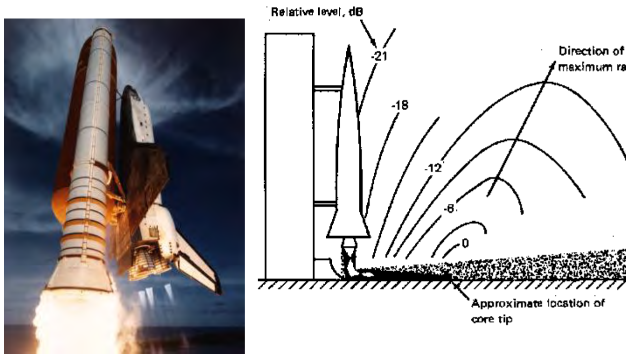

<Noise from rocket launcher>

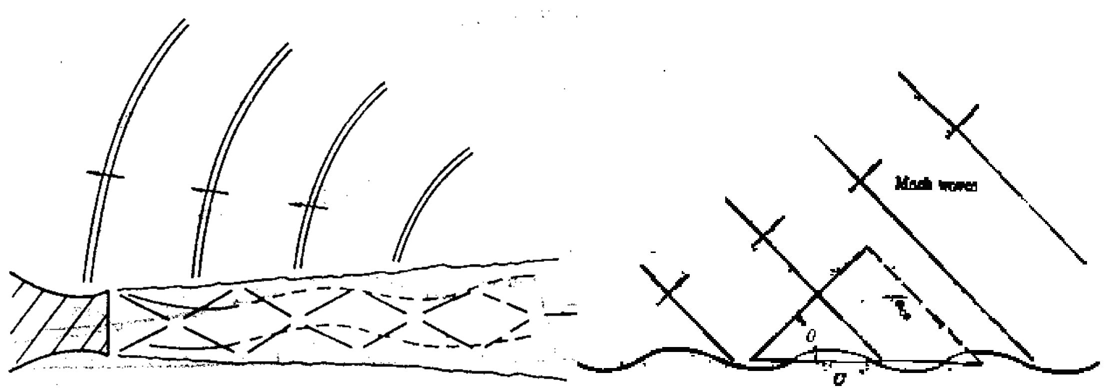

<Supersonic jet noise>

- Issues
  - ✓ Structure damage
  - ✓ Electronic Equipment
  - ✓ Generation mechanism: instability mode & shock cell reflection
  - ✓ Powell (1953)

$$\frac{1}{U_c} + \frac{1}{a_\infty} = \frac{1}{sf}$$

U_c : convection velocity

s : shock cell length

  - ✓ Tam (1988)

$$\frac{1}{U_c} + \frac{1}{a_\infty} = \frac{k_1}{2\pi f}$$

U_c : phase velocity

k_1 : fundamental wave number of the shock cell structure

AeroAcoustics Lab

Supersonic Flow

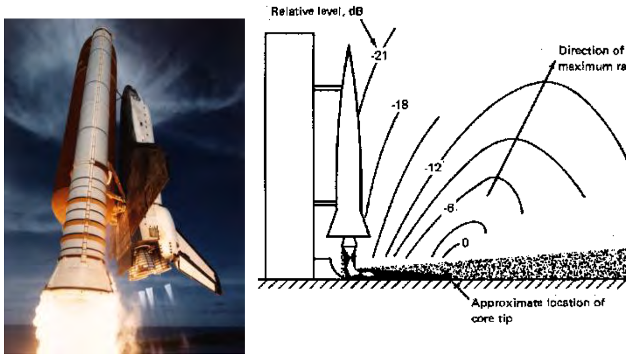

<Noise from rocket launcher>

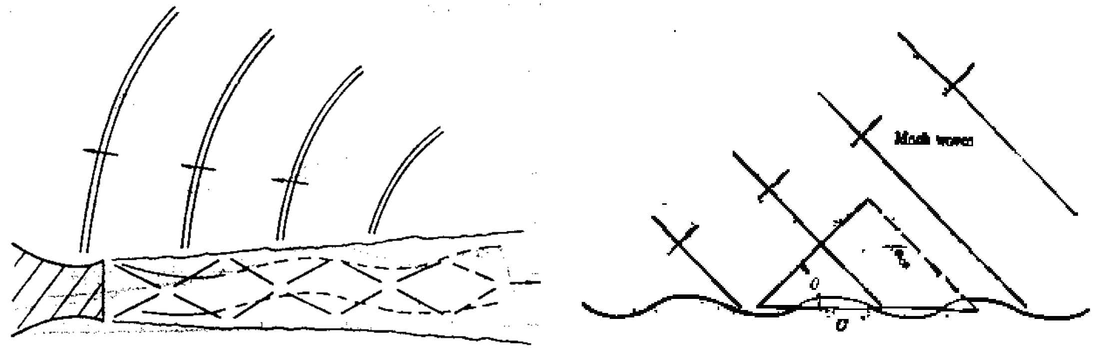

<Supersonic jet noise>

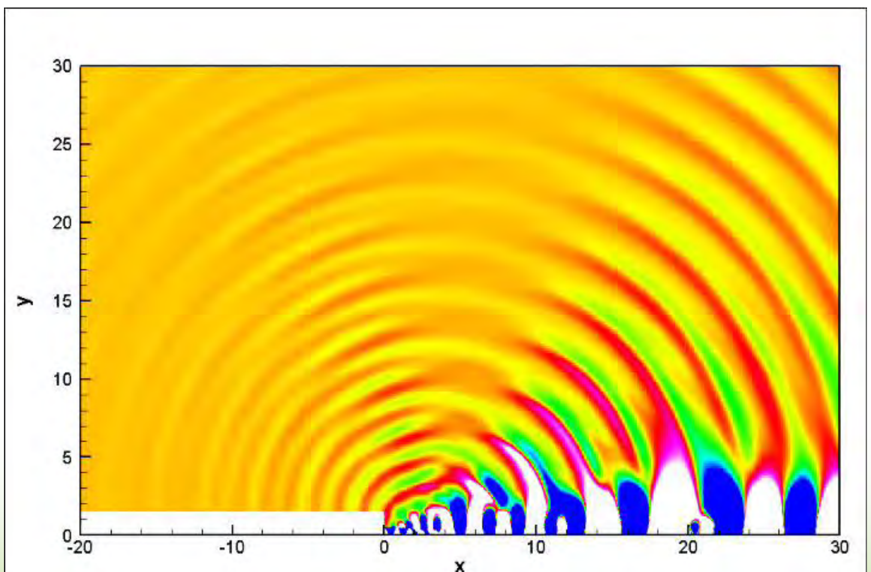

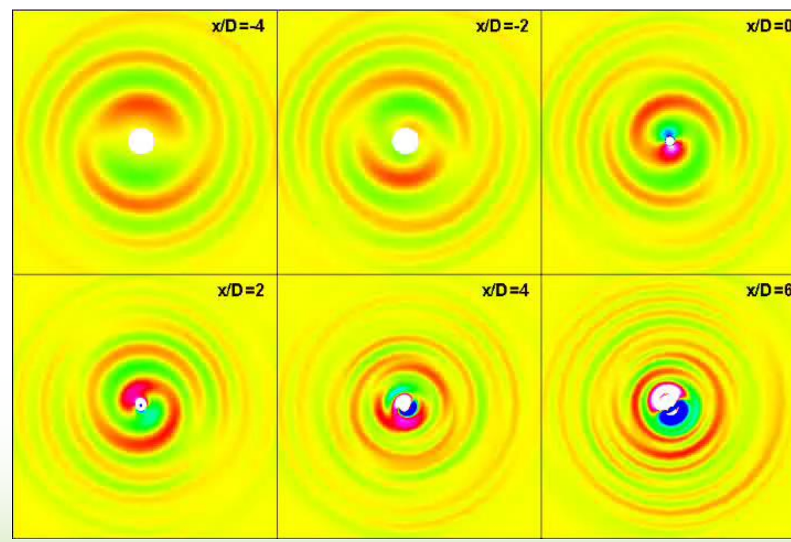

AeroAcoustics Lab

Jet Noise

- Rocket Noise
  - ✓ M=2.1, perfectly expanded condition
  - ✓ No shock cell structures
  - ✓ Only Mach waves are shown

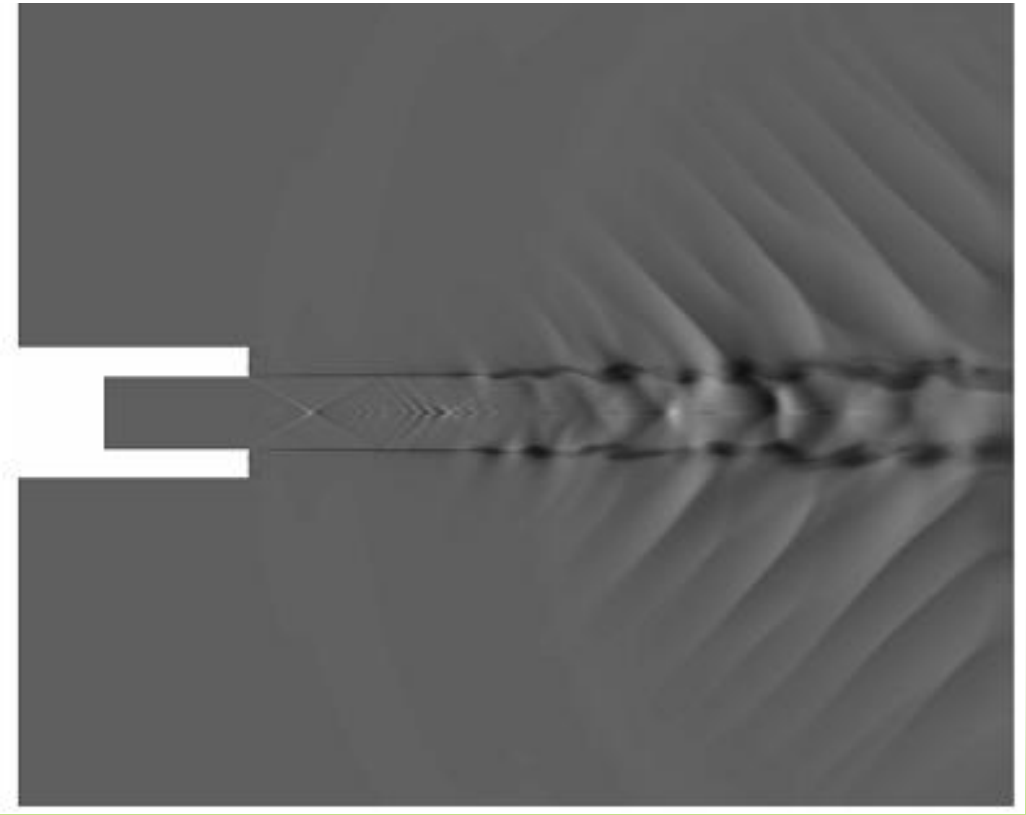

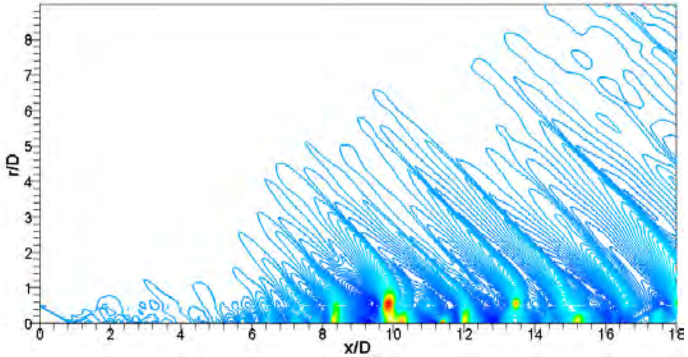

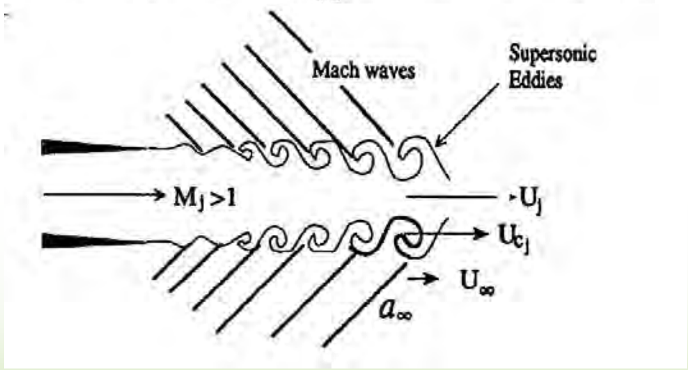

Jet Noise

- Screech Tone
  - M=1.18(A2 mode)
    - Two perturbations are observed at x/D=2.52 and x/D=5
    - A large perturbation is observed at the top of 3rd shock cell
    - Concentric circles show good agreement with wave fronts

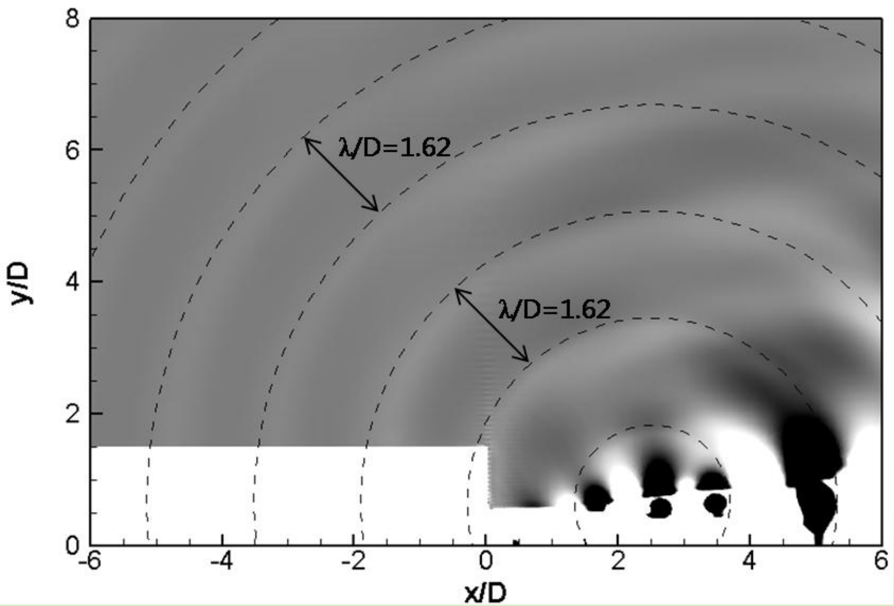

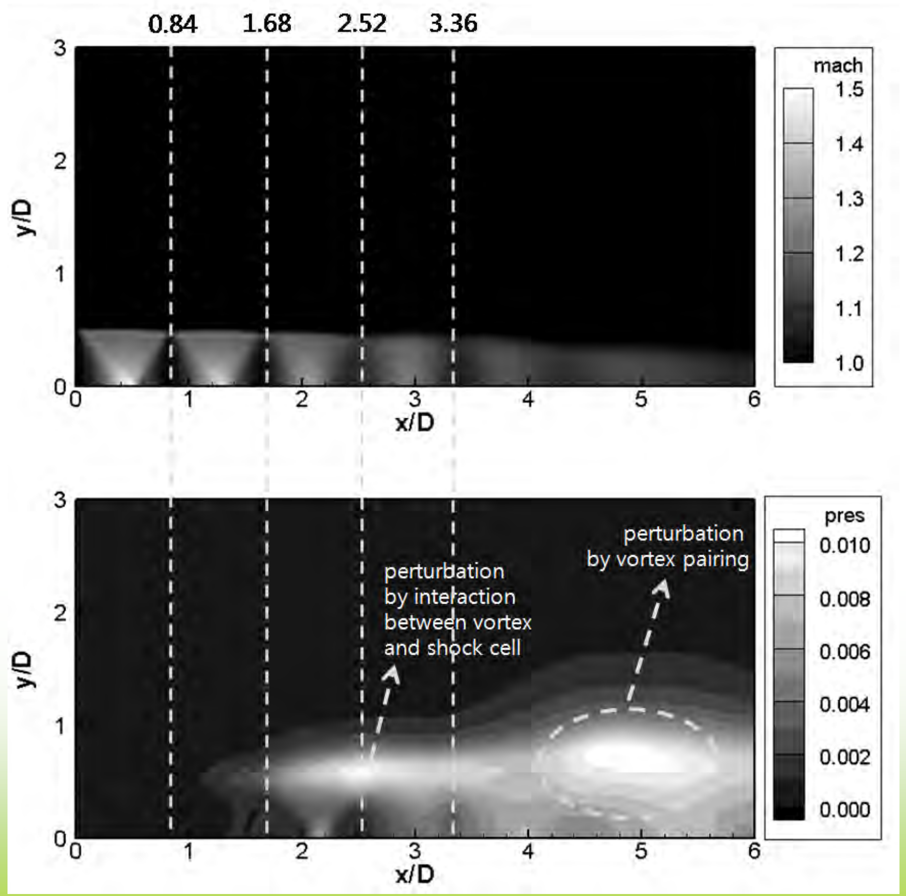

Jet Noise

- Screech Tone
  - ✓ At the initial stage, the pressure signal is not so stable and some irregular variation is observed

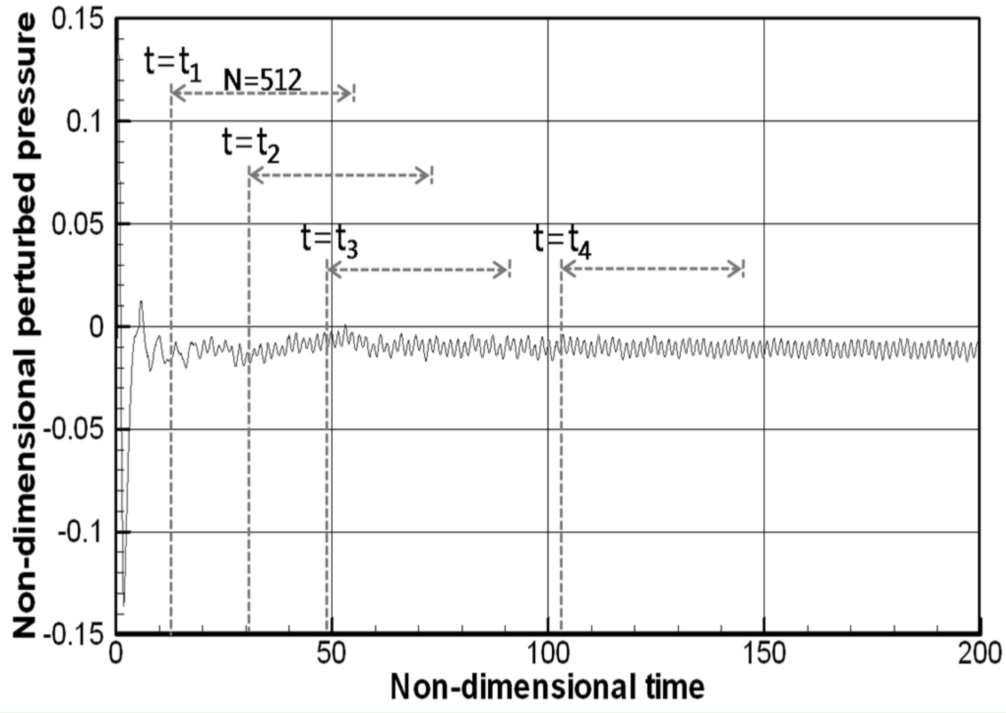

A pressure signal of M=1.18 jet

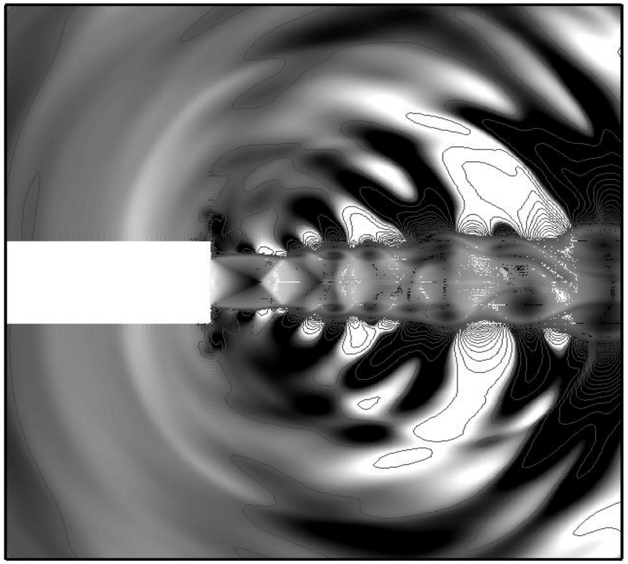

Sound Source

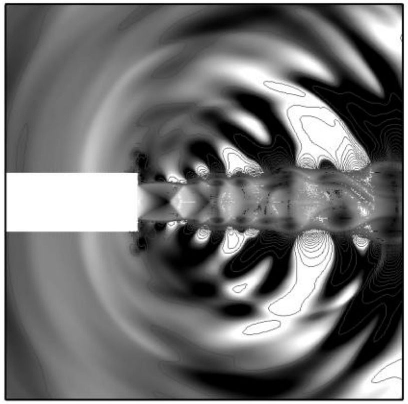

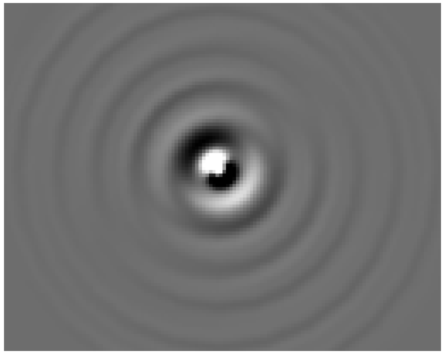

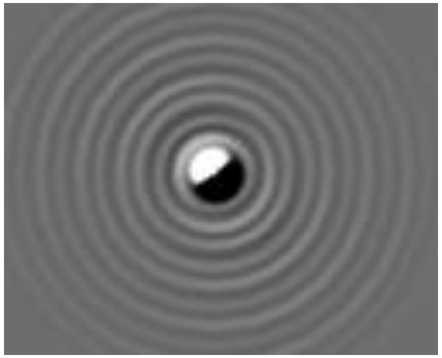

Jet Noise

- Screech Tone
  - ✓ M=1.18(A2 mode) : the components of both A1 and A2 modes exist at the beginning and A2 mode becomes dominant

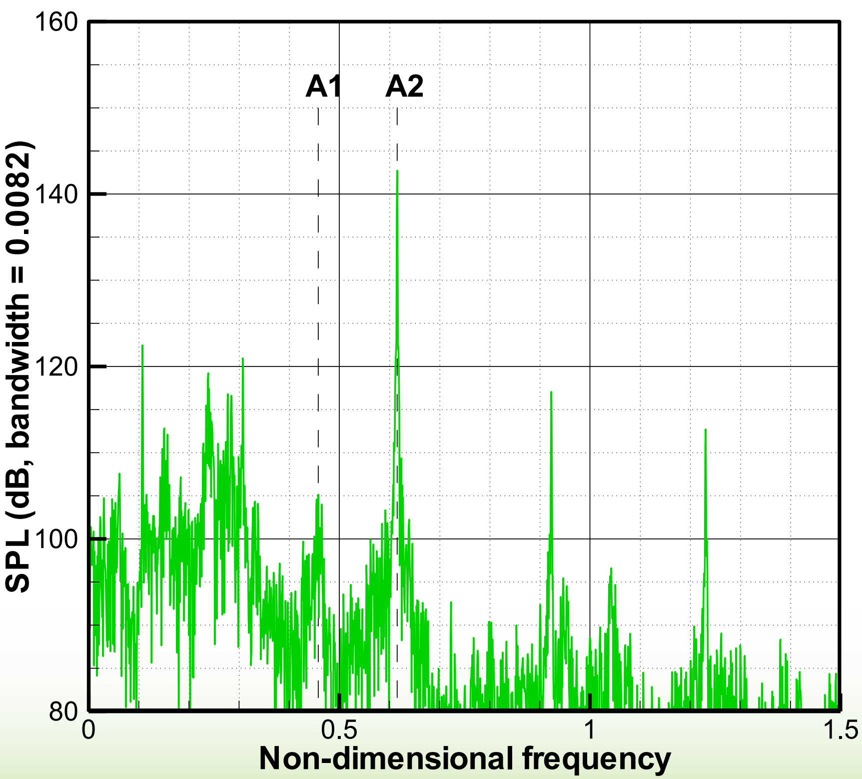

Long period (N=16,384)

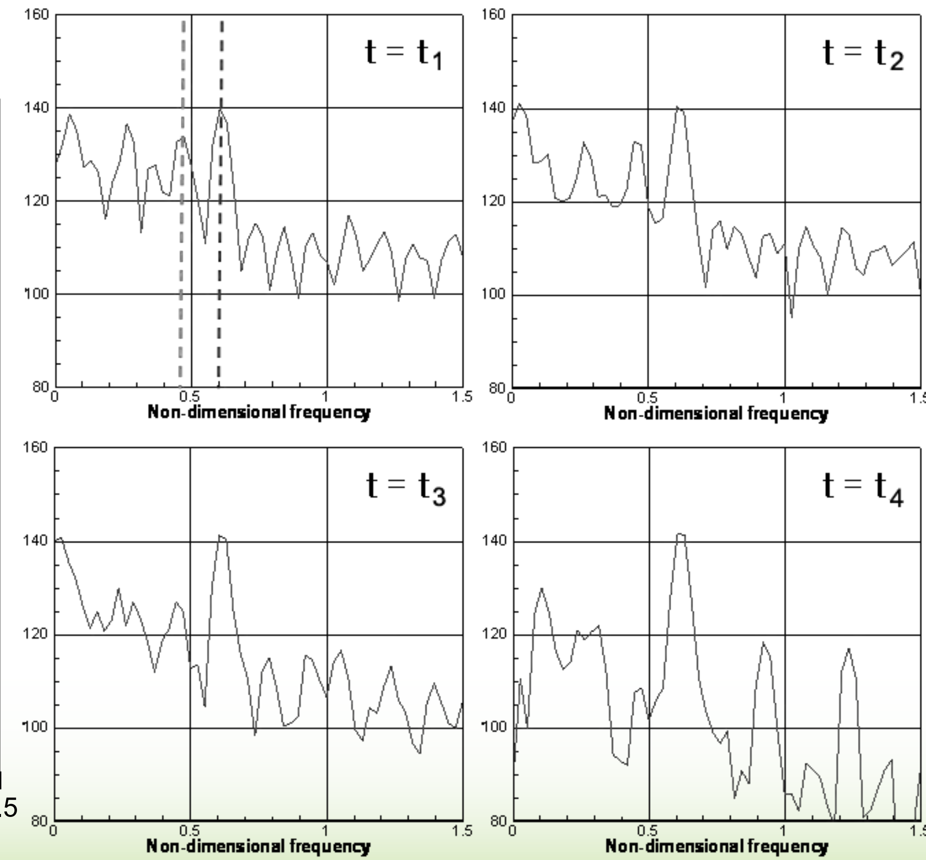

Short period (N=512)

Screech Tone

- Axisymmetric mode change : A1 mode
  - ✓ M=1.08

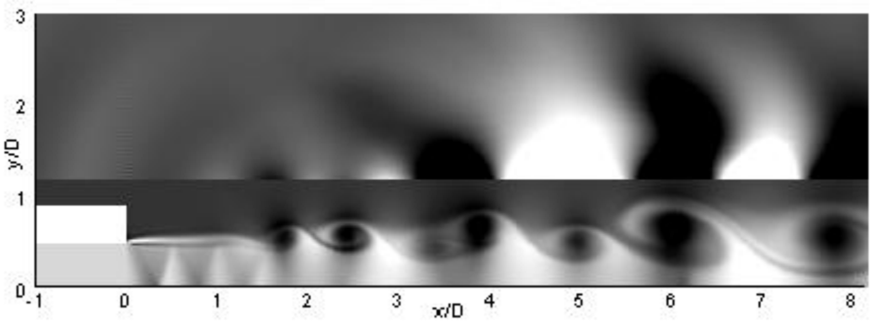

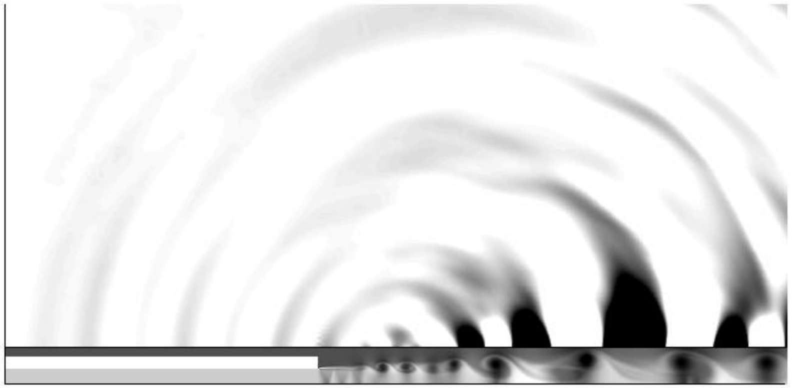

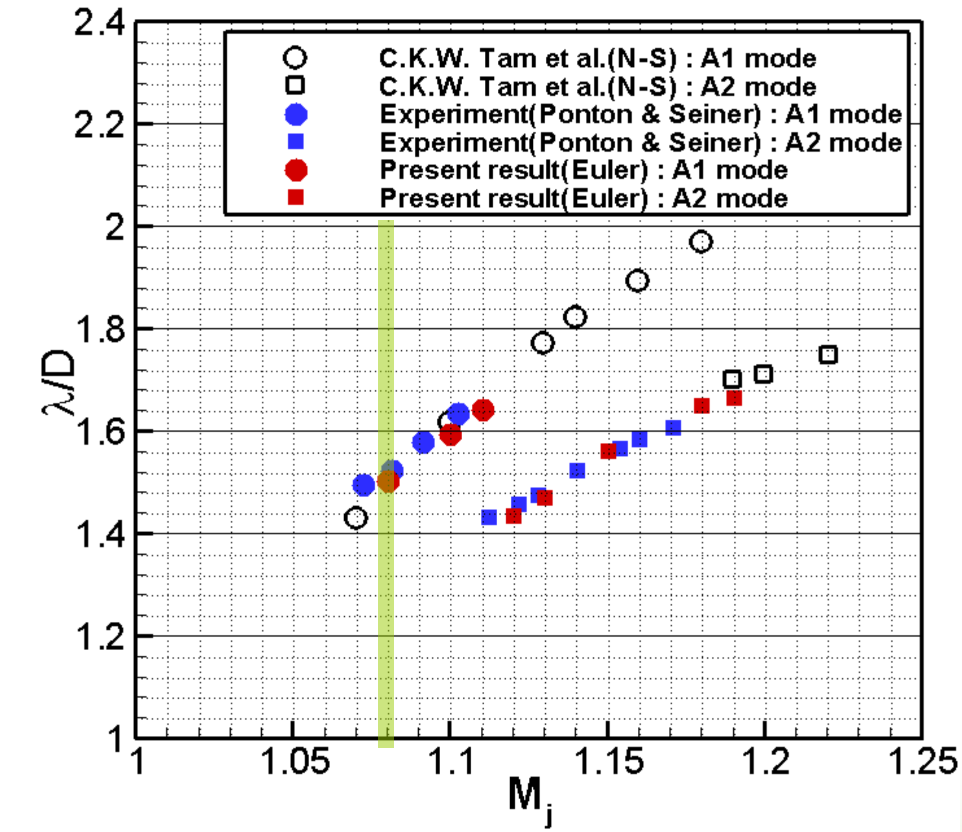

Screech Tone

- Axisymmetric mode change : A2 mode
  - ✓ M=1.18

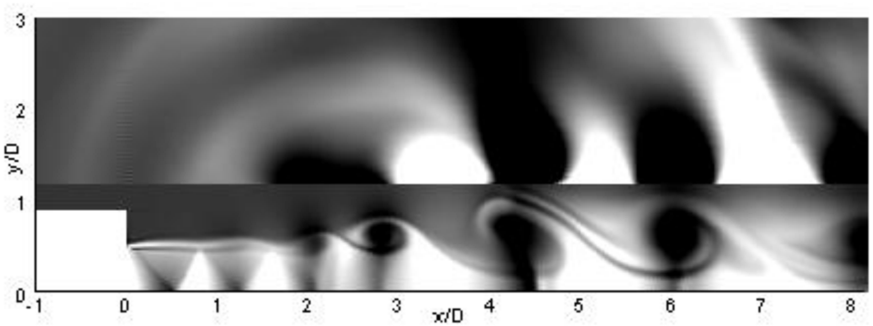

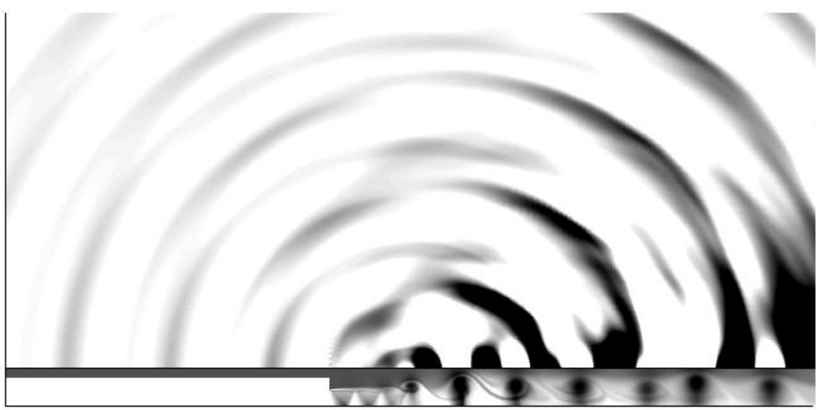

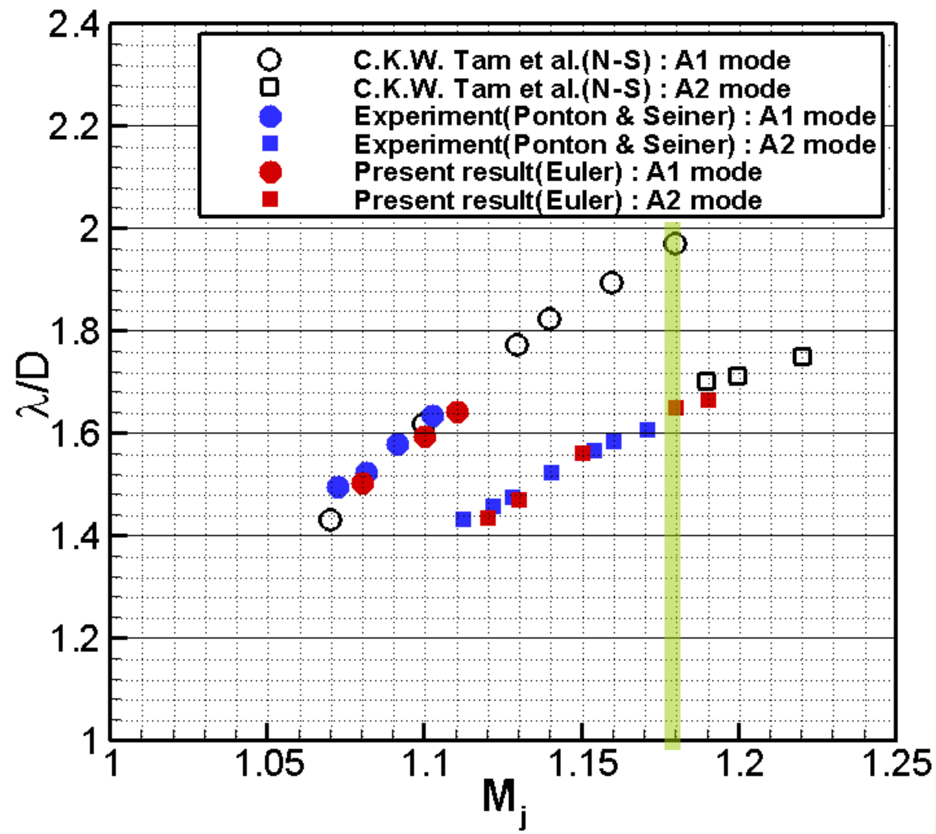

Jet Noise

- Screech Tone
  - ✓ Instantaneous density contour

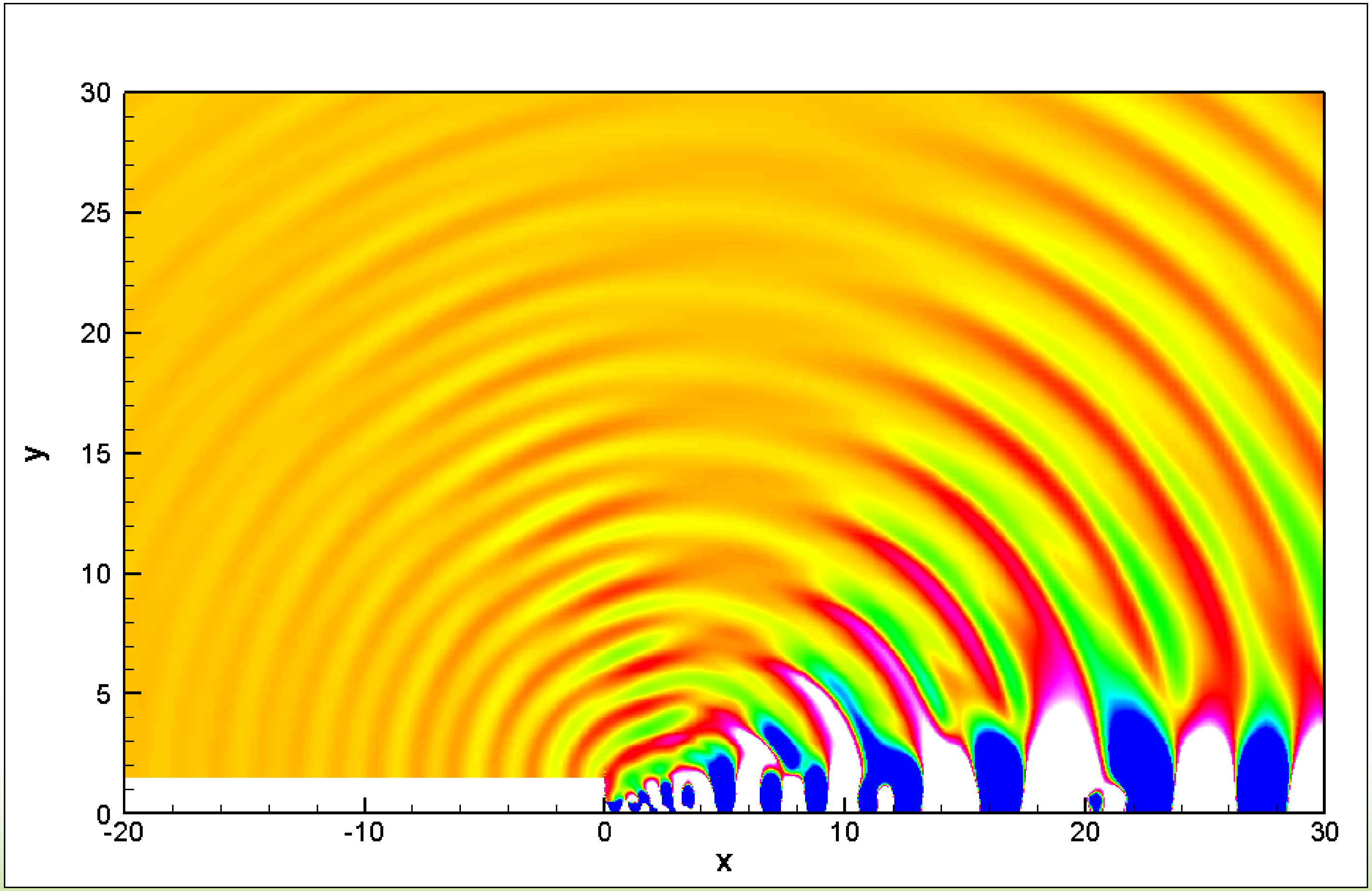

3 D Jet Screech

- Screech Tone
  - ✓ Two modes(A1&A2) are observed
  - ✓ Experimental results show rapid decrease of amplitude after Mach number 1.15 in 3D calculation

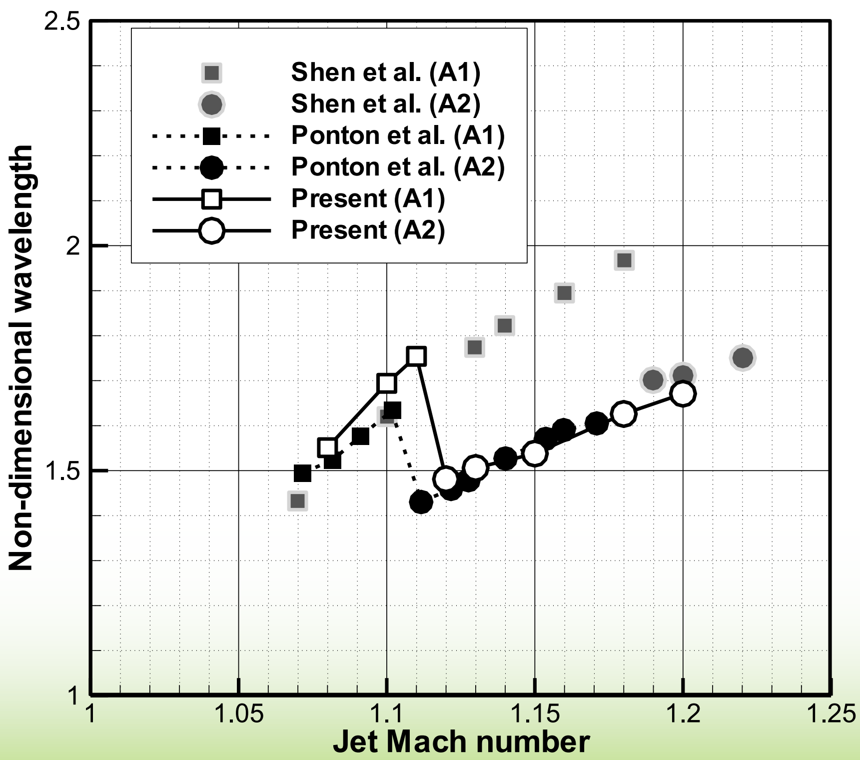

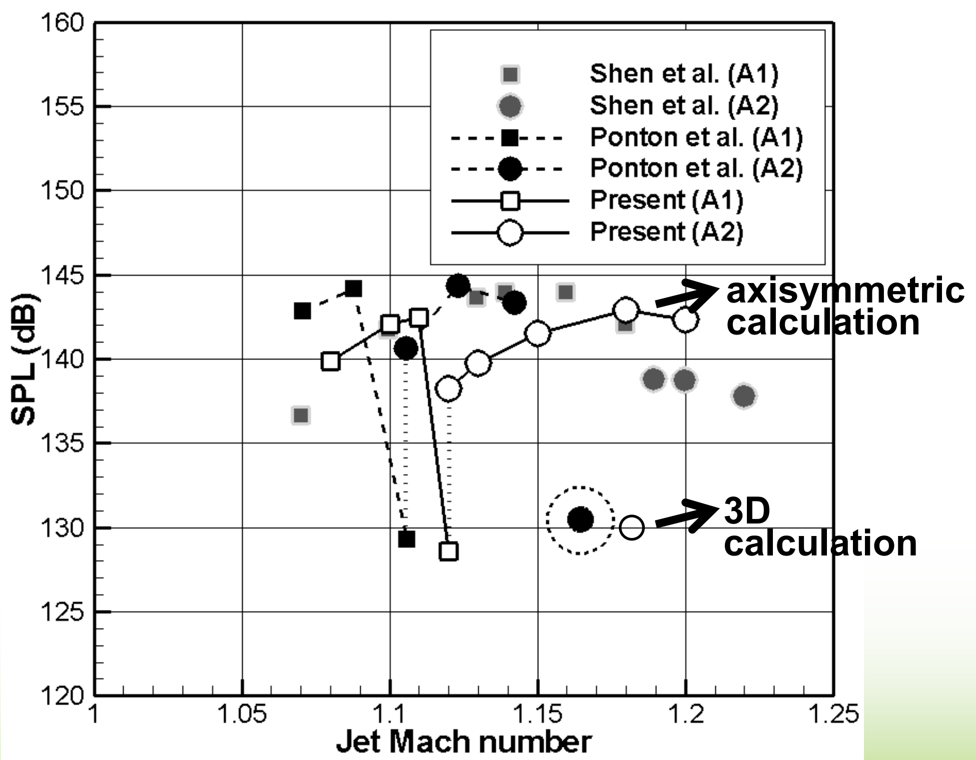

Supersonic Flow

- At the initial stage, the pressure signal is not so stable and some irregular variation is observed.

3D Mode : flapping, spiral mode

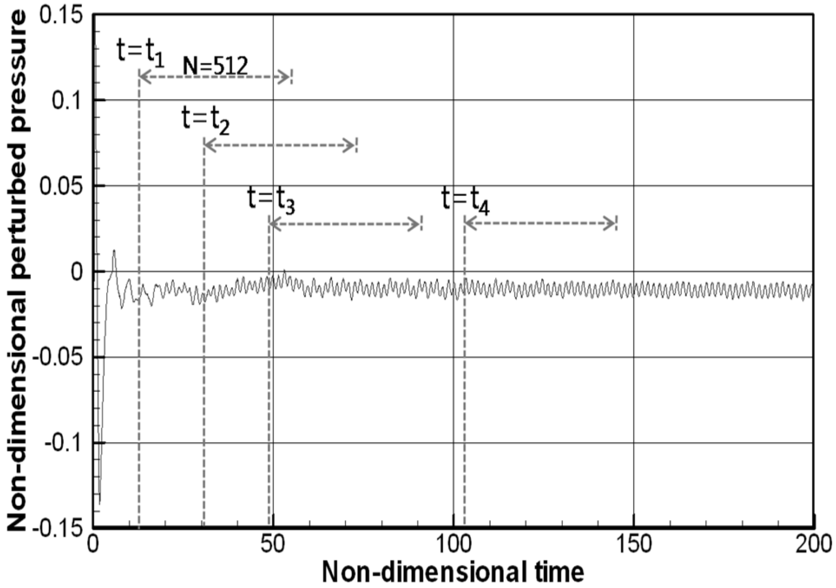

A pressure signal of M=1.18 jet

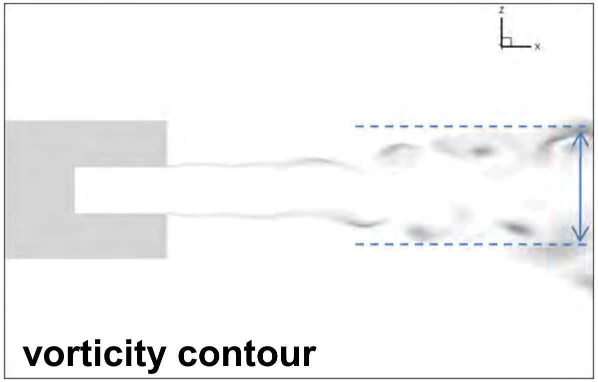

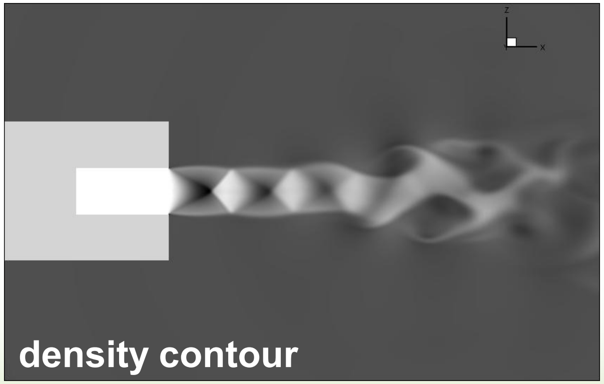

Screech Tone Noise

- 3D mode (M_j=1.43, B & C):
- Vorticity & Density Contours
  - ✓ Flapping mode (B)
  - ✓ Spiral mode (C)

Vorticity Contour

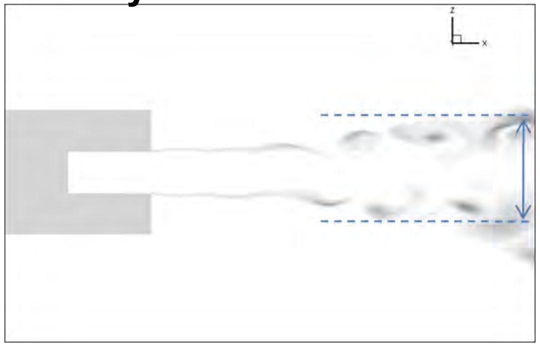

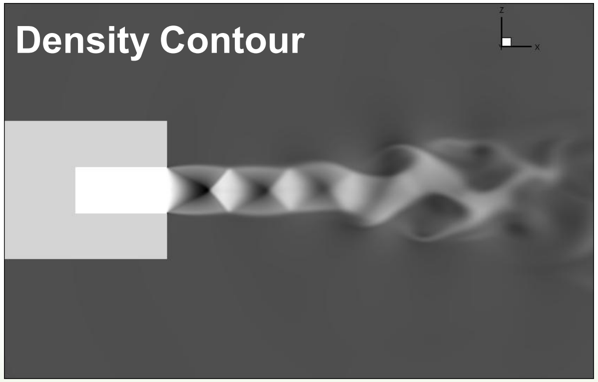

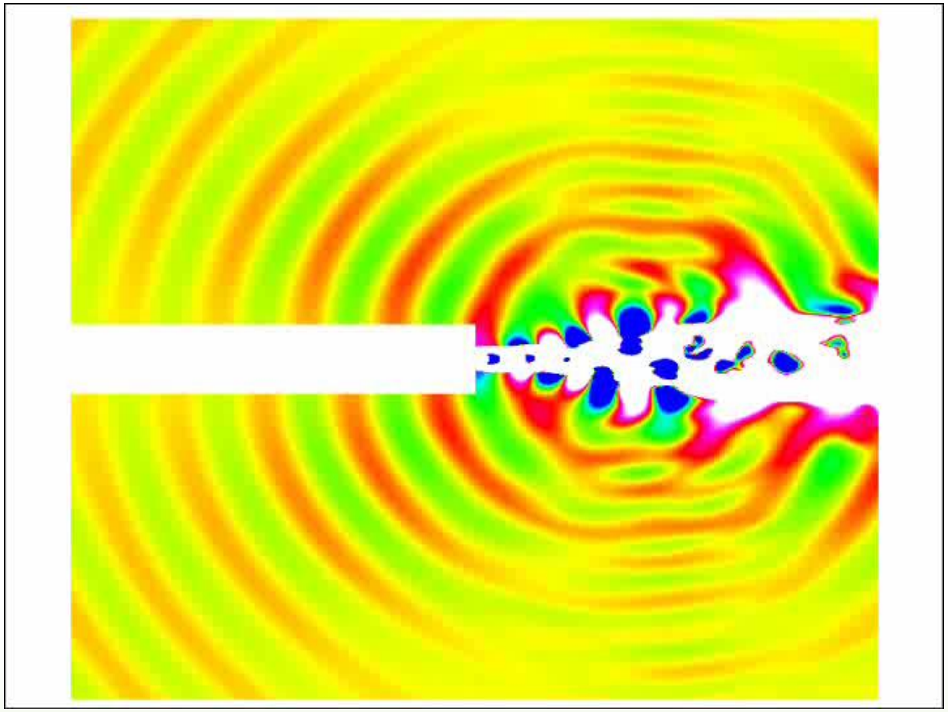

Instantaneous Density Contour

Screech Tone Noise

- 3D mode (M_j=1.43, B & C): Density Contour
  - ✓ Strong waves propagates up and down.

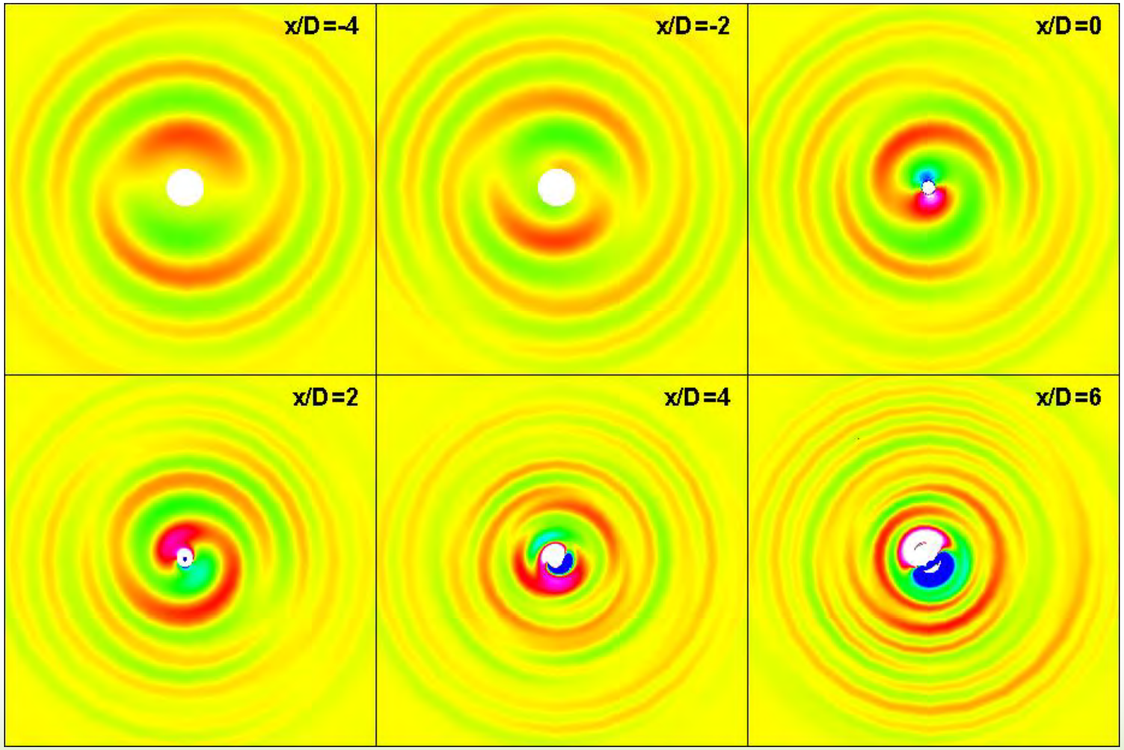

Sectional Variation

Screech Tone Noise

- 3D mode (M_j=1.43, B & C): Spectral Analysis
  - ✓ Two modes are observed.
    - B mode
    - C mode

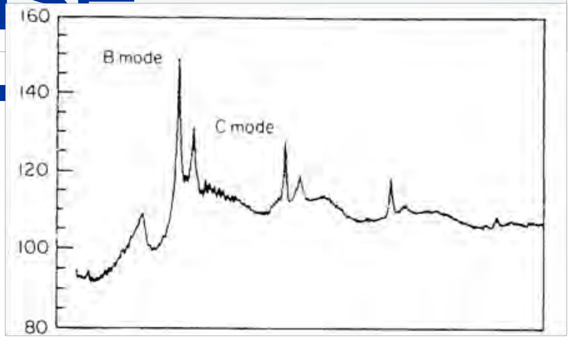

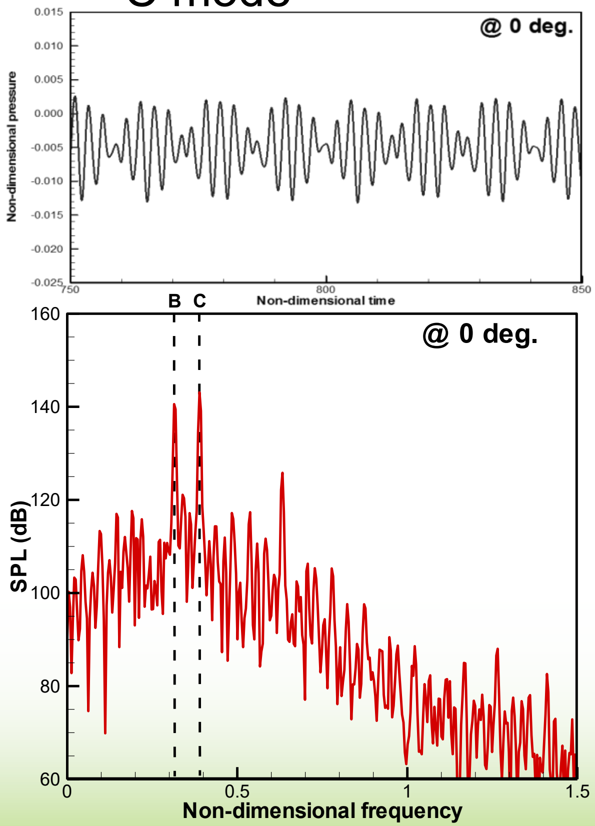

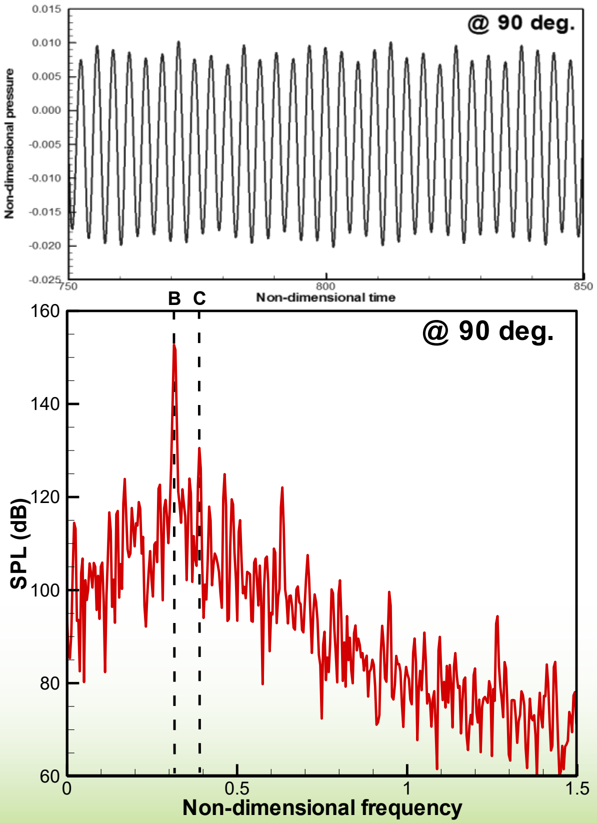

Screech Tone Noise

- 3D mode (M_j=1.43, B & C): Directivity
  - The directivities of B mode and C mode looks like the directivity of dipole and they are perpendicular each other

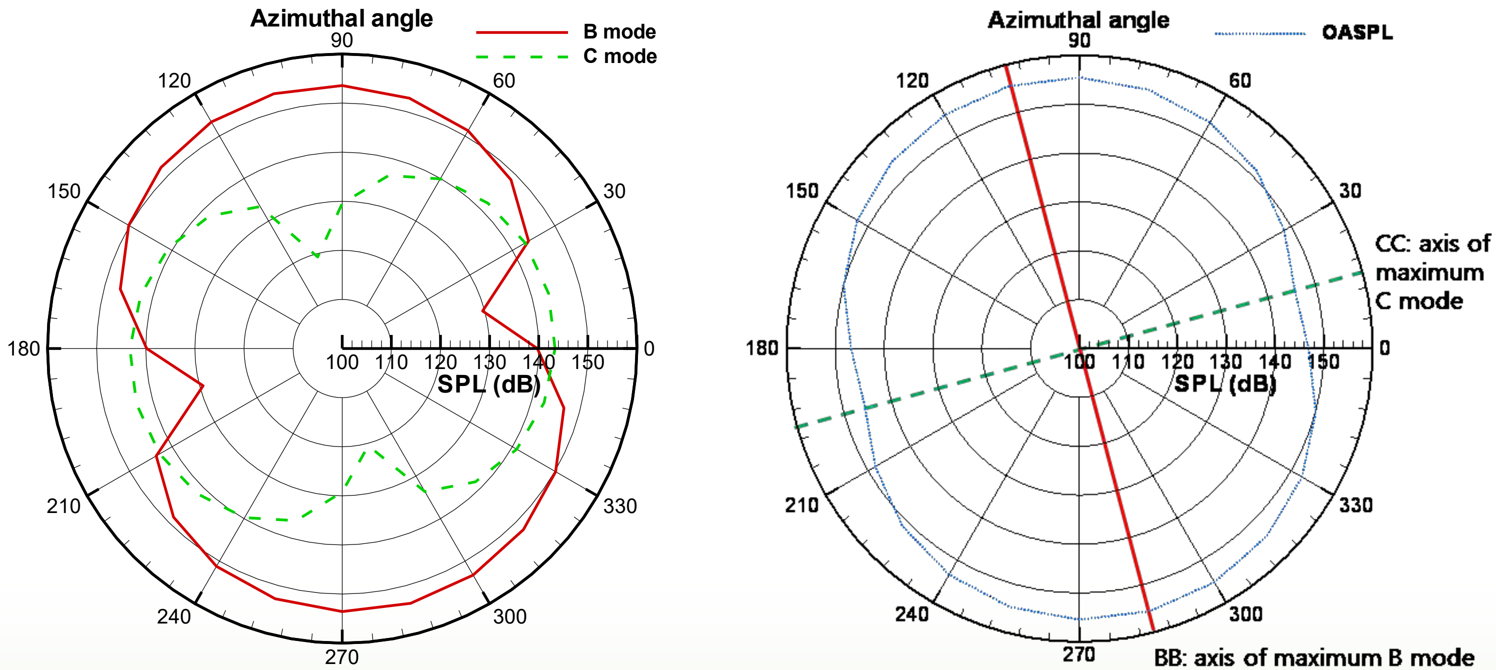

Screech Tone

- 3 dimensional supersonic jet : M=1.15

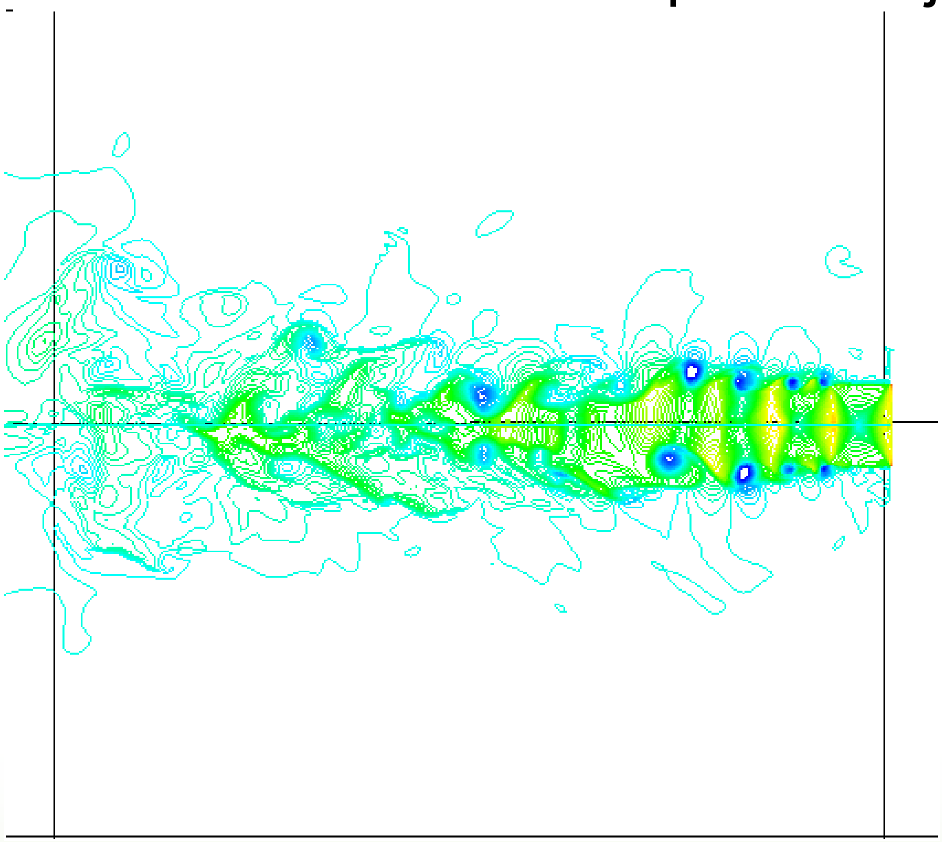

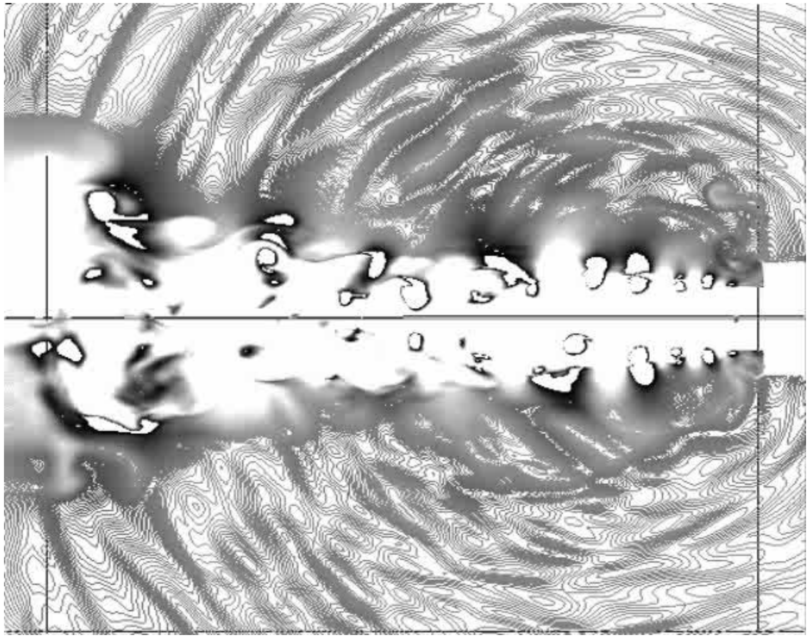

<Density contour 1(0.6<ρ/ ρ_0<1.7)>

<Density contour 2(0.95<ρ/ ρ_0<1.05)>

Screech Tone

- Downstream propagation

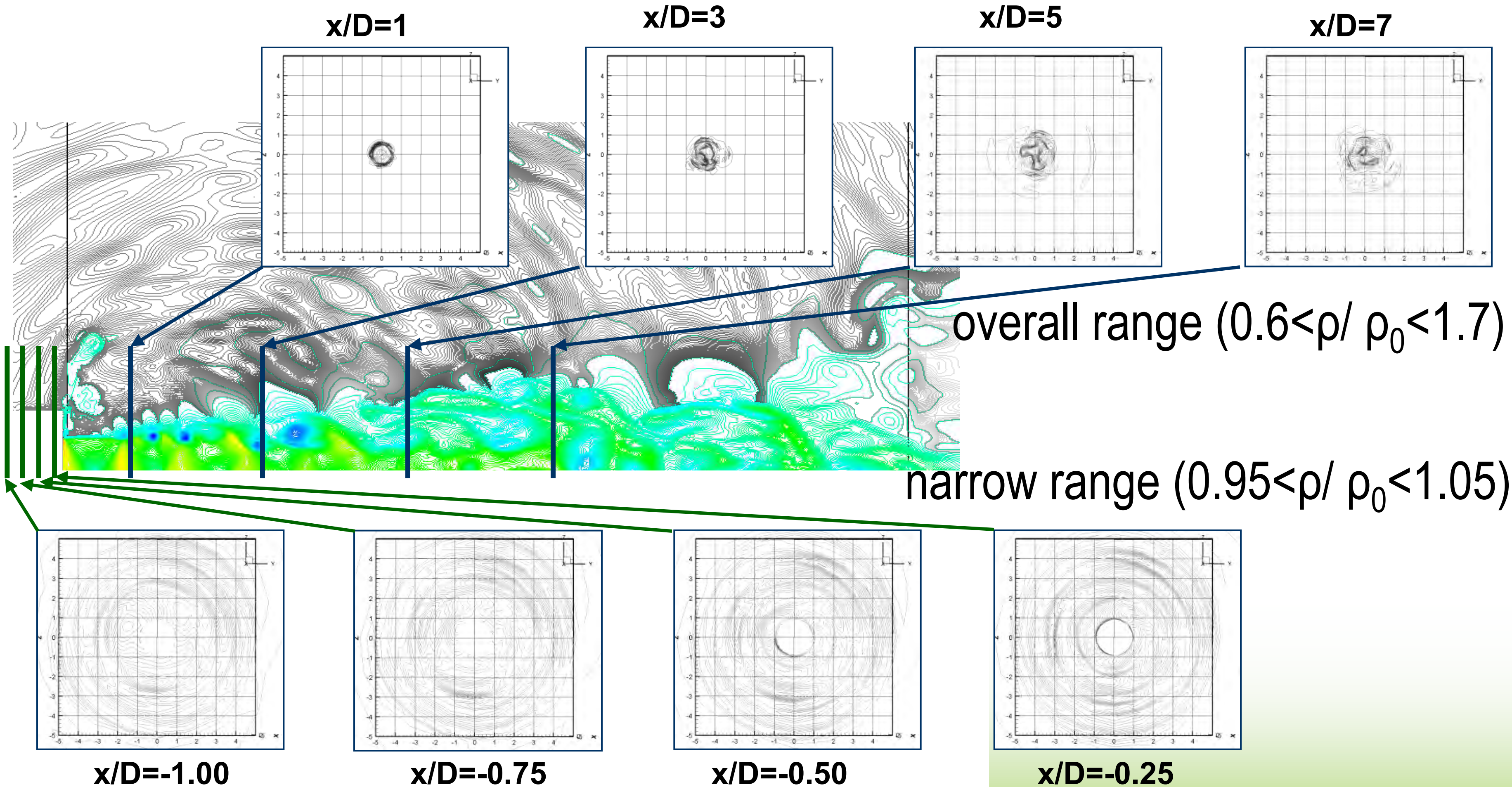

- Upstream propagation

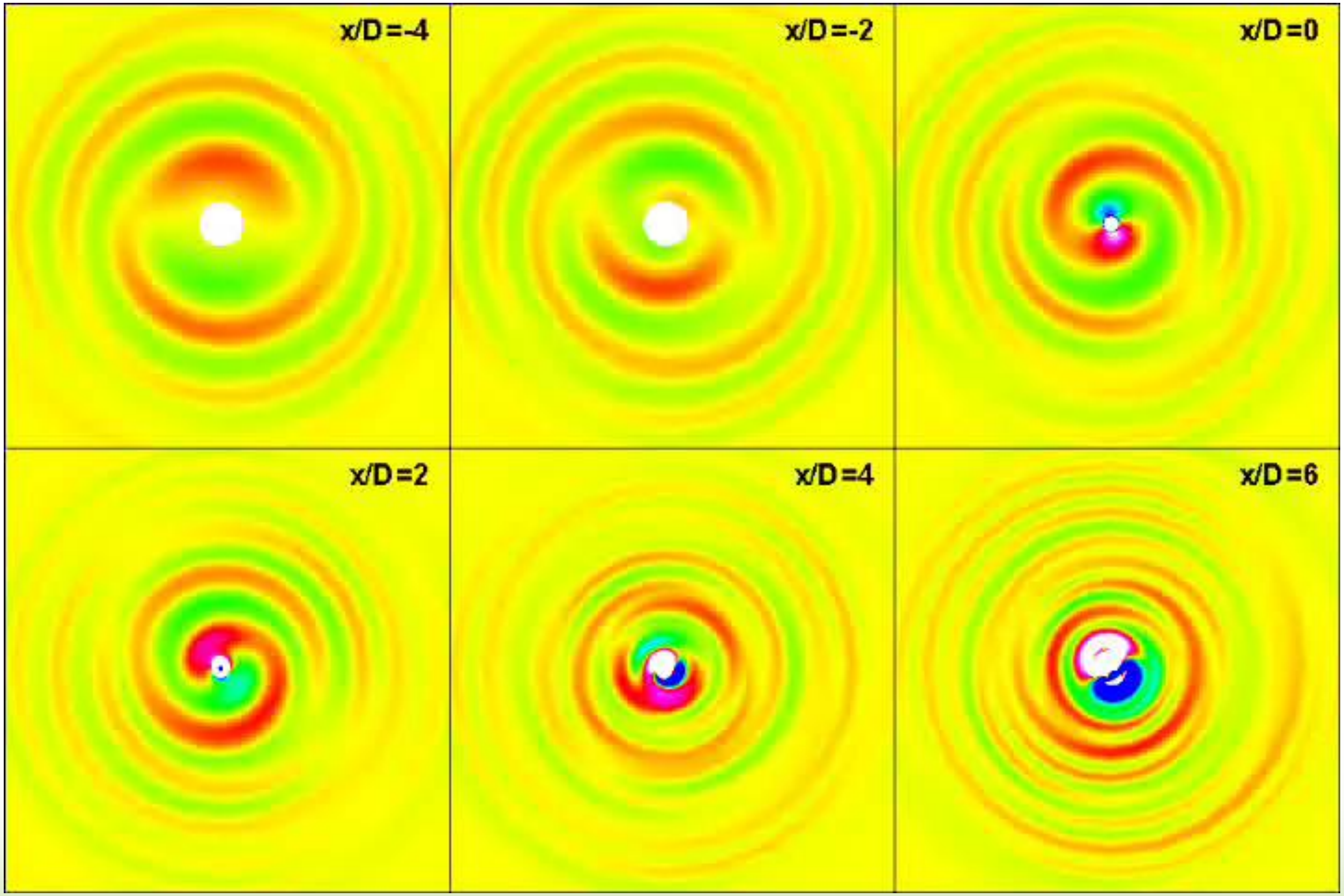
x/D=-4
x/D=-2
x/D=0
x/D=2
x/D=4
x/D=6

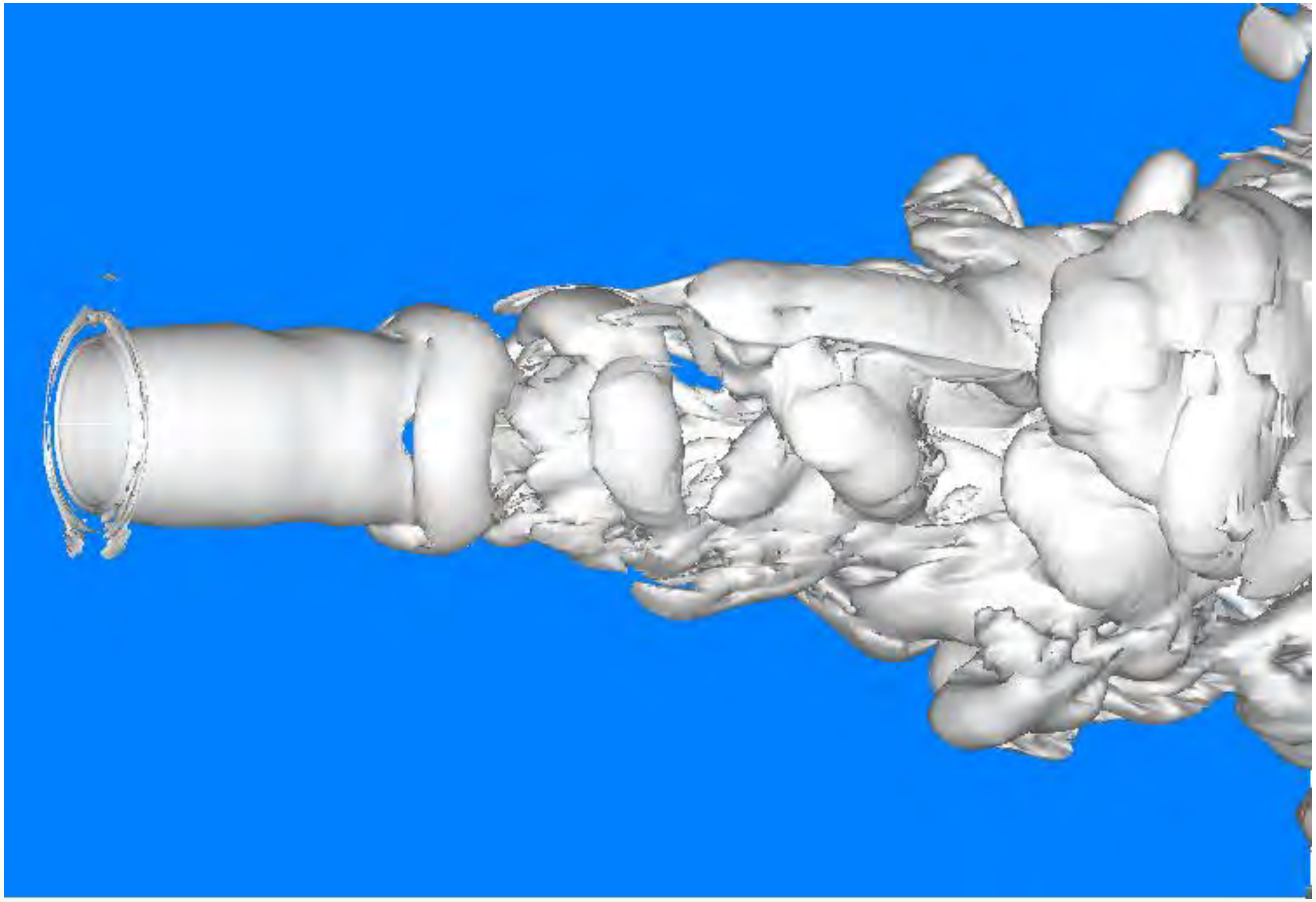

Screech Tone

- 3 dimensional effect

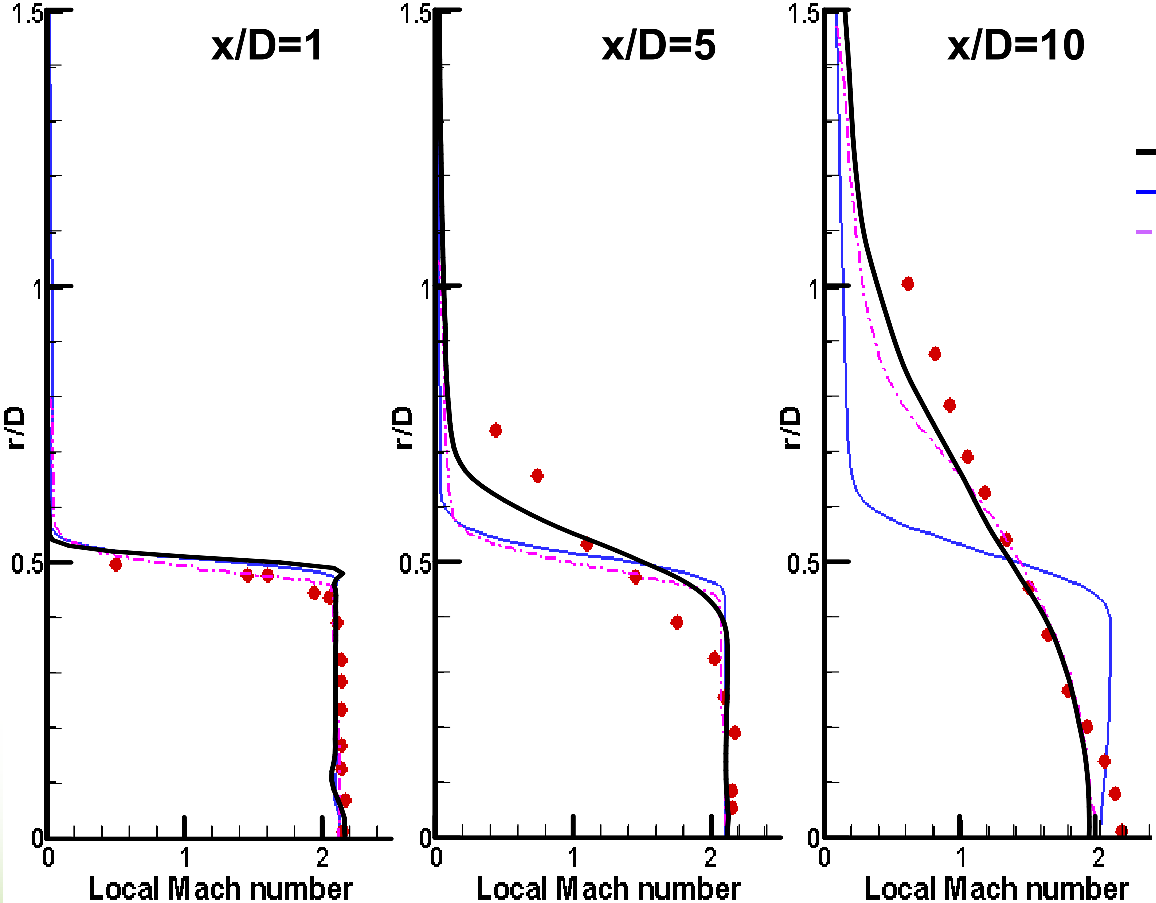

<Radial Mach number>

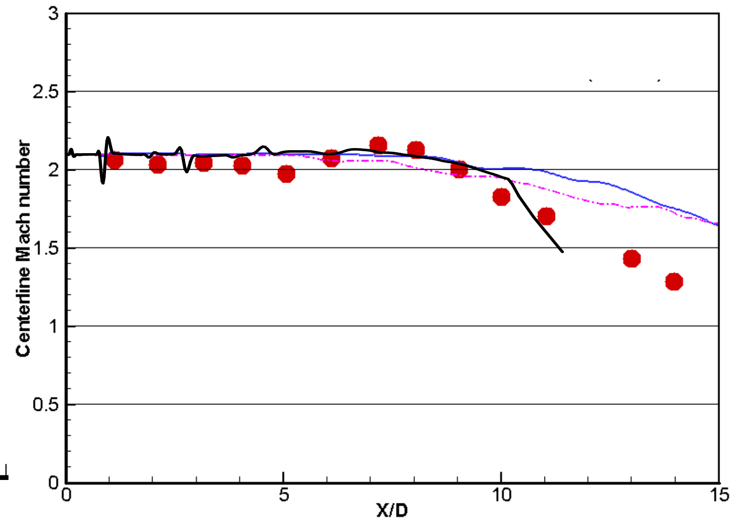

<Central Mach number>

AeroAcoustics Lab

Application

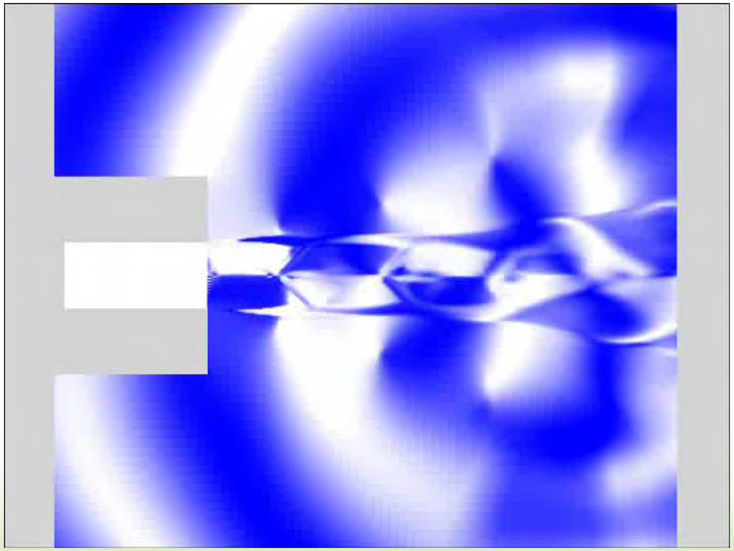

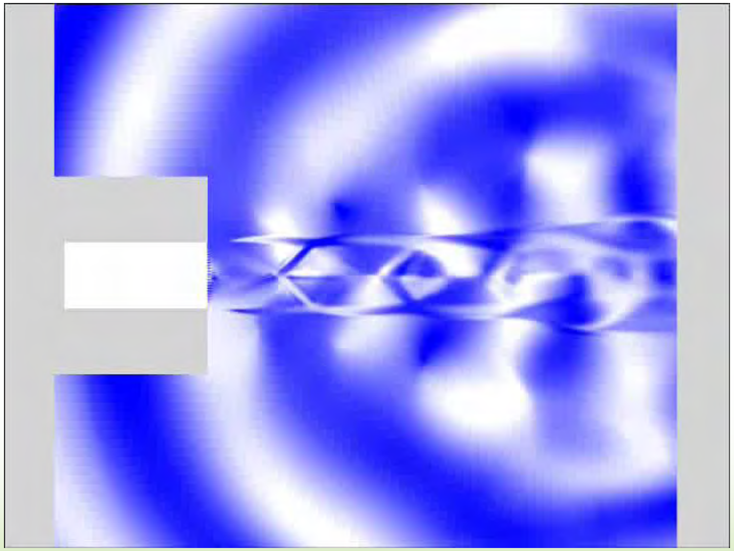

Naro Rocket

- Naro Rocket

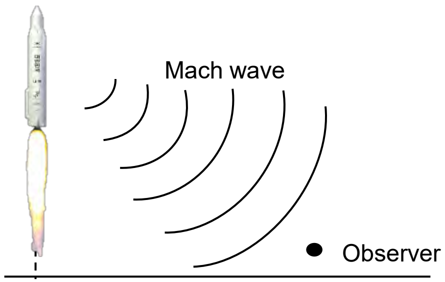

<나로 우주센터 발사장>

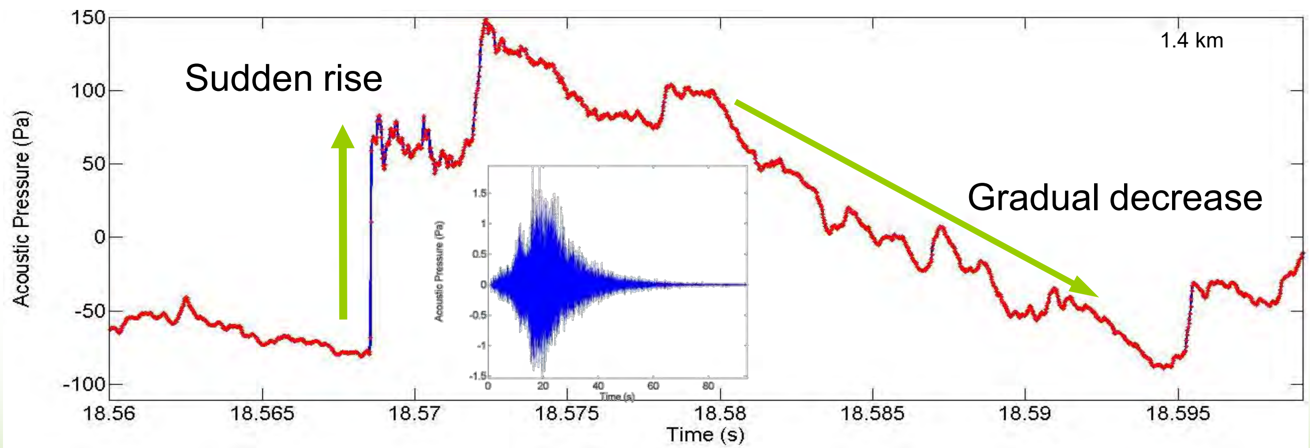

Jet Noise

- Naro Rocket Noise

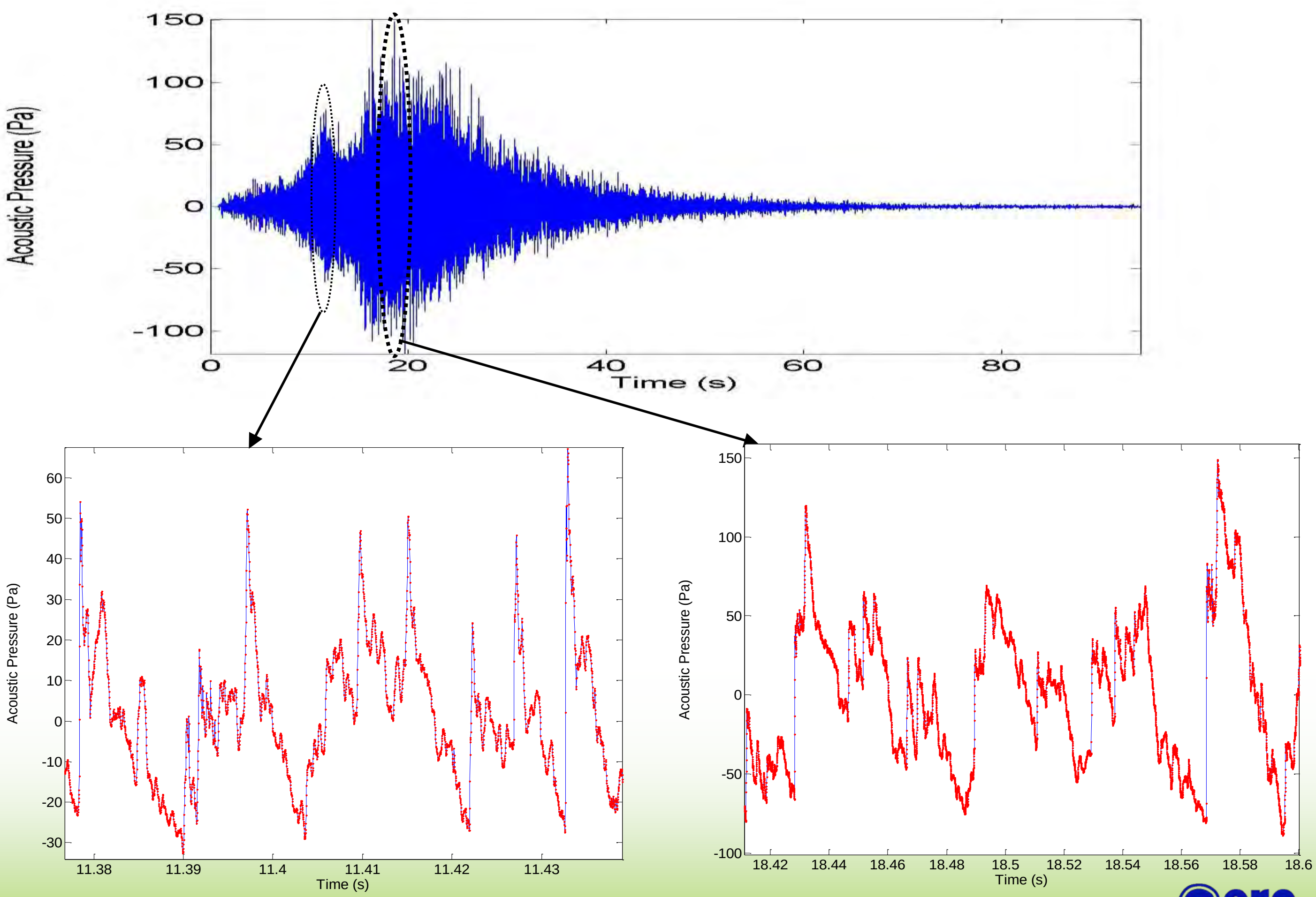

AeroAcoustics Lab

BVI Noise

Governing Equations
Optimized High Order Compact
Numerical Techniques

Blade Vortex Interaction

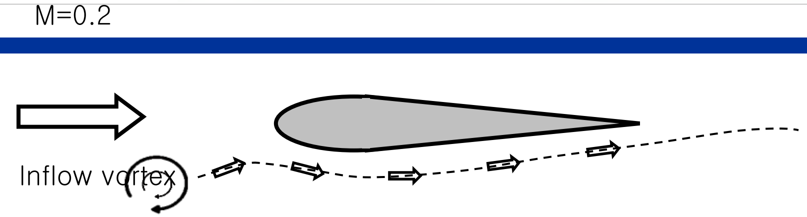

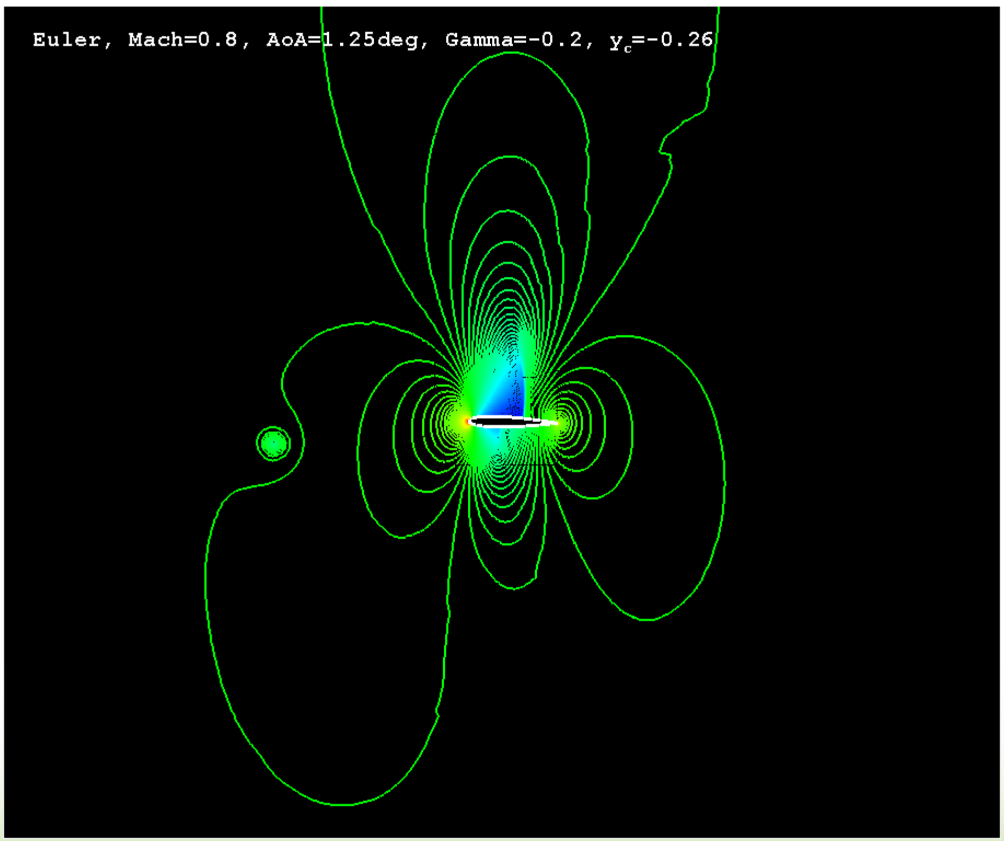

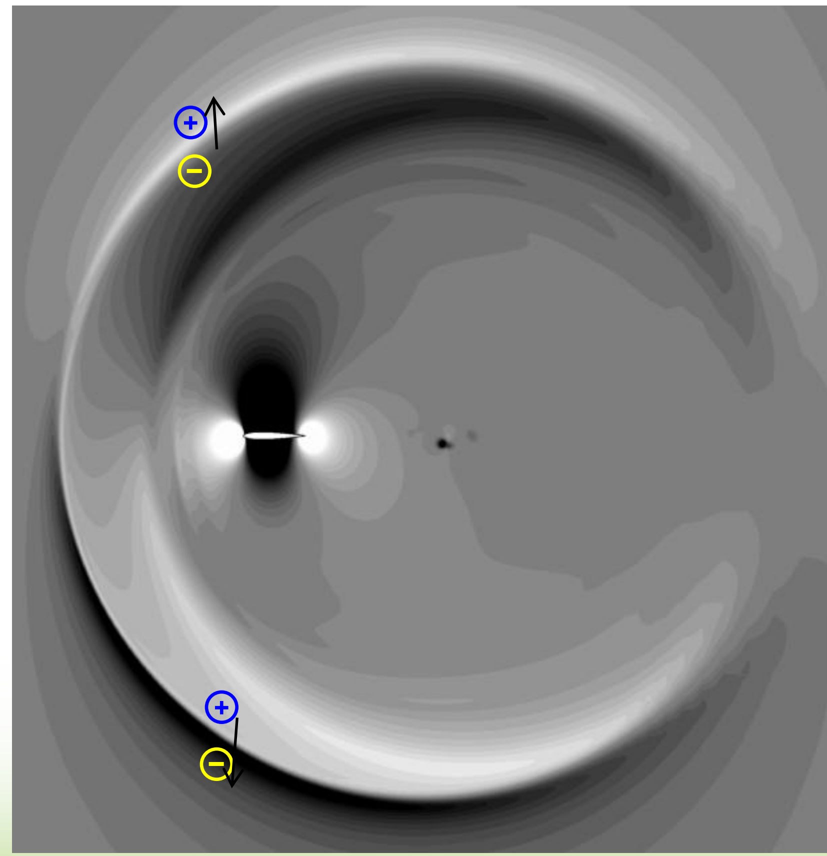

Simulation methods and validations

- Curle's Acoustic Analogy for Stationary Airfoil in a Uniform Flow

$$H(f)p'(\mathbf{x}) = -\oint_{f=0} F_i n_i \frac{\partial G(\mathbf{x};\xi)}{\partial \xi_i} dl - \int_{f>0} T_{ij} H(f) \frac{\partial^2 G(\mathbf{x};\xi)}{\partial \xi_i \partial \xi_j} d\xi$$

(Curle's equation)

dipole (loading) source :

$$F_i = p n_i$$

(surface pressure)

quadrupole source :

$$T_{ij} = \rho u_i' u_j' + (p - c_0^2 \rho)\delta_{ij}$$

← From FVM Simulation

(area Lighthill stress)

$$f = 0$$

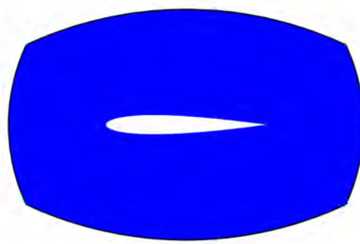

Artificial area truncation ~ 0.5 c

$$(f > 0)$$

- Implementation [Lockard, JSV 2000]

$$G(\mathbf{x};\xi) = \frac{i}{4\beta} \exp\left(\frac{ikM(x-\xi)}{\beta^2}\right) H_0^{(2)}\left(\frac{kR^*}{\beta^2}\right)$$

: Green function for 2D convective wave equation.

AeroAcoustics Lab

Simulation methods and validations

- Validation for BVI noise
  - ✓ Mach=0.5, y_v=-0.2

Pressure contour

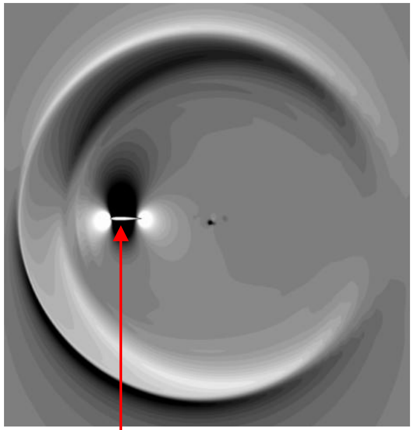

airfoil

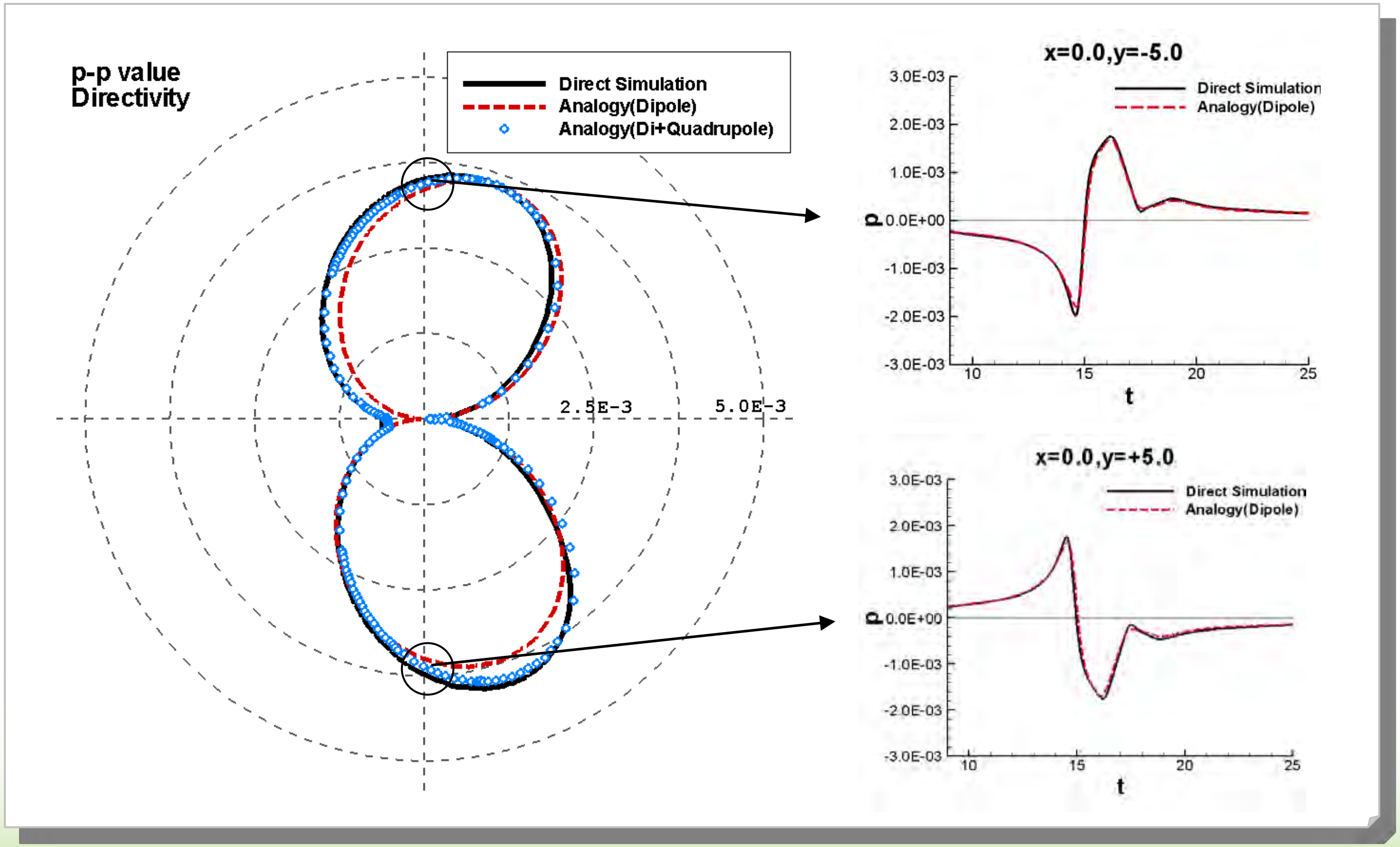

AeroAcoustics Lab

Whistle Noise

Governing Equations
Optimized High Order Compact
Numerical Techniques

Feedback Mechanism

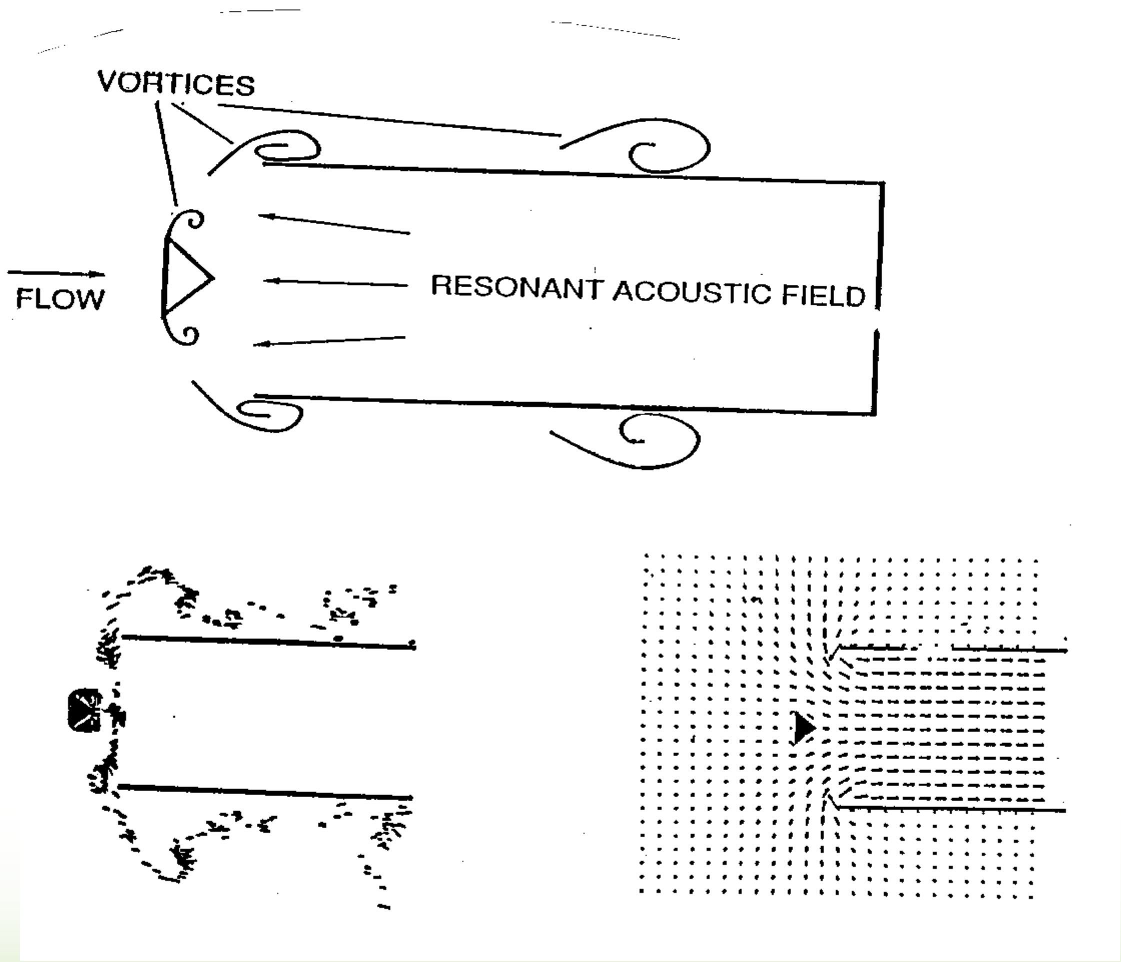

Acoustic Systems in Biology

- Sound production by vocal fold

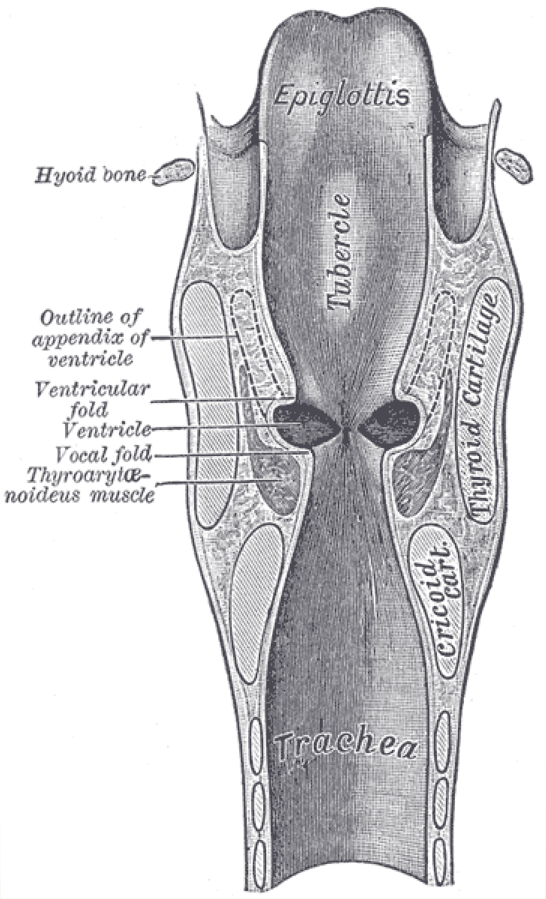

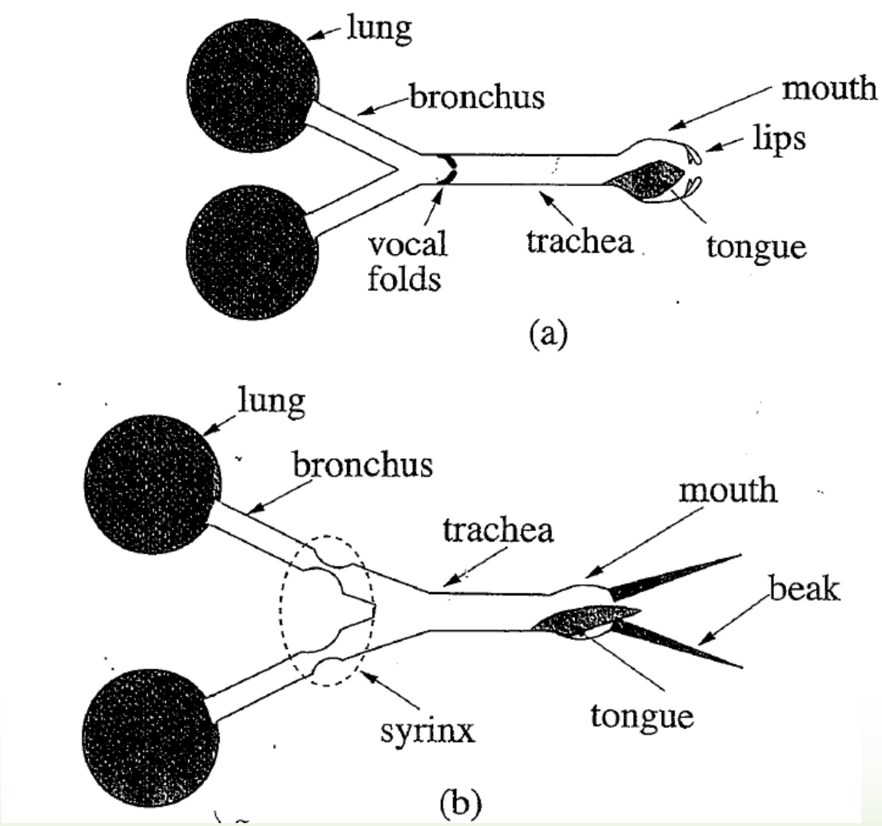

Laminar Whistle noise

- **Feedback Mechanism**

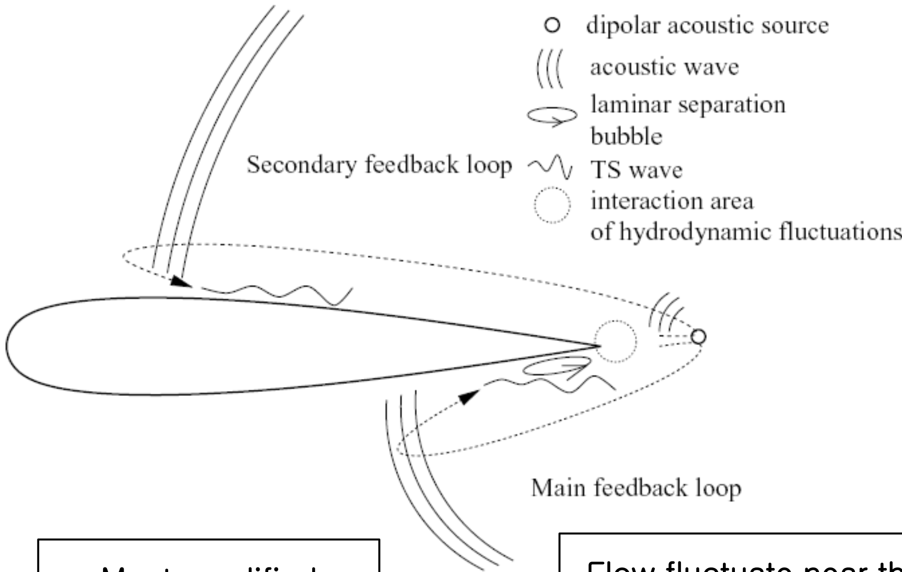

Numerical investigation of the tone noise mechanissm over laminar airfoil
G. Desquesnes et al.

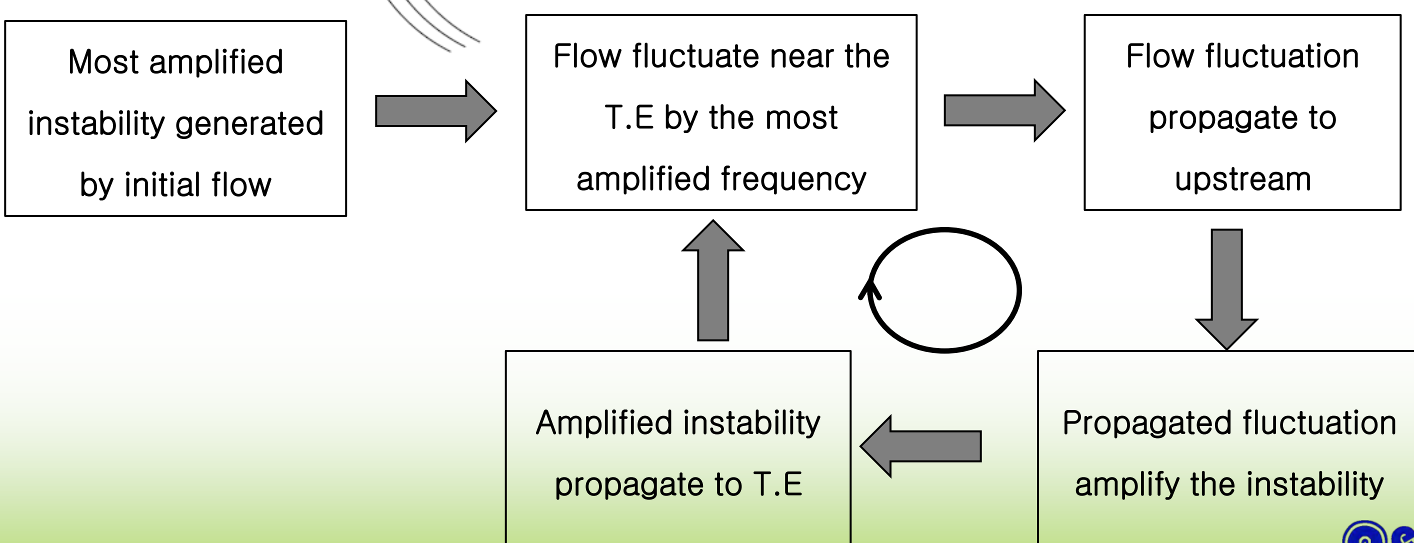

Laminar Whistle noise

- **Whistle noise on Laminar Airfoil**

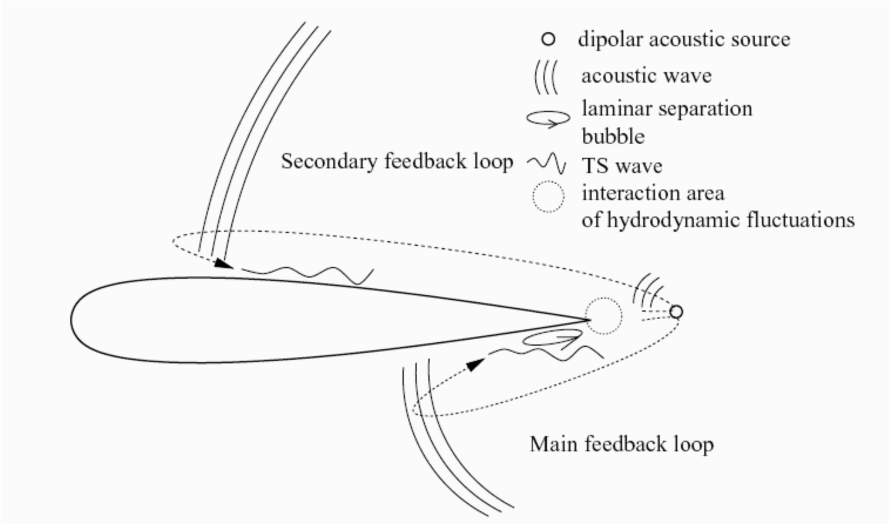

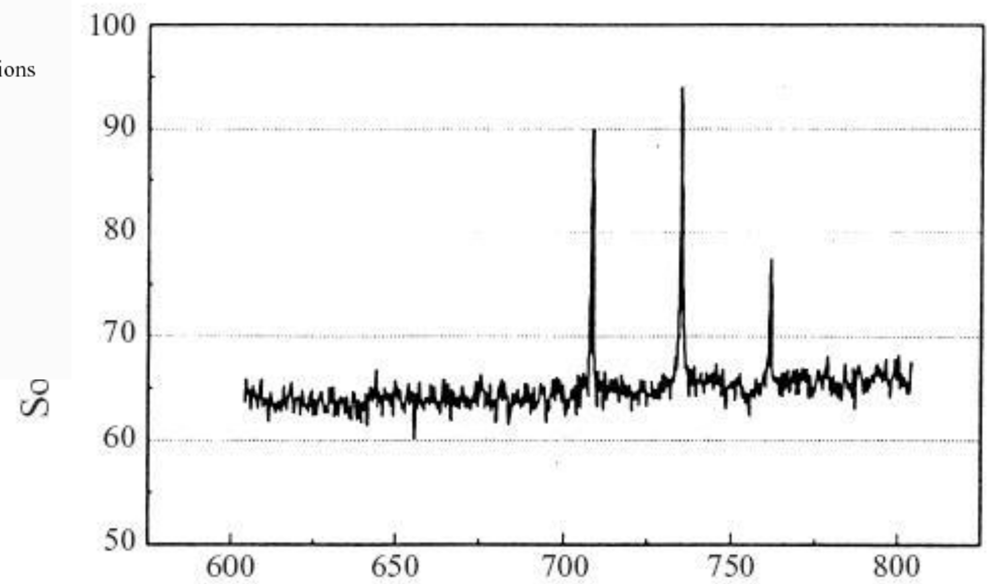

Sound spectrum for airfoil (Nash et al.)

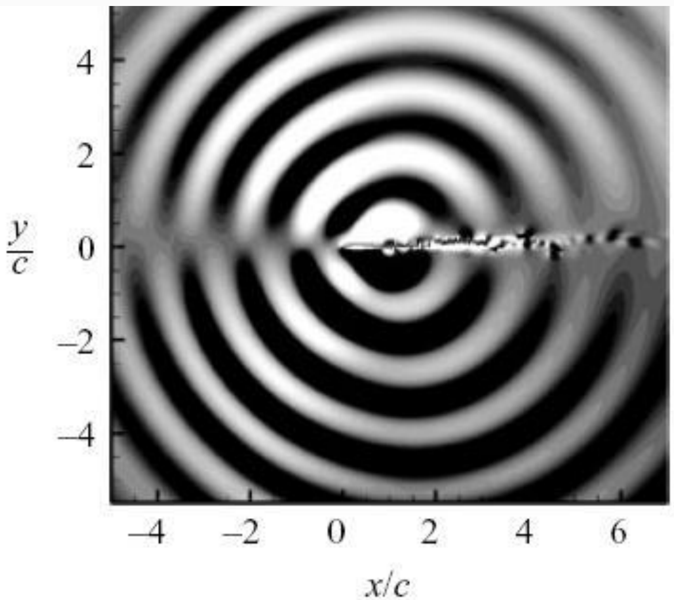

Pressure contour for airfoil (Desquesnes et al.)

Laminar Whistle Noise : Airfoil

• **Change of whistle noise as flow velocity change**

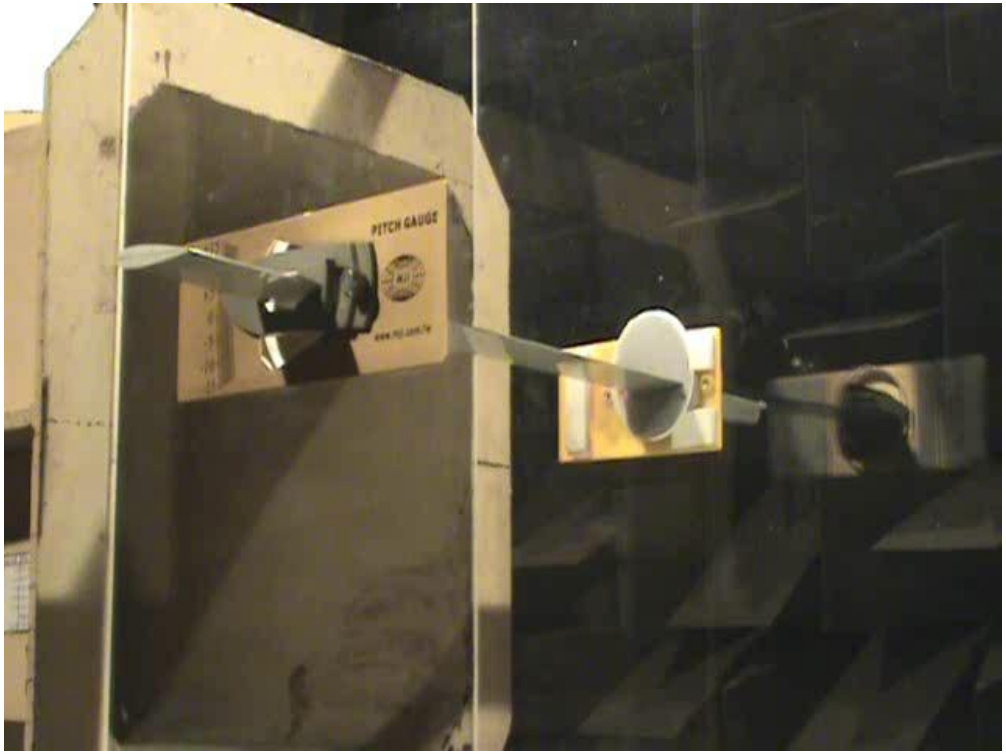

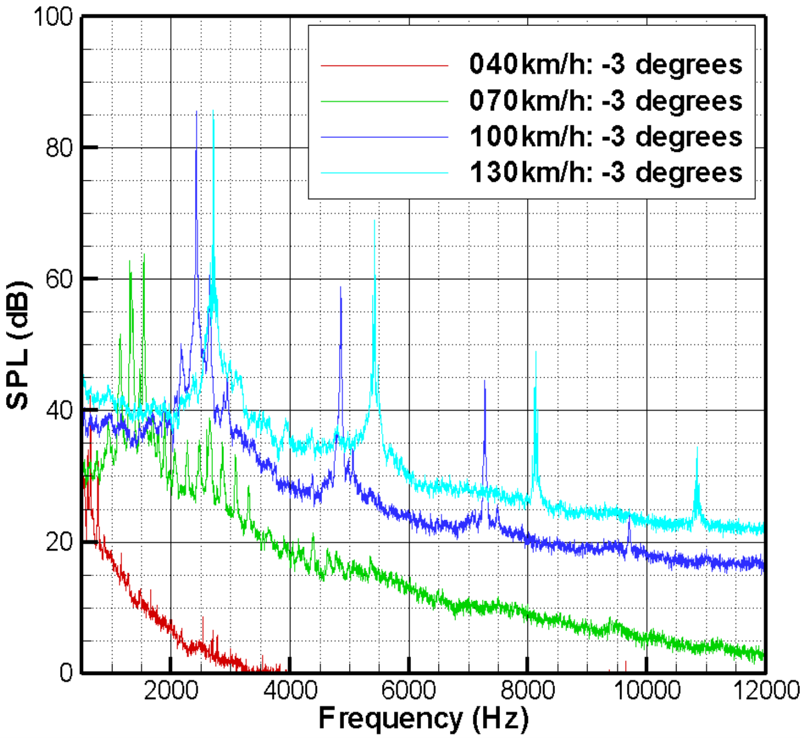

Inflow velocity : 0 → 130km/h

AeroAcoustics Lab

Acoustic Systems in Biology

- Silent Flight of Owl

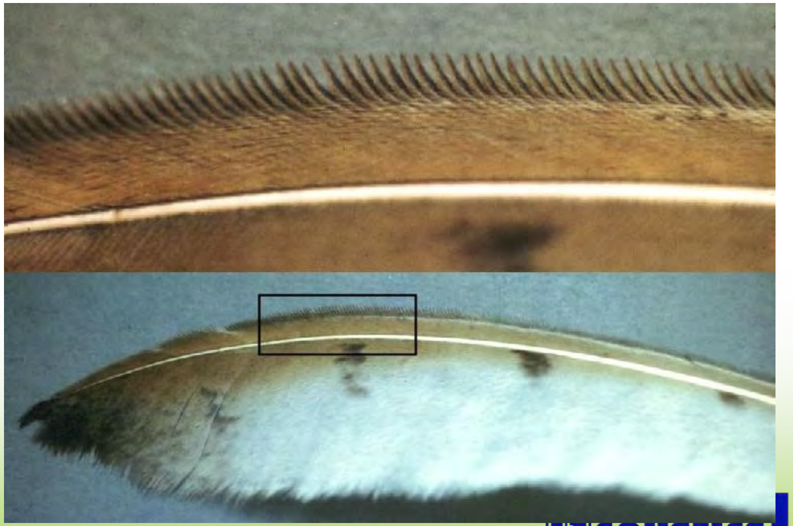

Laminar Whistle Noise : Car Side Mirror

- Whistle noise

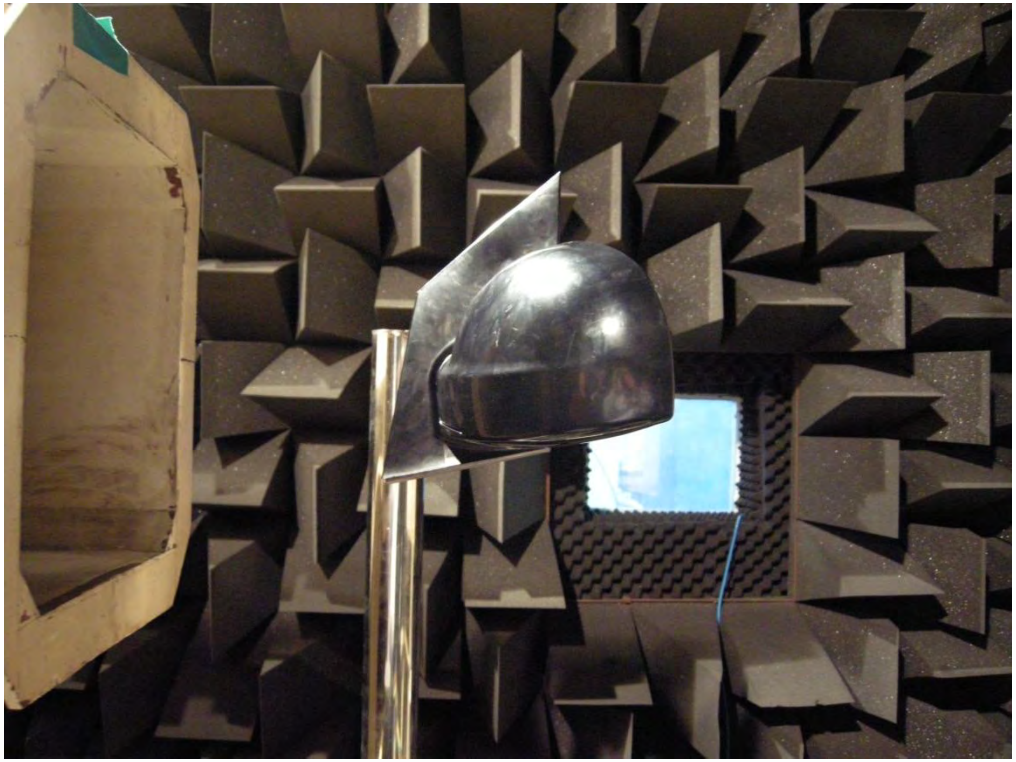

Real auto-vehicle side-mirror

Simplified side-mirror

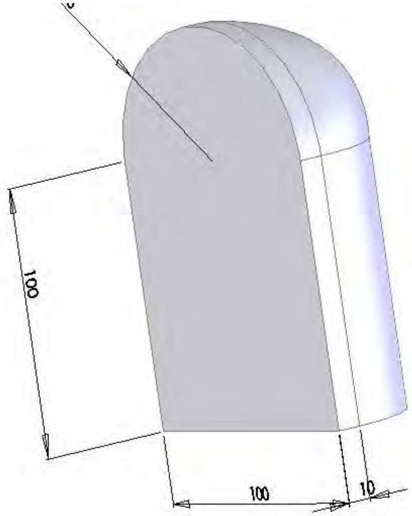

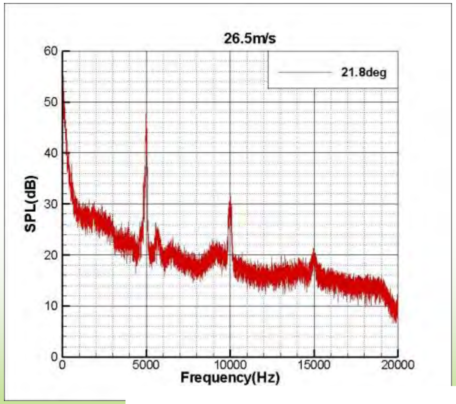

Noise spectrum

How people in science see each other

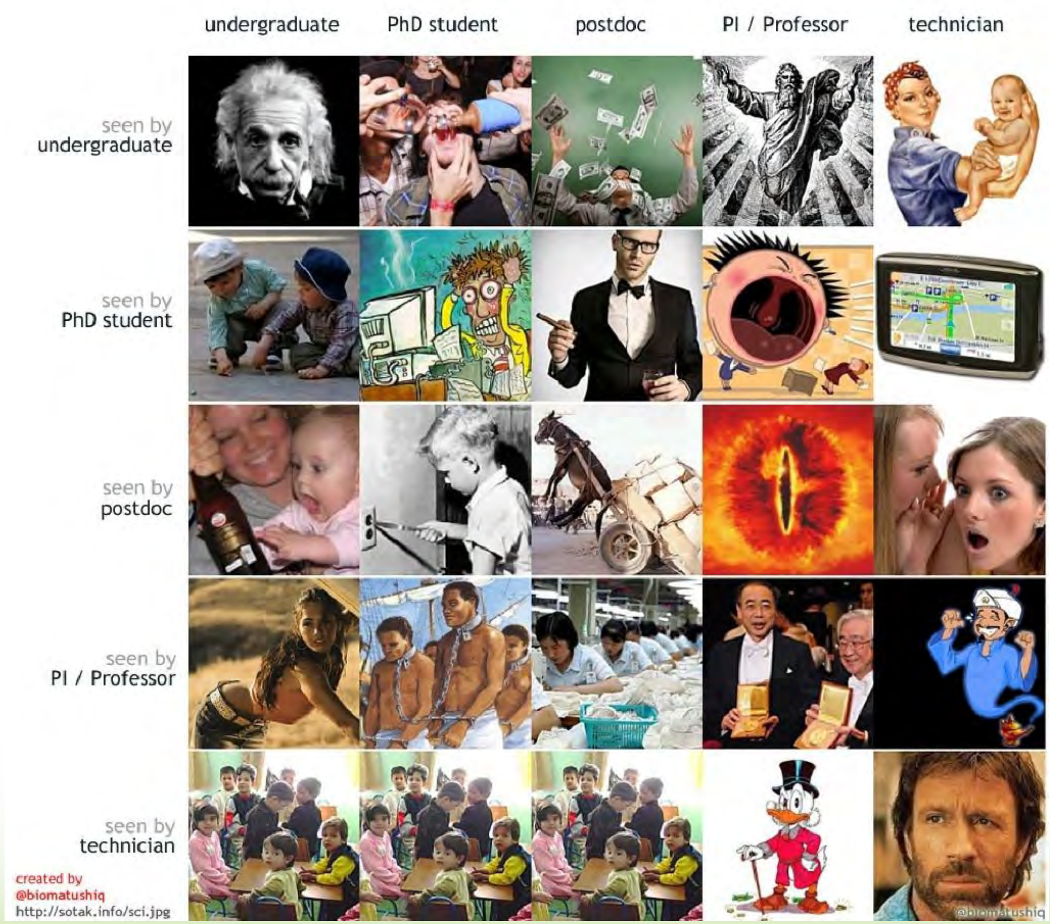

Acoustic –Flow Feed back

Locking Flow

- Example of flow locking

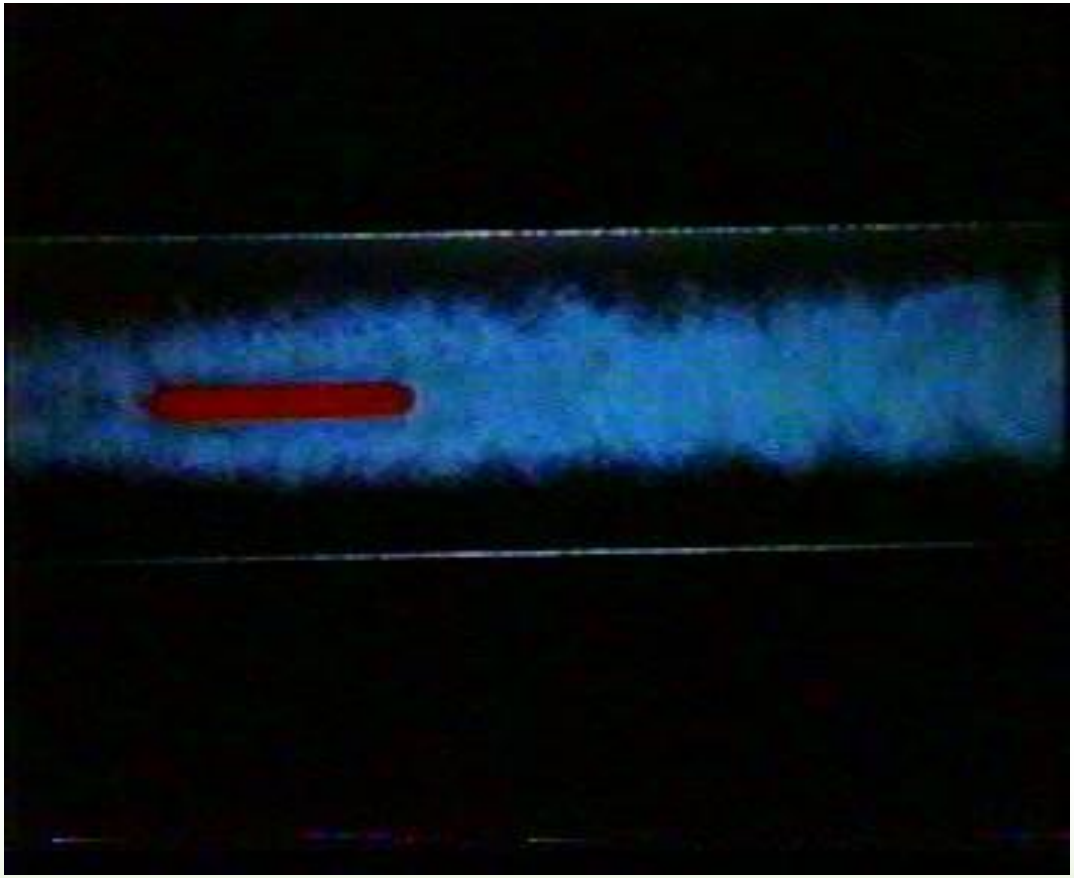

@ http://www.mae.cornell.edu/IJFD/1997_vol1/paper1/Parker.Flow.html

Locking Flow

- Analysis of locking flow
  - ✓ Resonance mode: Parker, 1967
  - ✓ Simple model: Welsh, 1984
  - ✓ Acoustic mode + flow: Stoneman, 1988

- A body in a duct

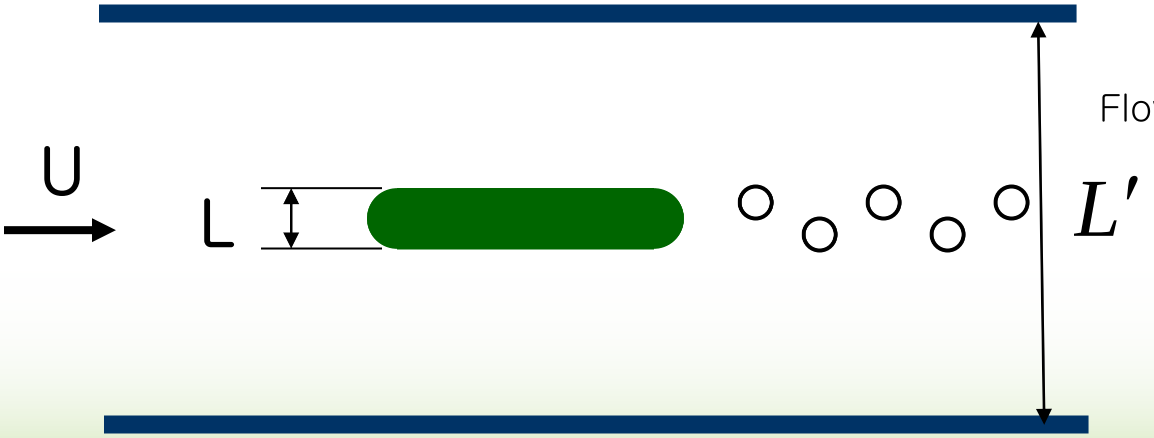

$$S_f = \frac{fL}{U}$$

Flow Strouhal No.

$$S_a = \frac{fL'}{a}$$

Acoustic Strouhal No.

U: flow velocity

a : acoustic speed

L : flow characteristic length

L' : acoustic characteristic length

Locking Flow

- Locking flow vs. unlocking flow
  - ✓ Pressure contour

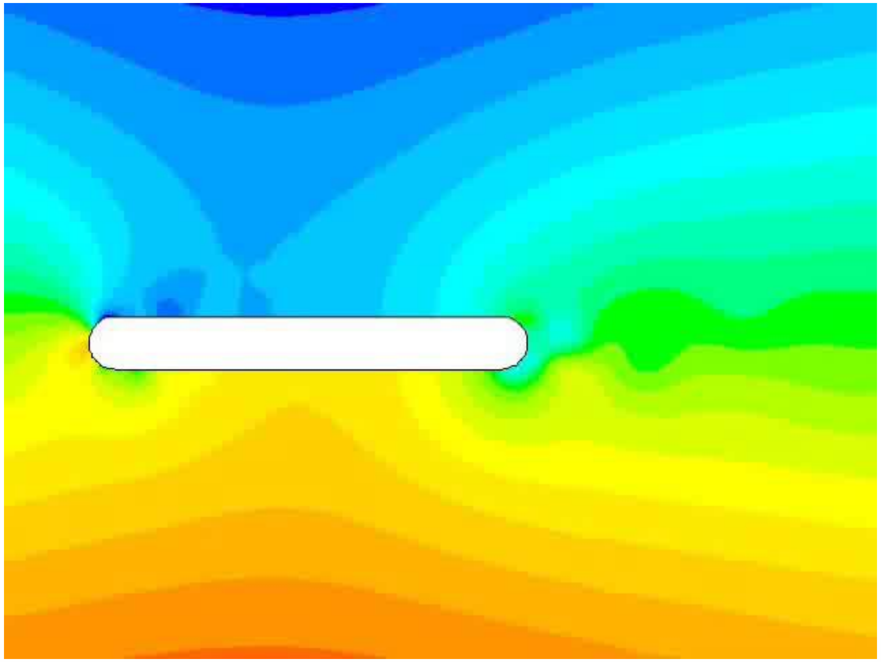

<Flow acoustic locking>

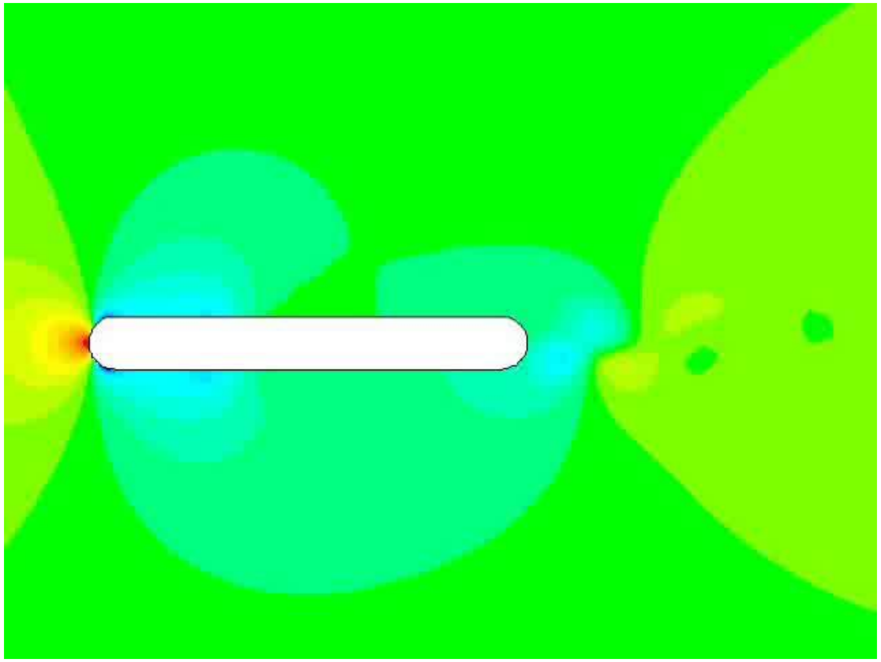

<Flow unlocking>

Applications of the developed numerical method

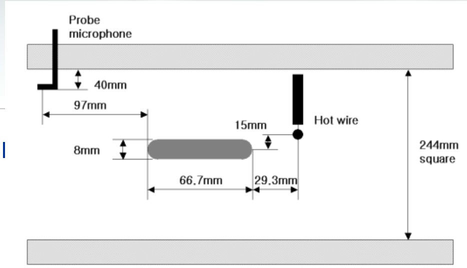

S.A.T. Stoneman, K. Hourigan, A.N. Stokes and M.C. Welsh “Resonant sound caused by flow past two plates in tandem in a duct”, J. Fluid Mech.(1988) Vol. 192, pp. 455-484

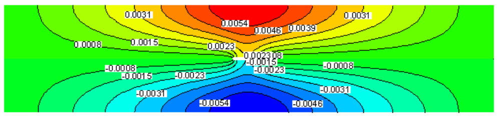

Resonance frequency 686 Hz

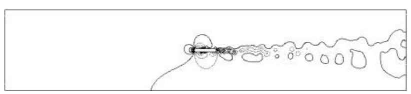

pressure contours

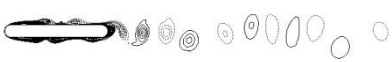

vorticity contours

Unlocked flow

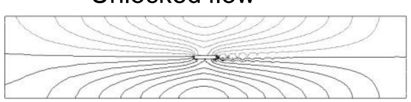

Acoustic resonant flow(locked flow)

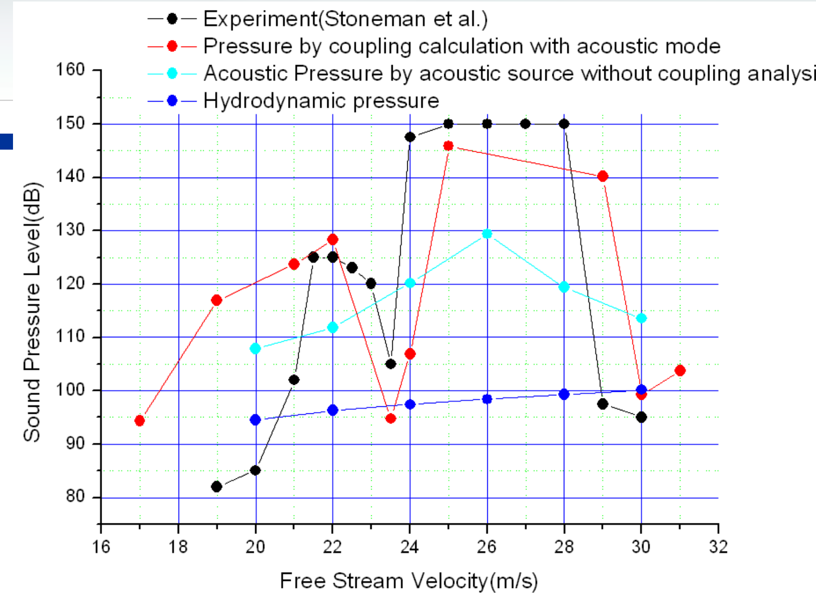

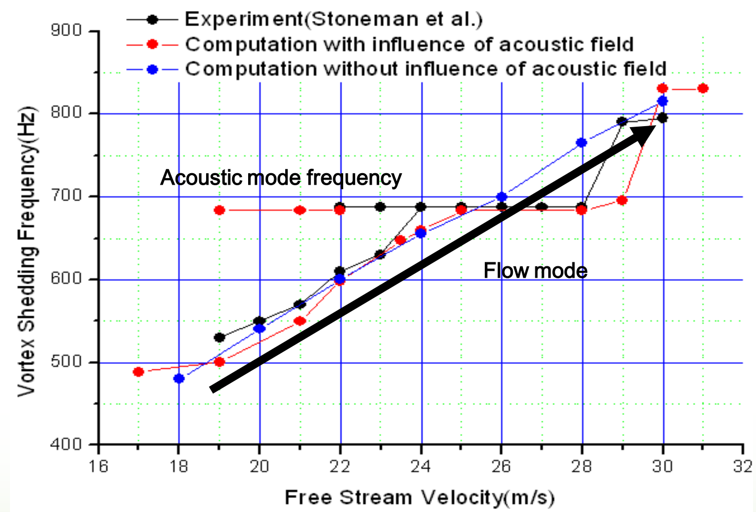

- Beat tones from the natural vortex shedding and acoustic resonant frequencies before the resonance flow
- Single vortex shedding frequency in the region of resonance flow
- Recover to natural incompressible flow after the resonance flow

AeroAcoustics Lab

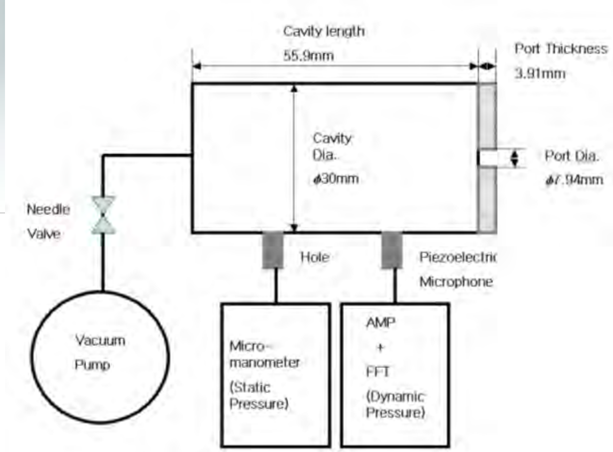

n in an
997,

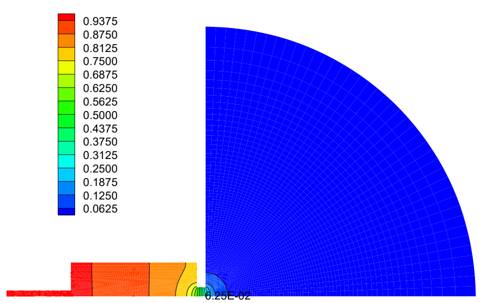

Resonance frequency=580Hz

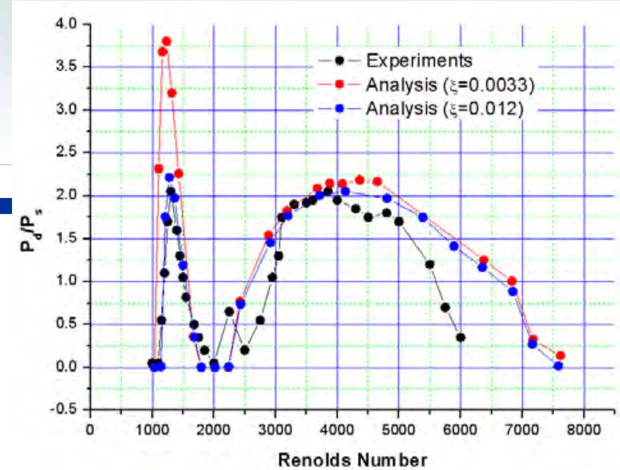

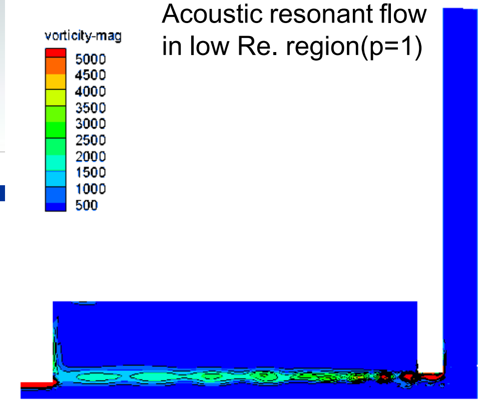

Acoustic resonant flow in low Re. region(p=1)

vorticity contours

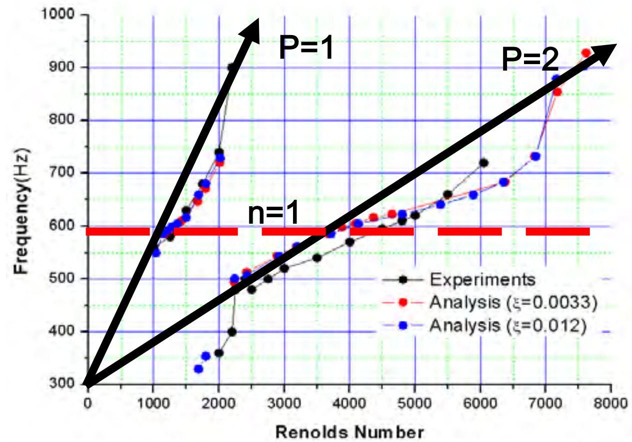

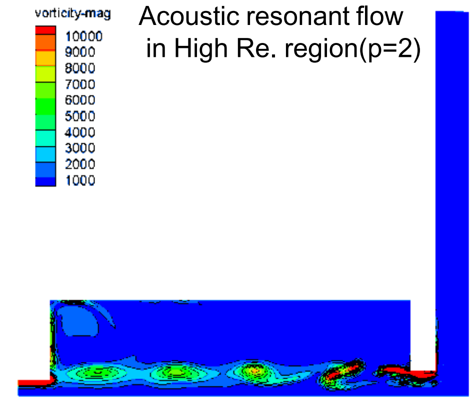

Acoustic resonant flow in High Re. region(p=2)

vorticity contours

- Two resonance regions depending on the suction velocities ranges
- Each of the resonant regions shows the different flow and vortex patterns
- Increase of the resonance frequencies according to the suction velocity
  - ✓ Aeroacoustic sources can generate the acoustic energy, as well as modify the resonance frequencies.

Incompressible Flow-Acoustic Feedback

- Special treatment
  - ✓ Governing equation
  - ✓ Numerical formulation (extension of Stoneman's formulation (1988))

- continuity equation $\nabla \cdot \vec{v} = S$ where $S = \frac{1}{\rho}\frac{D\rho}{Dt} \approx \frac{1}{\rho}\frac{\partial \rho}{\partial t}$

$$\rho(x, y, z, t) = A(t)\Phi(x, y, z)$$

- acoustic mode $k^2\Phi + \nabla^2\Phi = 0$ where $k = 2\pi f$

$$\rho - \rho_0 = \sum_m A_m \Phi_m$$

$$\sum_m \dot{A}_m \Phi_m + \rho_0 \nabla \cdot \tilde{u} = 0$$

$$\rho_0\left[\tilde{u}_t + (\tilde{u} \cdot \nabla)\tilde{u}\right] + \nabla p = \mu \nabla^2 \tilde{u}$$

Vortex Sound ;Howe

From the momentum equation,

$$\frac{\partial \mathbf{v}}{\partial t} + (\mathbf{v}\cdot\nabla)\mathbf{v} + \frac{1}{\rho}\nabla P = \nu\left(\nabla^2\mathbf{v} + \frac{1}{3}\nabla(\nabla\cdot\mathbf{v})\right) \quad \text{- - - (1)}$$

$$\frac{1}{\rho}\nabla P = \nabla\left(\int\frac{dP}{\rho}\right)$$

$$\nabla\times\boldsymbol{\omega} = \nabla\times\nabla\times\mathbf{v} = \nabla(\nabla\cdot\mathbf{v}) - \nabla^2\mathbf{v}$$

$$(\mathbf{v}\cdot\nabla)\mathbf{v} = \boldsymbol{\omega}\times\mathbf{v} + \nabla\left(\frac{1}{2}v^2\right)$$

Crocco's equation

$$\frac{\partial \mathbf{v}}{\partial t} + \boldsymbol{\omega}\times\mathbf{v} + \nabla B = -\nu\left(\nabla\times\boldsymbol{\omega} - \frac{4}{3}\nabla(\nabla\cdot\mathbf{v})\right) \quad \text{- - - (2)}$$

Incompressible

where $B = \int\frac{dP}{\rho} + \frac{1}{2}v^2$

AeroAcoustics Lab

Integral Solution for Boundary

Finally the integral solution is given as

$$B(\mathbf{x},t) = \oint_{S+} \left(B\nabla G + G\frac{\partial \mathbf{v}}{\partial \tau} \right) \cdot d\mathbf{S} - \int_V H\,(\boldsymbol{\omega} \times \mathbf{v}) \cdot \nabla G\, d^3 y$$

$$+ \nu \oint_{S+} \left(\boldsymbol{\omega} \times \nabla G \right) \cdot d\mathbf{S}$$

AeroAcoustics Lab

Vortex Sound in f resonant flows

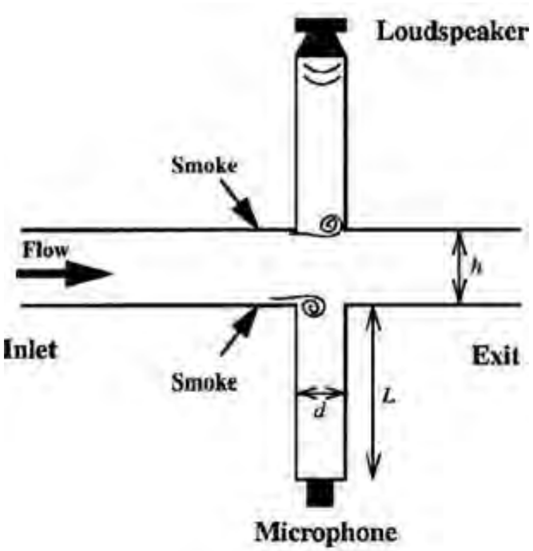

Quarter-wave resonator

Hydrodynamic mode

Vortex shedding at branch edge

First mode, $p = 1$

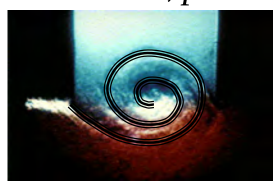

Second mode, $p = 2$

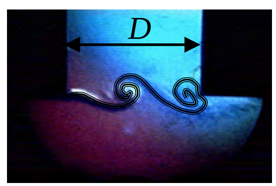

$$f_p = \frac{U_0}{D} \cdot \mathrm{St}_p$$

Acoustic modes

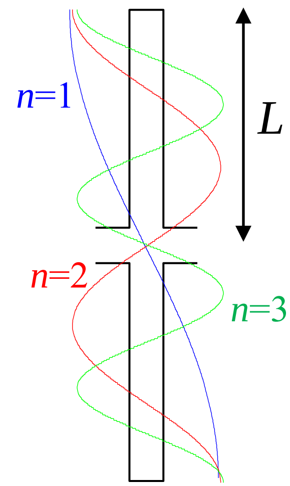

$$f_n = \frac{c}{L} \cdot \frac{2n-1}{4}$$

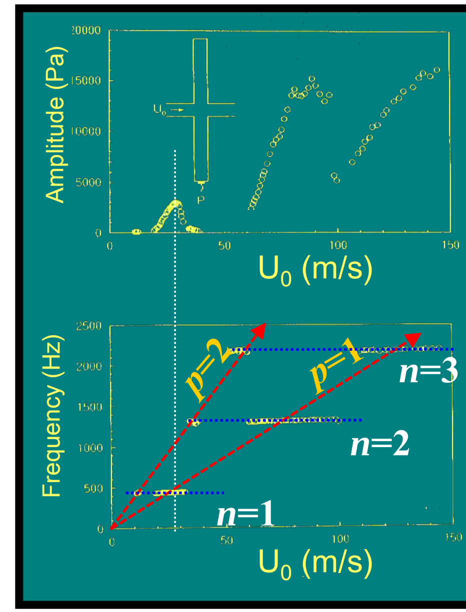

- Compressible effects are only come from acoustic resonance phenomena.
- Acoustic resonance is defined by the geometries of system.
- Unsteady incompressible flow analysis is faster and lighter than compressible flow analysis and can accurately capture the aeroacoustic sources.
- The strong points of unsteady incompressible flow analysis and acoustic modes can be combined.

Aero Acoustics Lab

Previous studies for acoustic resonant flows

Continuity Equation

$$\rho_0 \nabla \cdot \tilde{u} = 0$$

Momentum Equation

$$\rho_0 \left[\frac{\partial \tilde{u}}{\partial t} + (\tilde{u}\cdot\nabla)\tilde{u} \right] + \nabla p = \mu \nabla^2 \tilde{u}$$

- Using the results of mode analysis
- Fixed acoustic resonant frequency
- Acoustic excitation on boundary zones
- Neglecting the feedback effects from flows
- Parametric case studies according to acoustic velocity
- 1 way coupled method

$$v_b = v(x)\sin(2\pi f t)$$

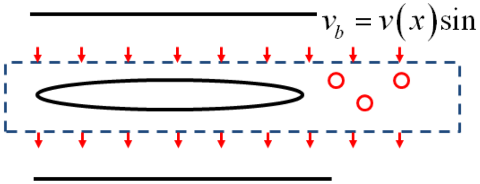

S.A.T. Stoneman, K. Hourigan, A.N. Stokes and M.C. Welsh "Resonant sound caused by flow past two plates in tandem in a duct", J. Fluid Mech.(1988) Vol. 192, pp. 455-484

B. T. Tan, M. C. Thompson, K. Hourigan "Flow past rectangular cylinders: receptivity to transverse forcing", J. Fluid Mech.(2004),Vol. 515, pp. 33-62

Hemant, K. Chaurasia, Mark C. Thompson, "Three-dimensional instabilities in the boundary-layer flow over a long rectangular plate", J. Fluid Mech.(2011),Vol. 681, pp. 411-433

This study

Continuity Equation

$$\rho_0 \nabla \cdot \tilde{u} = -\sum_m \dot{A}_m \Phi_m$$

Before starting flow analysis

Momentum Equation

$$\rho_0 \left[\frac{\partial \tilde{u}}{\partial t} + (\tilde{u}\cdot\nabla)\tilde{u} \right] + \nabla p = \mu \nabla^2 \tilde{u}$$

2nd order ordinary differential Equation

for the nth coefficients of the acoustic modes

$$\begin{aligned}\ddot{A}_n + \nu k_n^2 \dot{A}_n + \omega_n^2 A_n = \Bigg[& -\rho_0 \int \nabla\Phi_n \cdot (\tilde{\omega}\times\tilde{u})\, dV \quad \text{Volume source} \\ & - \int \left(p + \frac{\rho_0 u^2}{2} \right) \frac{\partial \Phi_n}{\partial n}\, dS \quad \text{Acoustic radiation} \\ & - \rho_0 \frac{d}{dt} \int \Phi_n \tilde{u}\cdot\tilde{n}\, dS \Bigg] \frac{1}{\int \Phi_n^2\, dV} \quad \text{wall vibration}\end{aligned}$$

The Eigen value problem of Helmholtz equation

$$k_m^2 \Phi_m + \nabla^2 \Phi_m = 0$$

$$\Phi_m \big|_{far} = 0 \qquad \frac{\partial \Phi_m}{\partial n}\bigg|_{wall} = 0$$

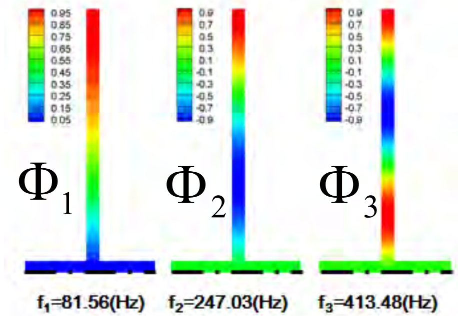

Acoustic modes

Quarter-wave resonator example

The strong points of the developed numerical method

- The magnitude and frequency of acoustic fields are defined by aerodynamic acoustic sources.
- Computational time can be reduced by using the ordinary differential equations and incompressible flow solver.
- Wall vibrations conditions and acoustic radiations loss can be considered by the surface integral terms of ordinary differential equations

AeroAcoustics Lab

Acoustic Liner

Governing Equations
Optimized High Order Compact
Numerical Techniques

Acoustic Liner

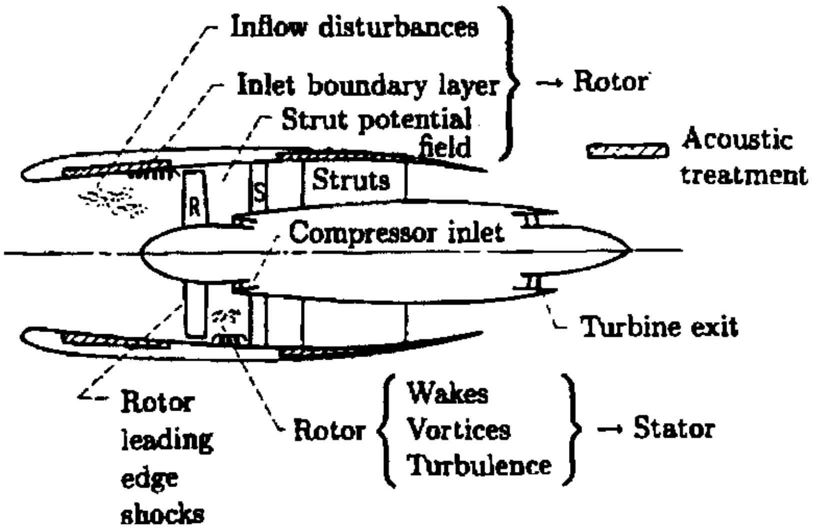

Perforated Liner (Resonator Array)

Noise of a typical aero-engine (turbofan)

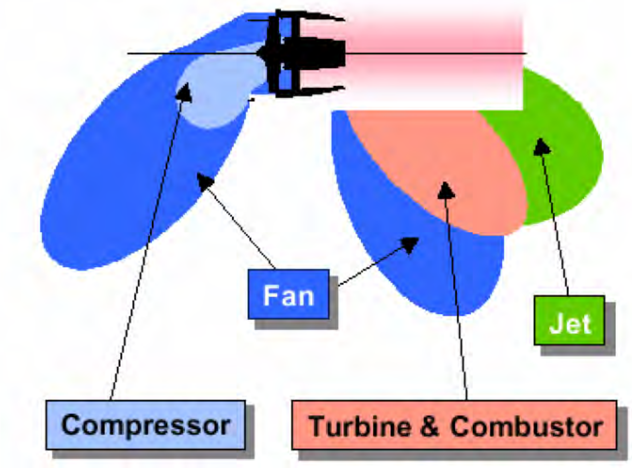

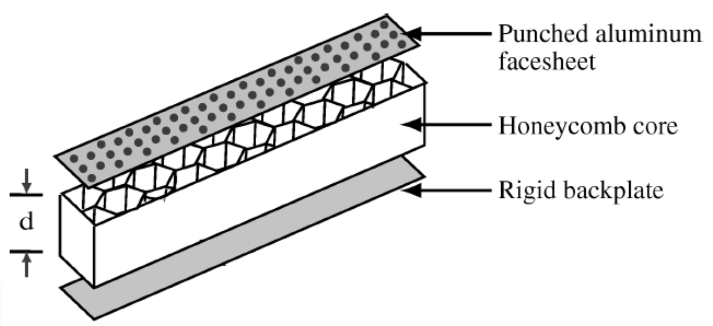

Perforate Liner
(Helmholtz resonator type)

Acoustic Liner
installed in Turbofan Engine Nacelle

Perforated Liner (Resonator Array)

- CAA simulation of Helmholtz Resonator
  - ✓ Experimental Data : Measurement of single Helmholtz resonator by Hersh-Walker

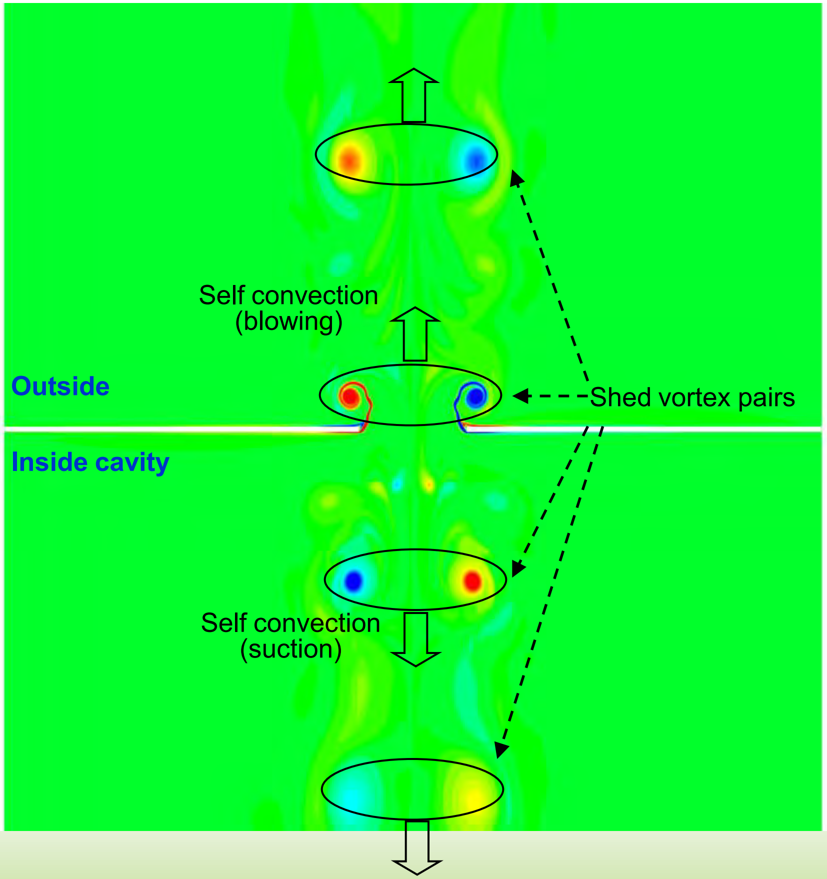

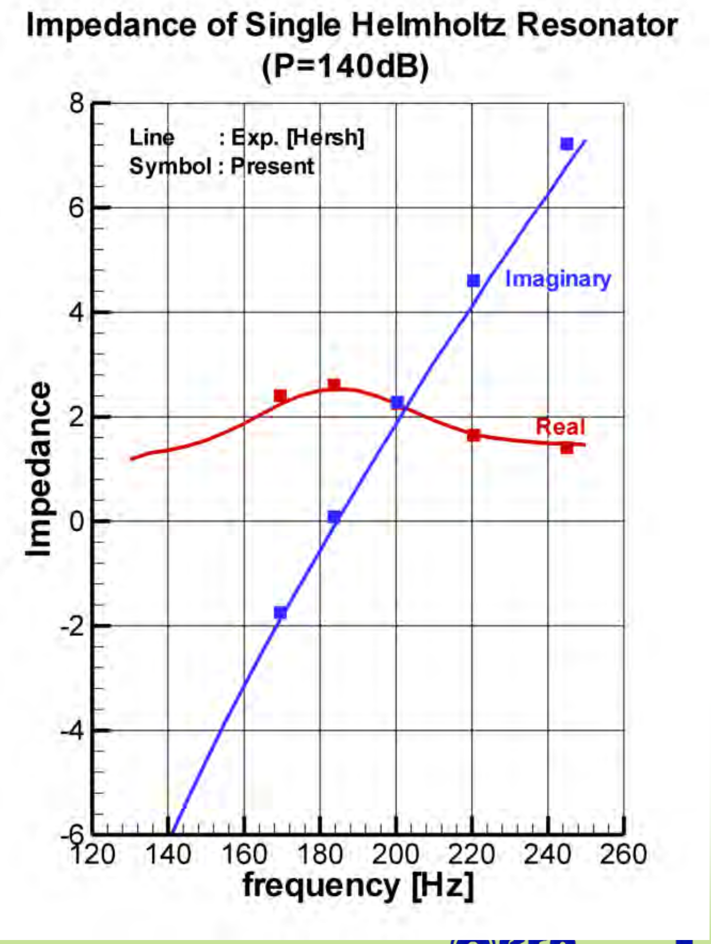

Jet Noise

- Nonlinear Impedance at Acoustic Liner
  - ✓ Property : Acoustic Impedance

$$Z = p'/v_n = R + i\,X$$

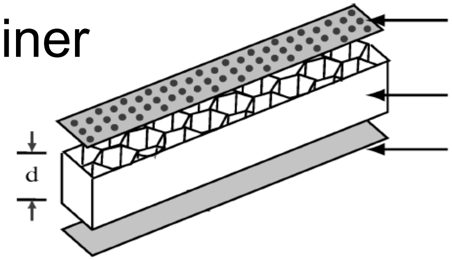

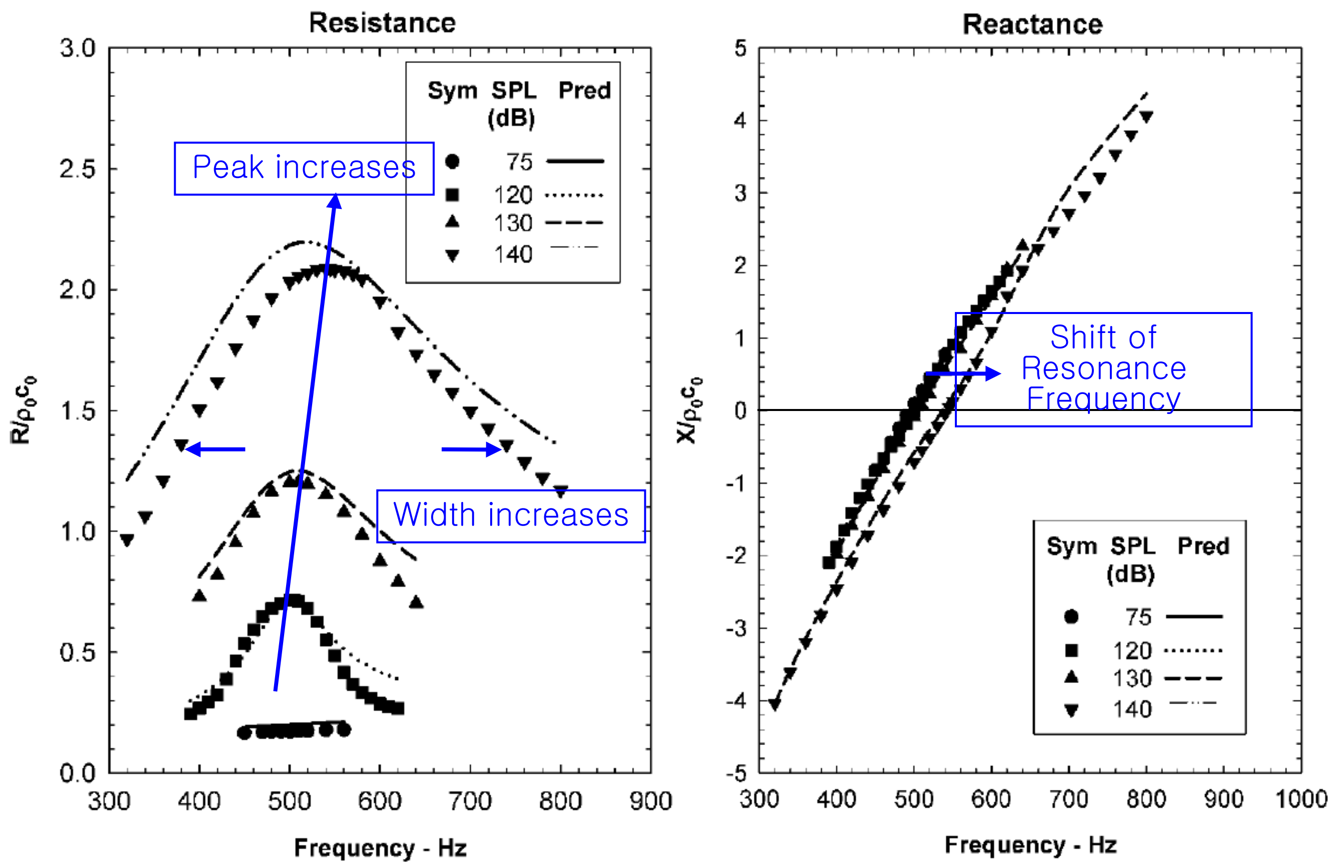

Jet Noise

- Tubular Liner
  - ✓ Single hole simulation of NASA CT-57 liner
    - Experimental data : NASA grazing impedance tube
    - Theory : Zwikker-Kosten narrow tube

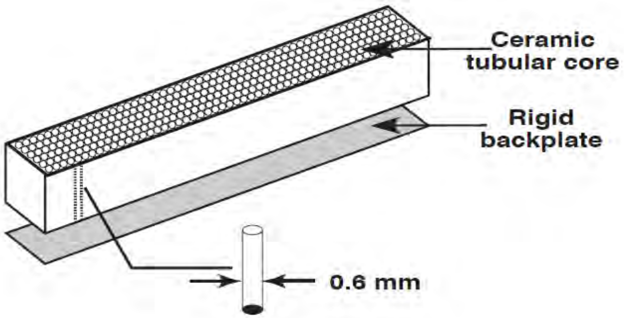

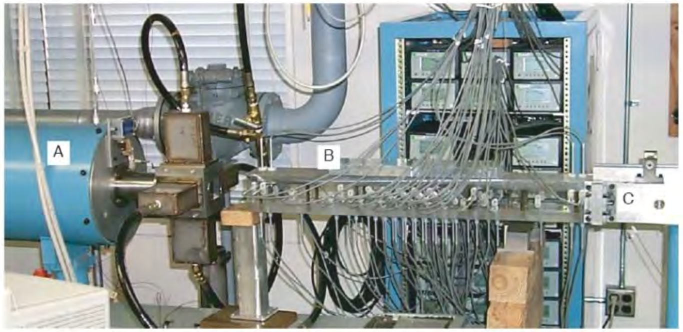

A. Air source plenum B. Top-mounted liner fixture C. Termination

Real term

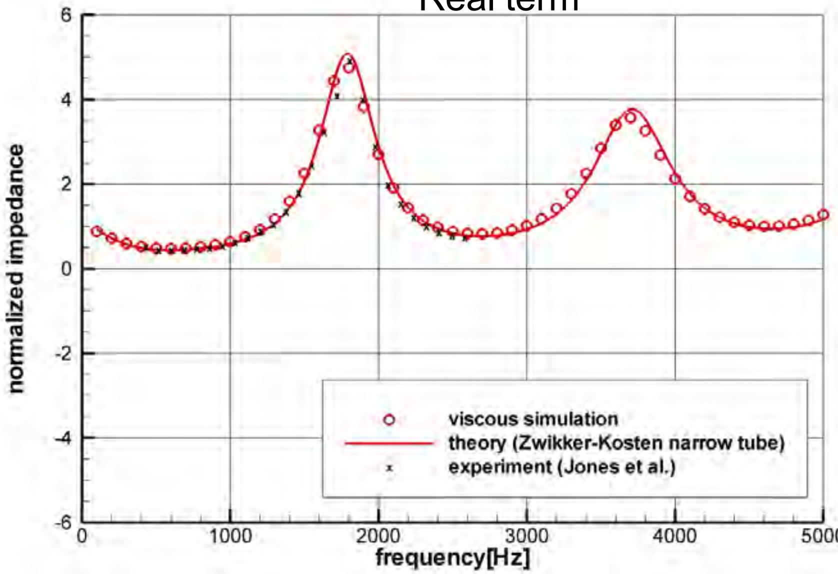

Imaginary term

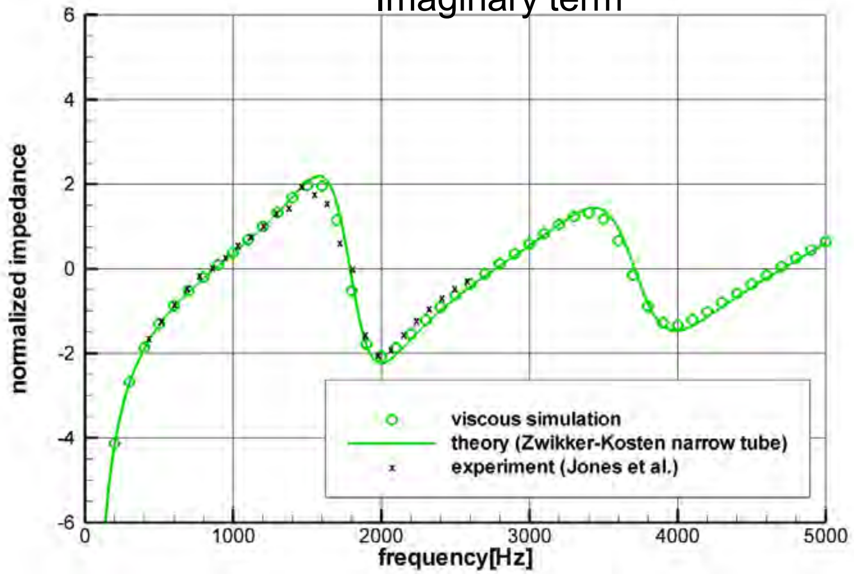

Acoustic Liner

- Nonlinear Propagation

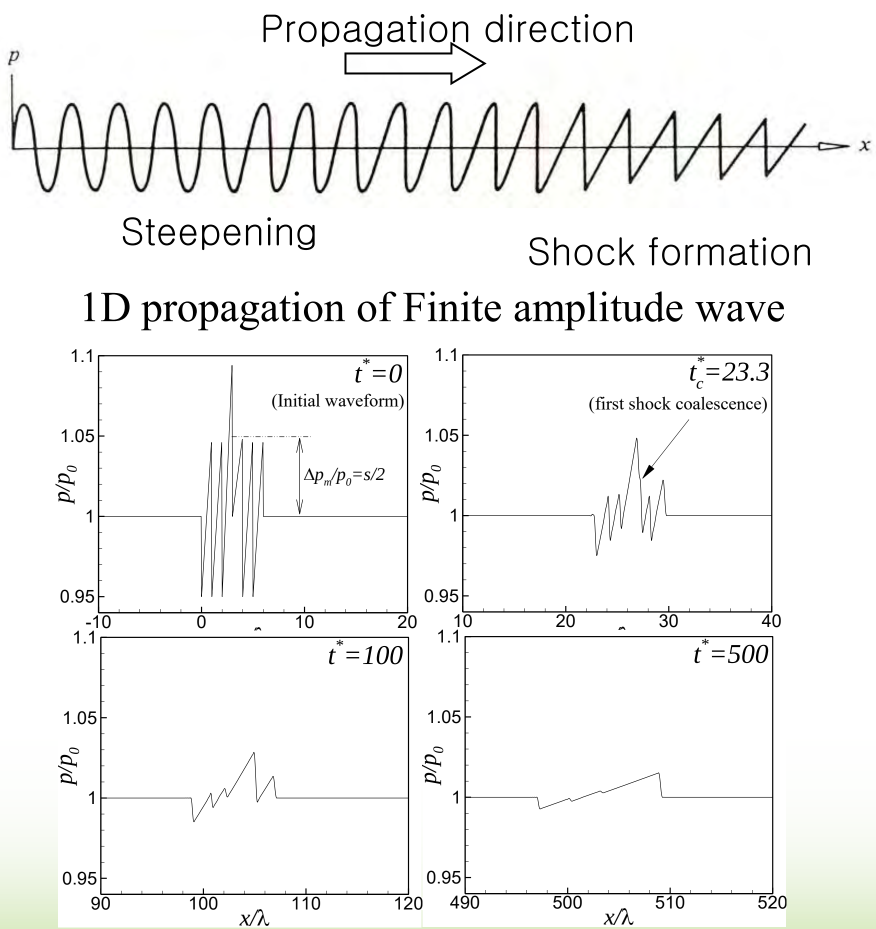

Sonic boom propagation [Shim, Lee AIAA2001]

Acoustic Liner

- Impedance Boundary Condition for Locally Reacting Liner
  - ✓ TDIBC implementation methods

$$Z(\omega) = v(\omega) / p(\omega)$$

	Frequency-domain impedance model	Time-domain conversion	Imposing boundary condition
Tam et al. (AIAA 1996)	narrow band (spring-mass-damper)	numerical integral/derivative	coupling of LEE and impedance equation
Ozyoruk et al. (JCP 1998)	broadband model for CT liner	z-transform approximation	coupling of LEE and impedance equation
Fung et al. (AIAA 2000,2001)	several broadband models	modified numerical convolution integral	characteristic approach

Not suitable for multi freq. simulation

Not suitable for Euler equation

Acoustic Liner

- Lined Duct Propagation
  - ✓ NASA Langley Grazing Impedance Tube Configuration
  - ✓ Liner Impedance : constant depth ceramic tubular(CT) liner
  - ✓ Sound Source
  - SPL : 120 dB, 140 dB, 160 dB
  - Waveform : Sinusoidal , Sawtooth

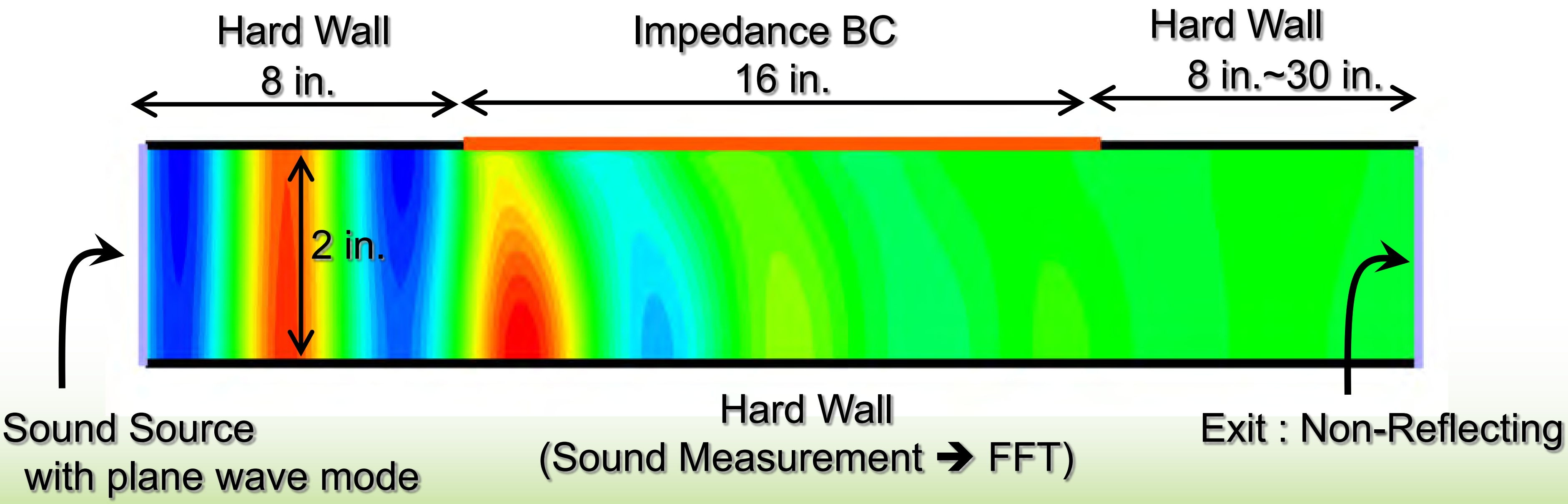

Acoustic Liner

- Lined Duct Propagation
  - ✓ Experimental Data [Jones, 2003]
    - NASA Langley Grazing Impedance Tube
    - CT57 liner, M=0 case, 140 dB source
  - ✓ Simulation :
    - LEE equation
    - Educed impedances for 140 dB source by NASA Langley*

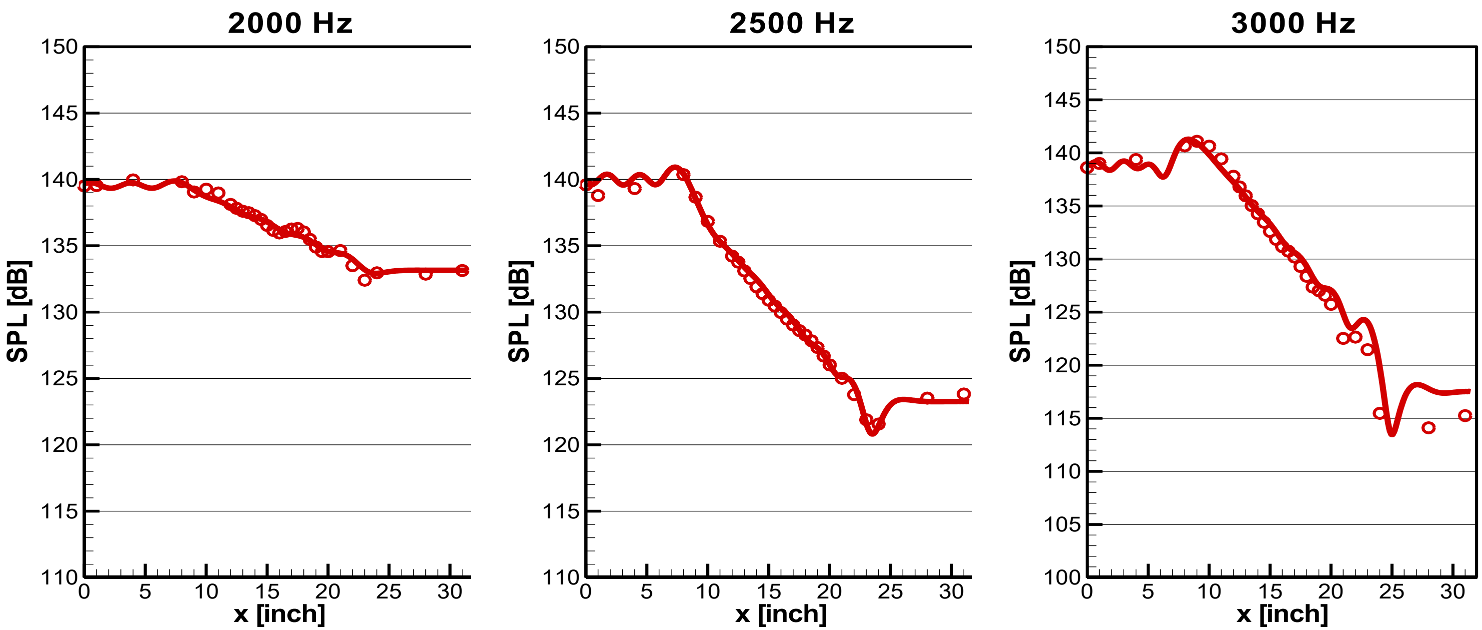

Acoustic Liner

- Lined Duct Propagation with Nonlinear Effect
  - ✓ sinusoidal wave, fundamental freq=1 kHz (CT73 liner)

120 dB | 140 dB | 160 dB

Linear regime → Nonlinear regime

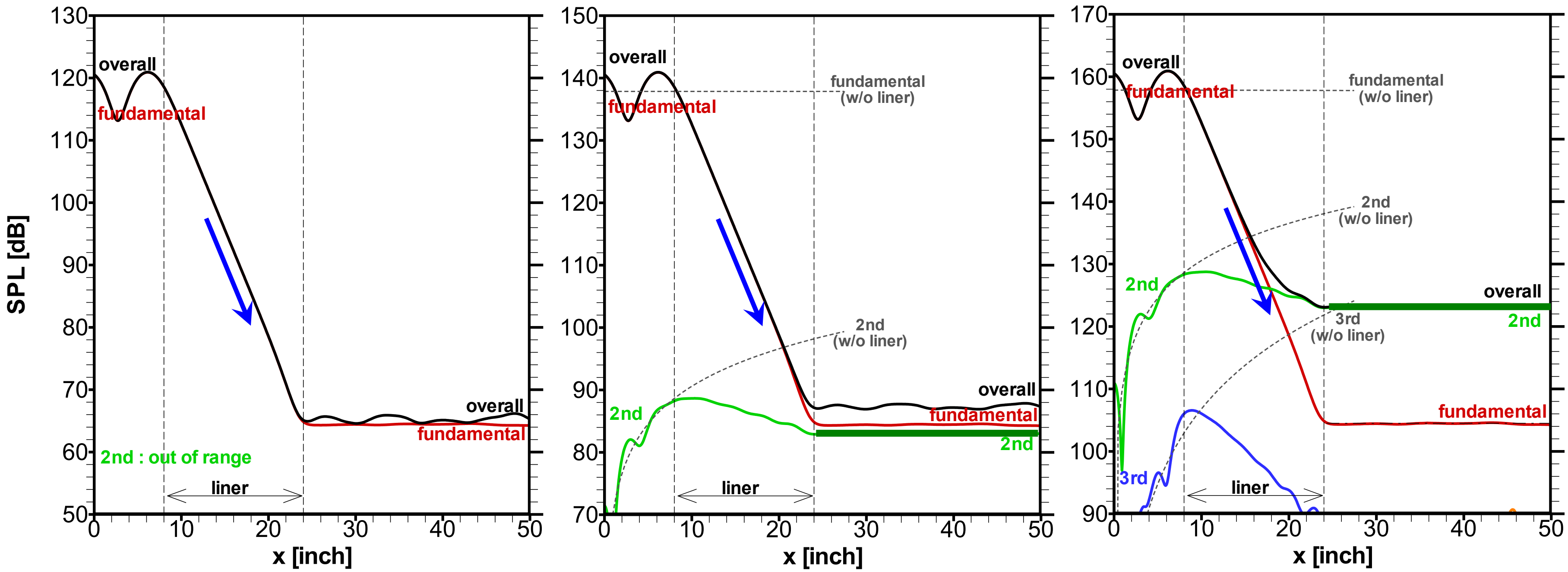

- SPL curve over liner region is not changed.
- SPL of 2nd harmonic component dominates one of source frequency

Orifice

- Direct Simulation of Resonator
  - ✓ Simulation of nonlinear characteristics of thin orifice

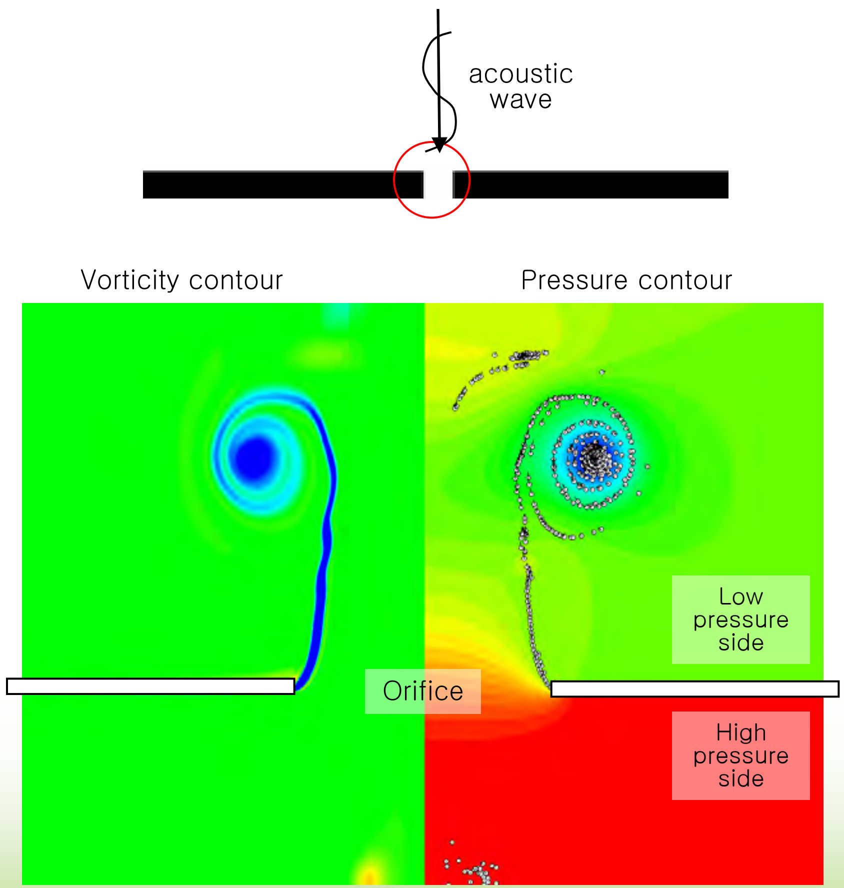

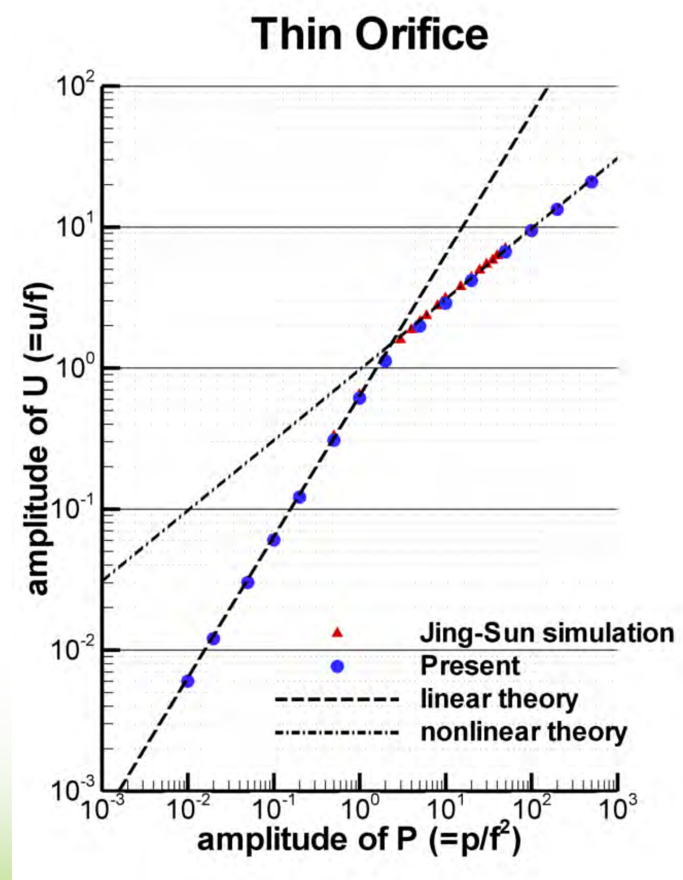

Orifice

- Direct Simulation of Resonator
  - Simulation of nonlinear characteristics of thin orifice

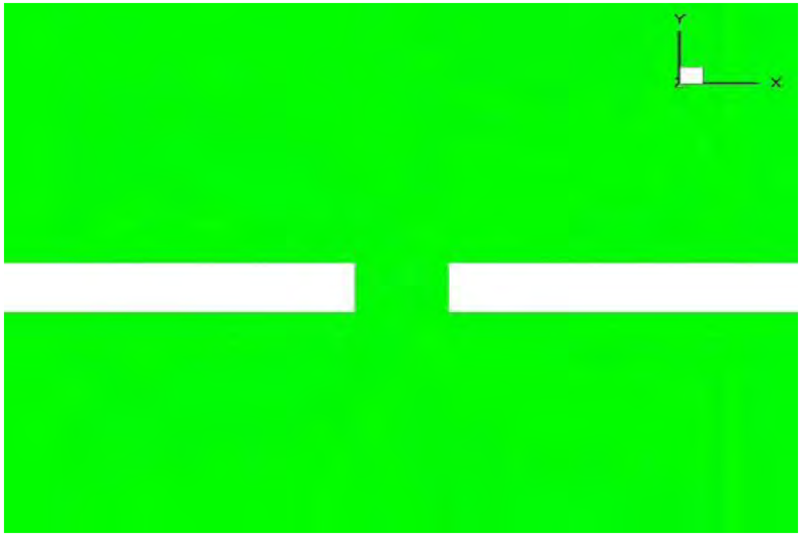

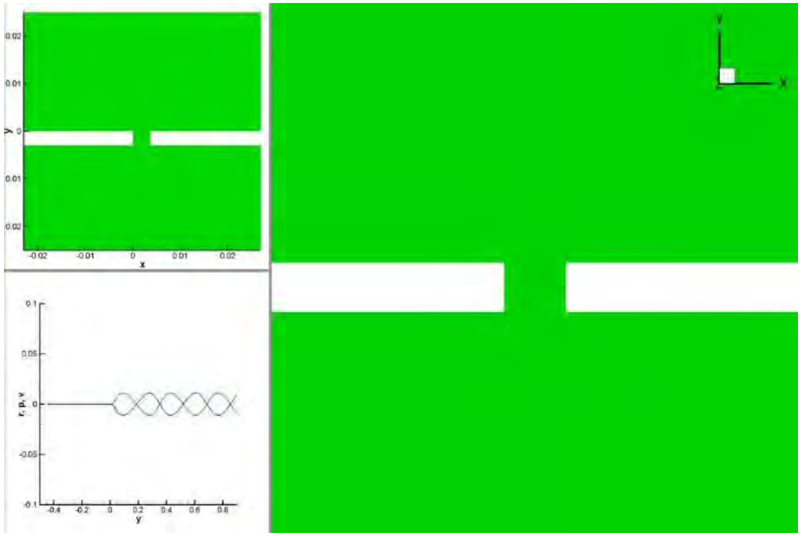

Orifice

- Helmholtz Resonator
  - ✓ Hersh-Walker's experiment
    - Case of thick neck Helmholtz resonator

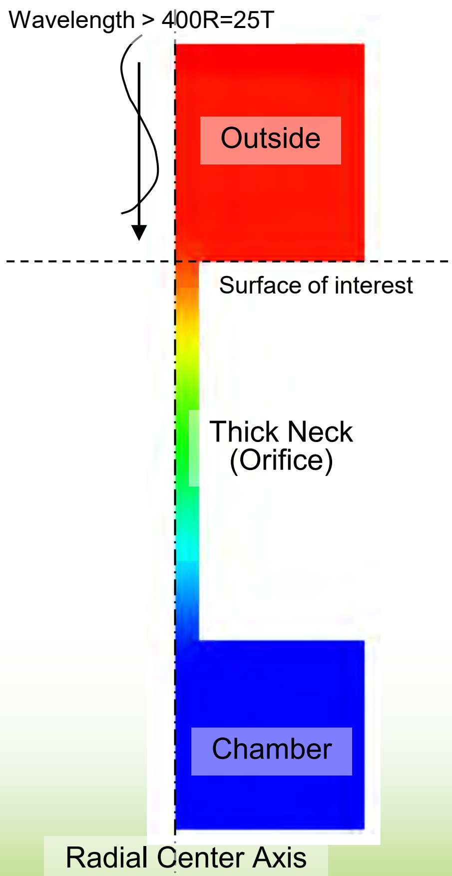

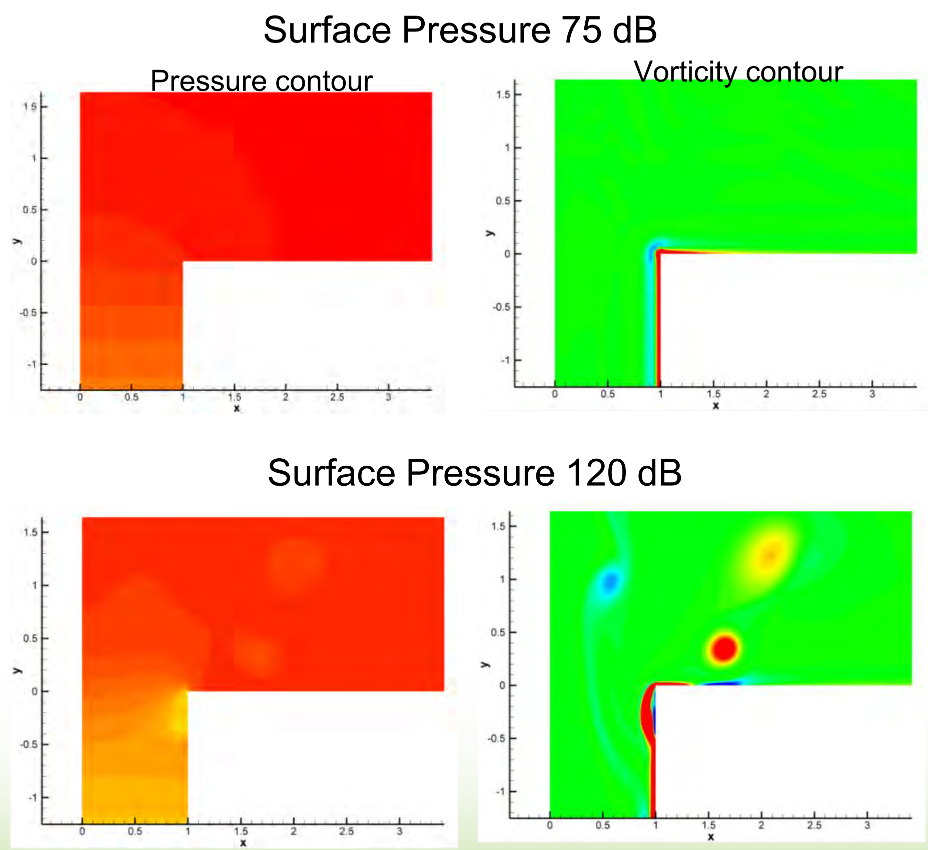

Orifice

- Helmholtz Resonator

Impedance for 75dB

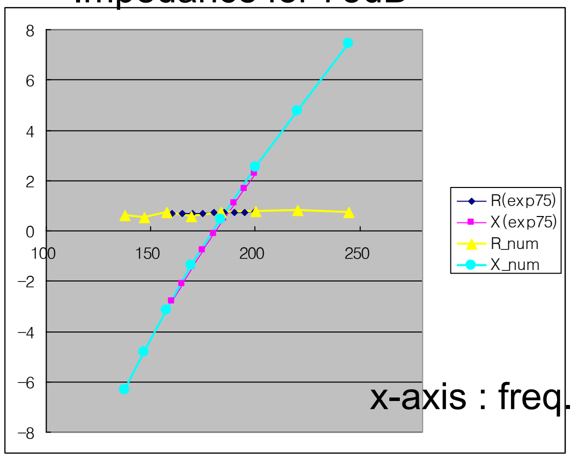

120dB

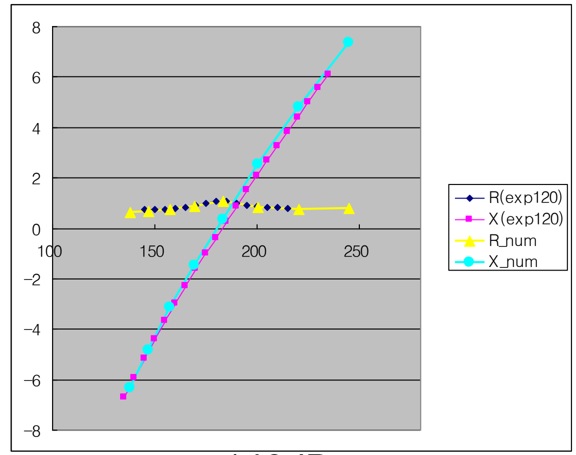

x-axis : freq.(Hz)

130dB

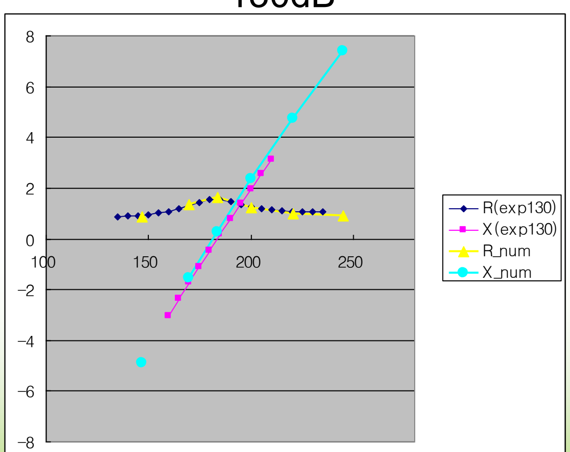

140dB

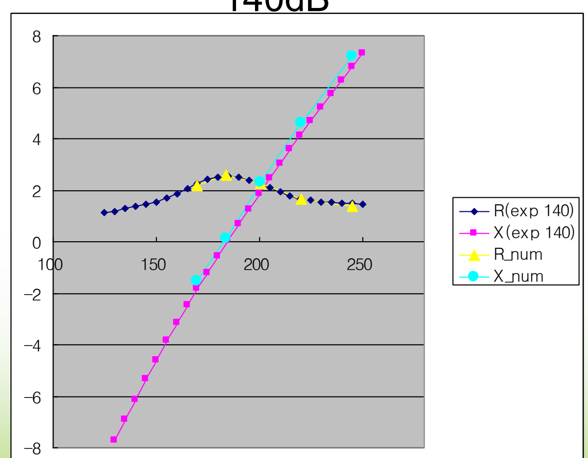

Single Orifice Simulation

- Impedance w.r.t. Pressure

Real
(Resistance)

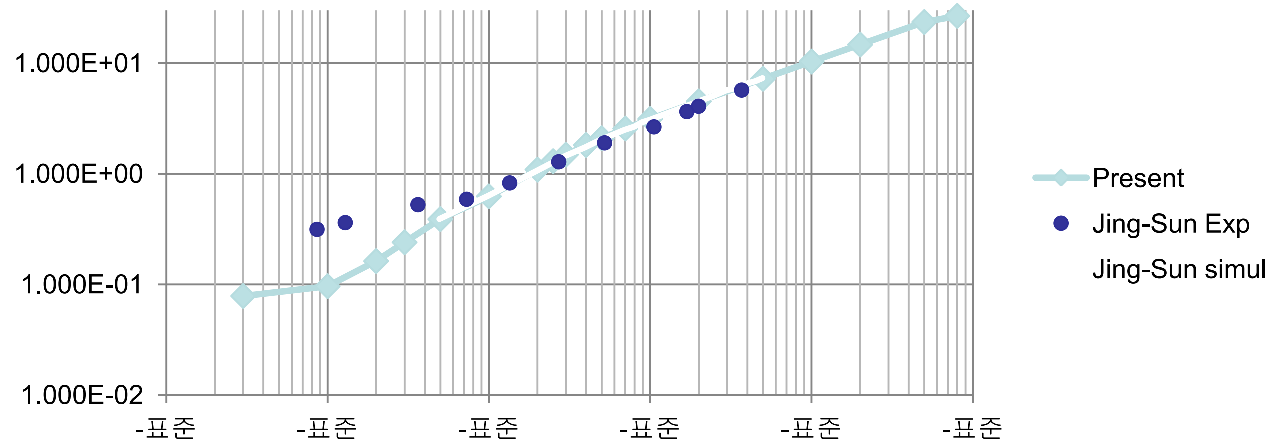

Imaginary
(Reactance)

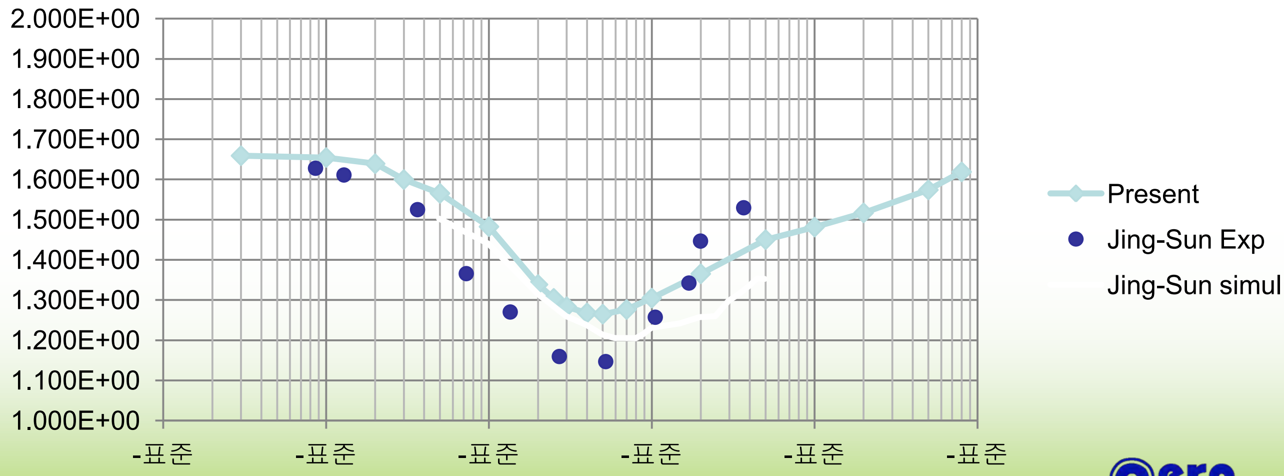

Non-dimensional Pressure

CFD Simulation

$\widehat{P} = 1$

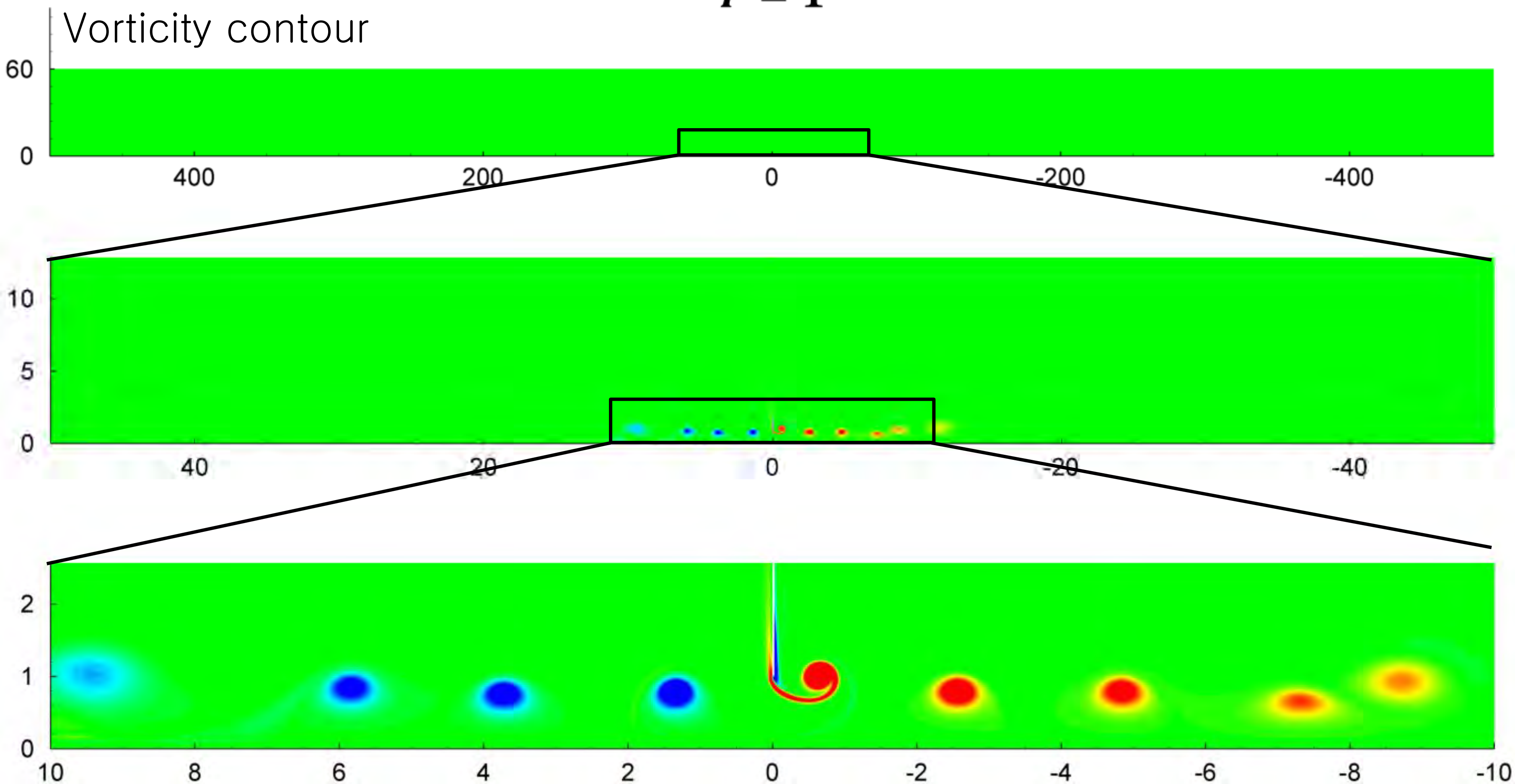

CFD Simulation

$\widehat{P} = 1$

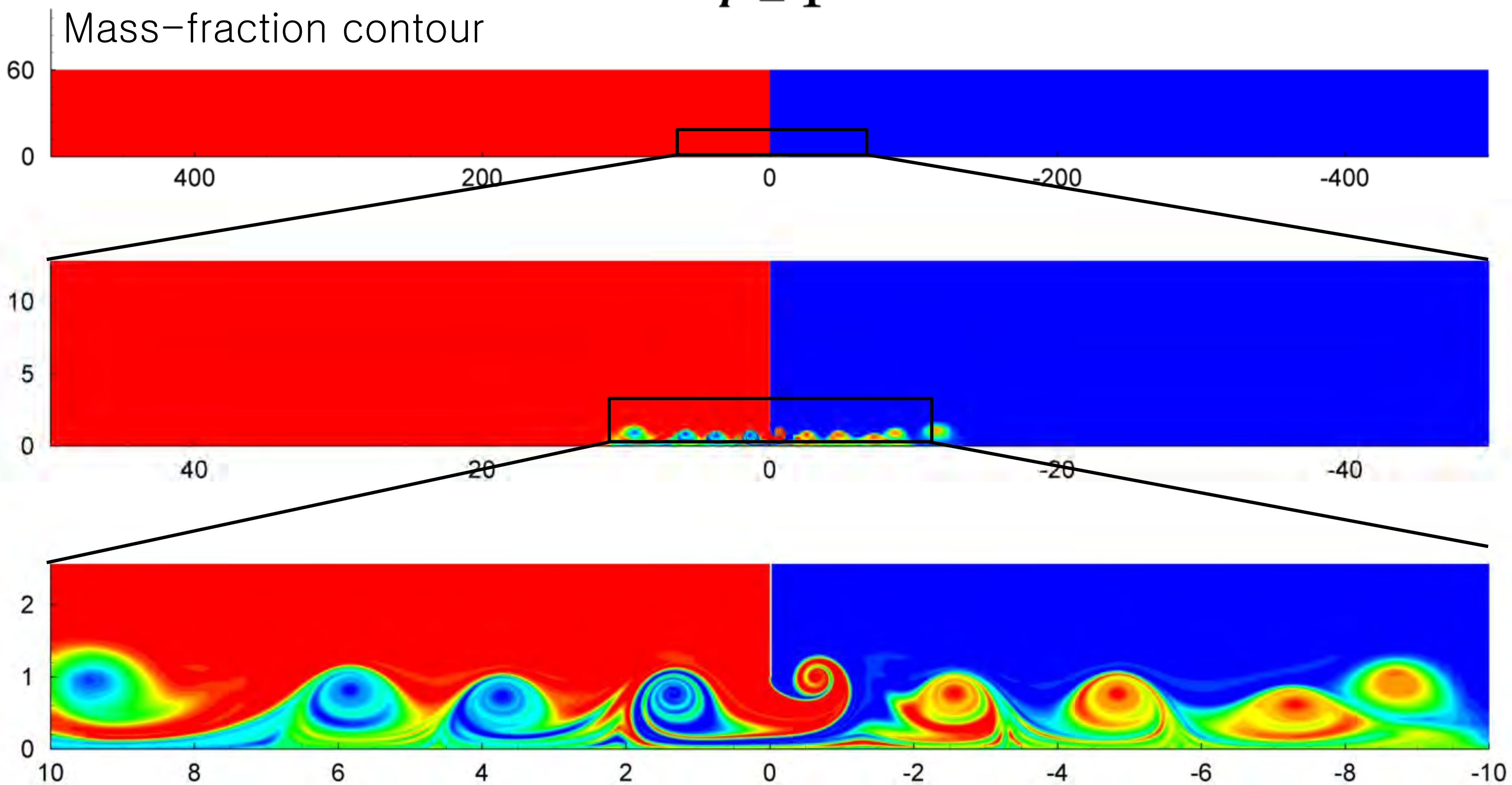

CFD Simulation – Animation

$\hat{P} = 1$

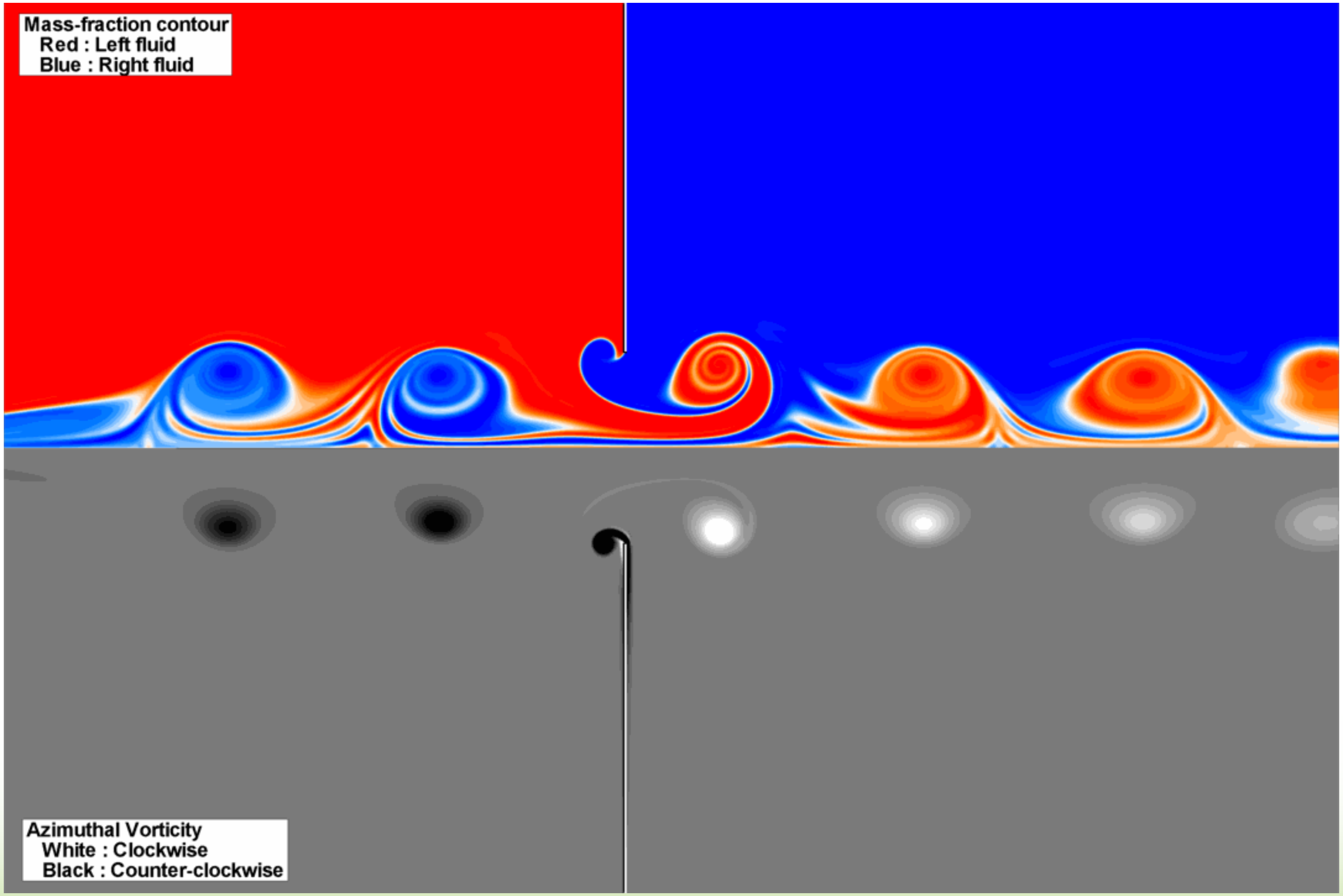

CFD Simulation – Wake

$$\hat{P} = p/(\rho\omega^2 R_0^2) = 0.0001$$

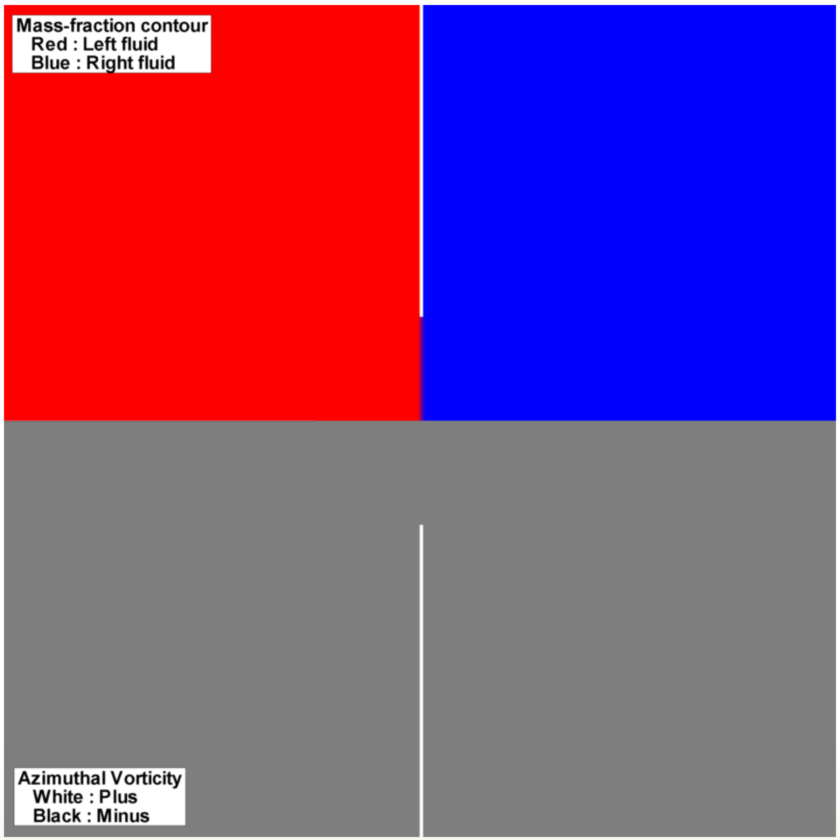

At infinitesimal amplitude, no wake obviously.

$$\hat{P} = p/(\rho\omega^2 R_0^2) = 0.1$$

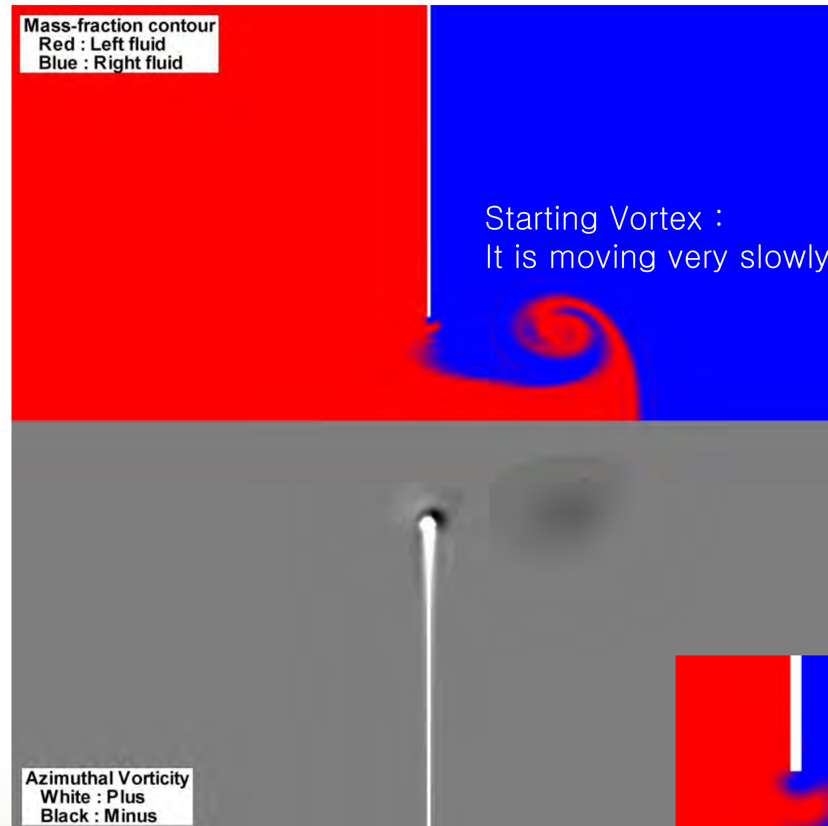

Zoom
near Edge

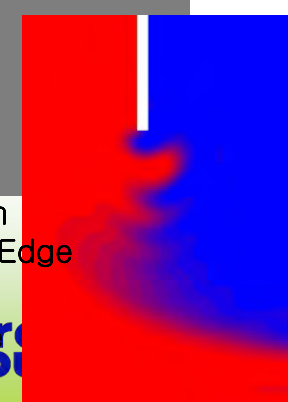

Oscillating small-amplitude wake
cannot travel away.

CFD Simulation – Wake

$$\hat{P} = p/(\rho\omega^2 R_0^2) = 1$$

$$\hat{P} = p/(\rho\omega^2 R_0^2) = 10$$

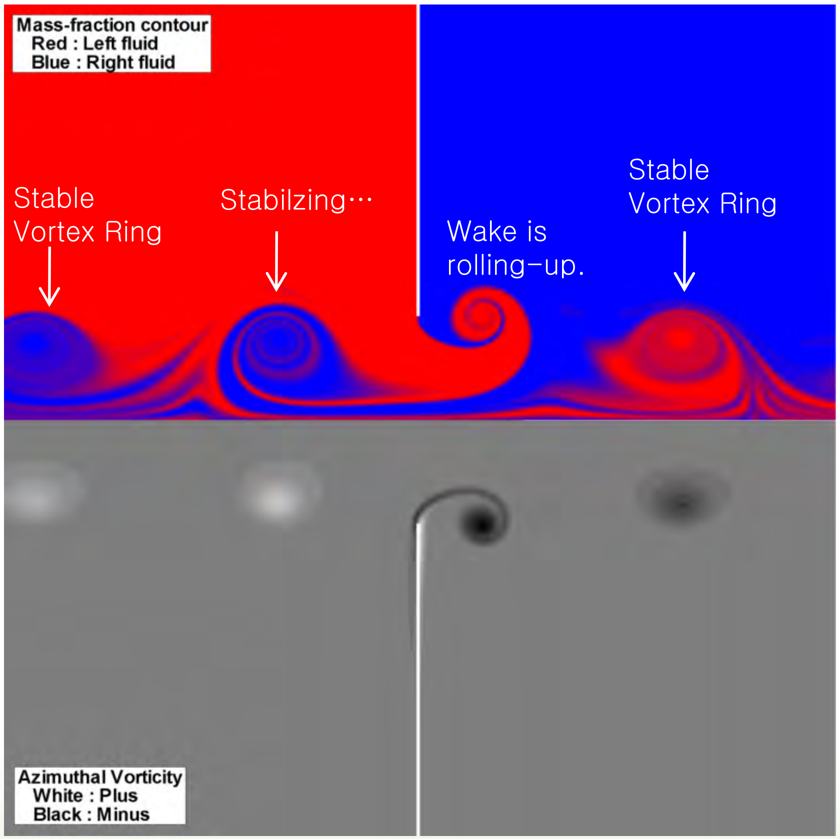

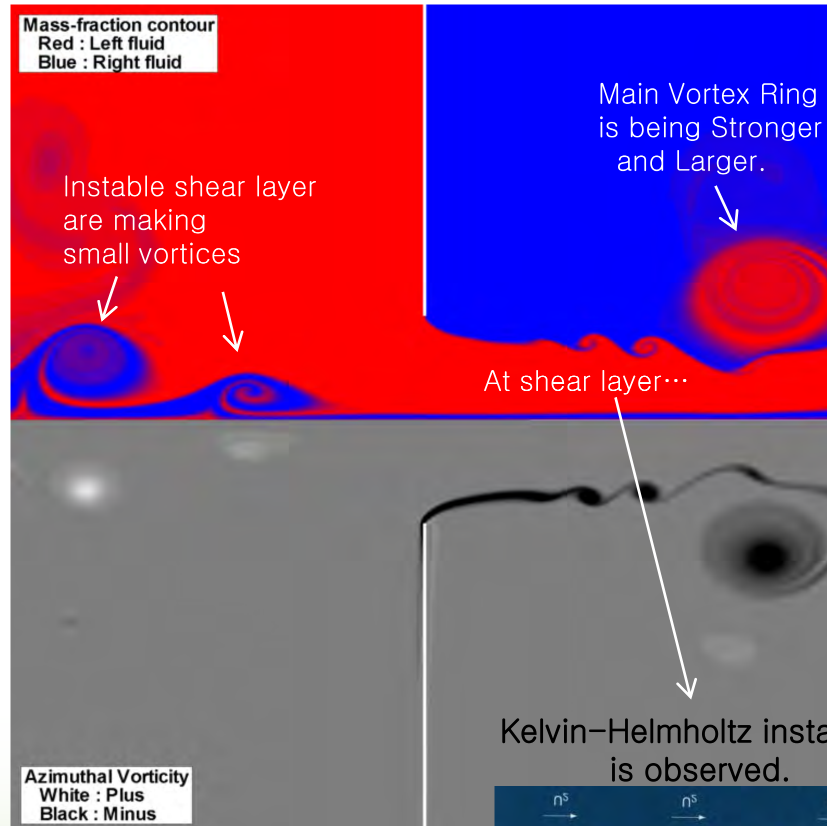

Regular and stable wake pattern.

Kelvin-Helmholtz instability is observed.

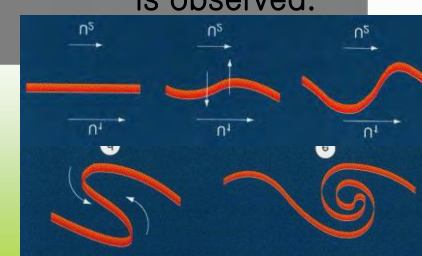

CFD Simulation – Wake

$$\hat{P} = p/(\rho\omega^2 R_0^2) = 100$$

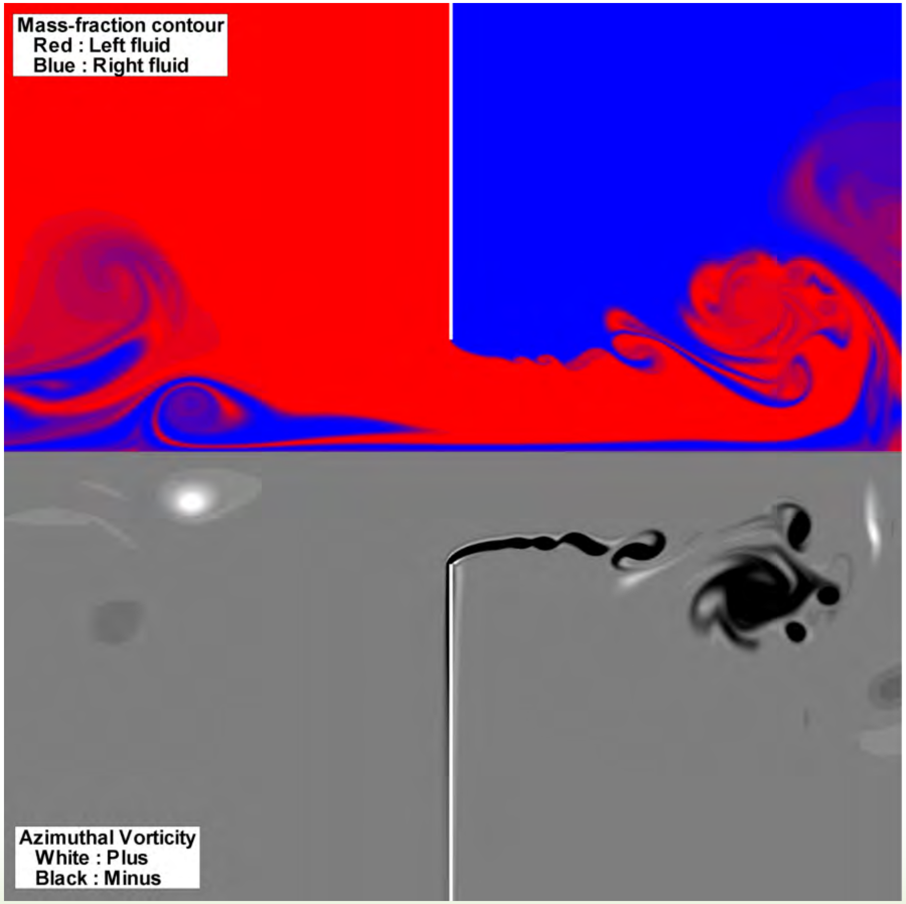

Turbulent

Impedance(Reactance) vs. Wake Pattern

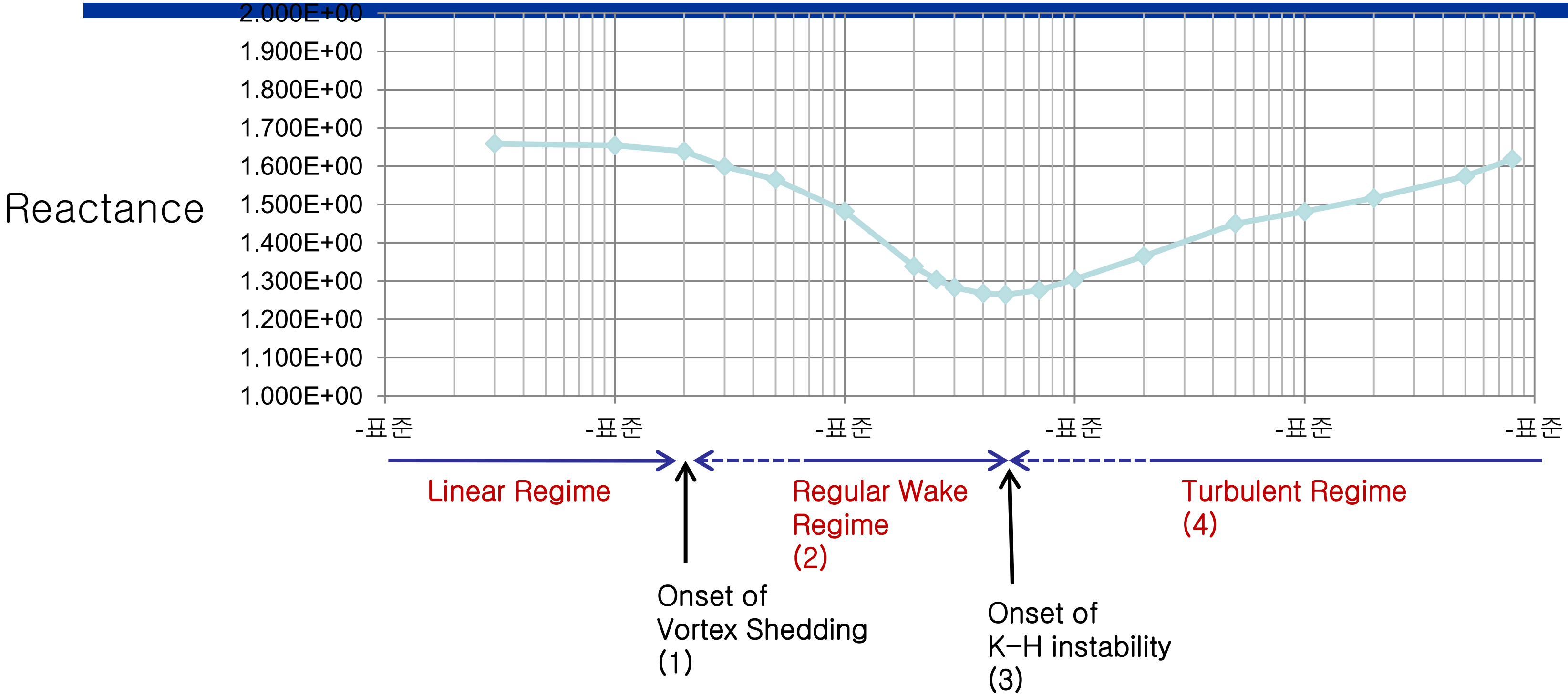

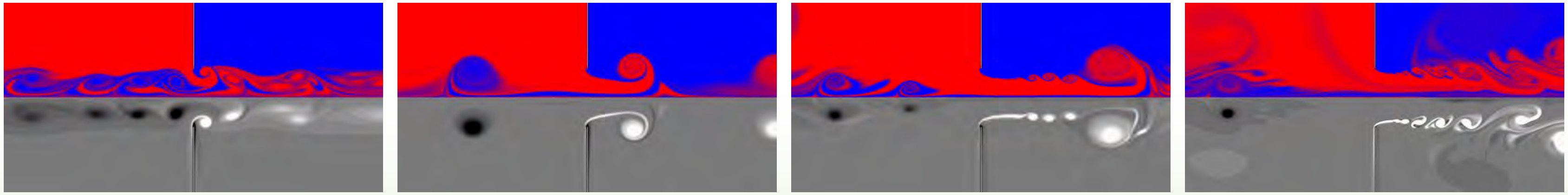

(1) (2) (3) (4)

Duct acoustics

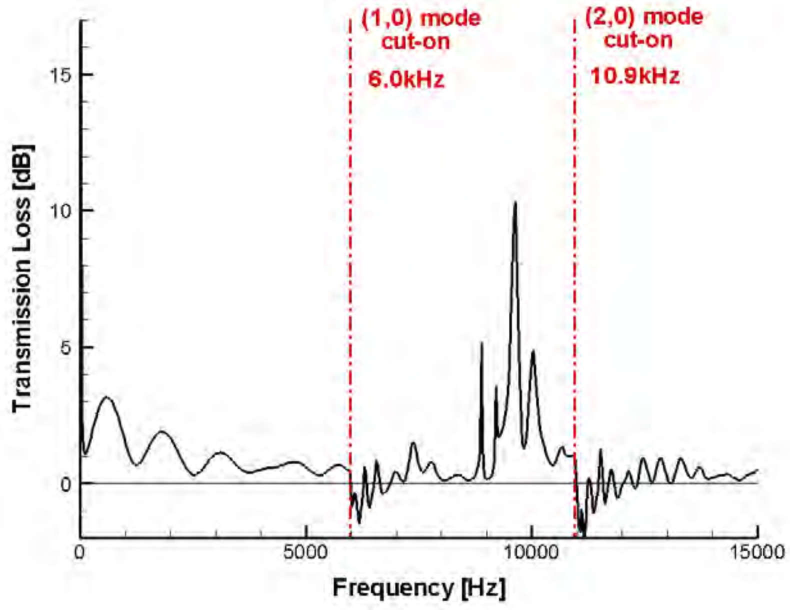

- 6.0 kHz higher Mode Propagation
- 9.8 kHz Cut Off
- Resonator for Silencer

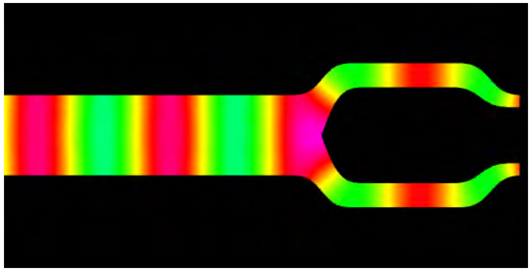

2.9 kHz : Plane wave mode

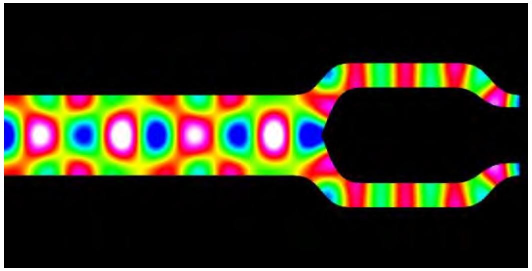

7.8 kHz : (1,0) mode

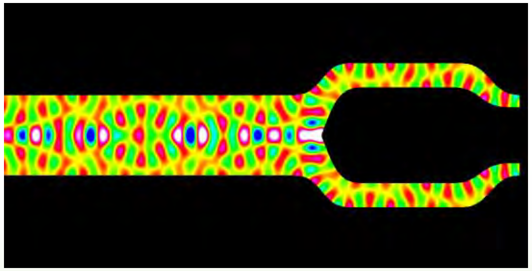

11.8 kHz : Higher modes

Sound Propagation in Duct

- Helmholtz Resonator in a Duct

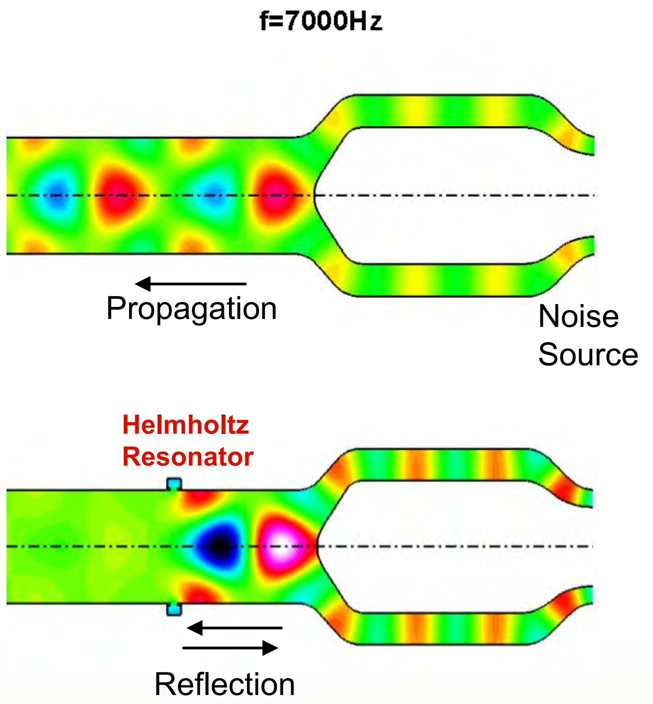

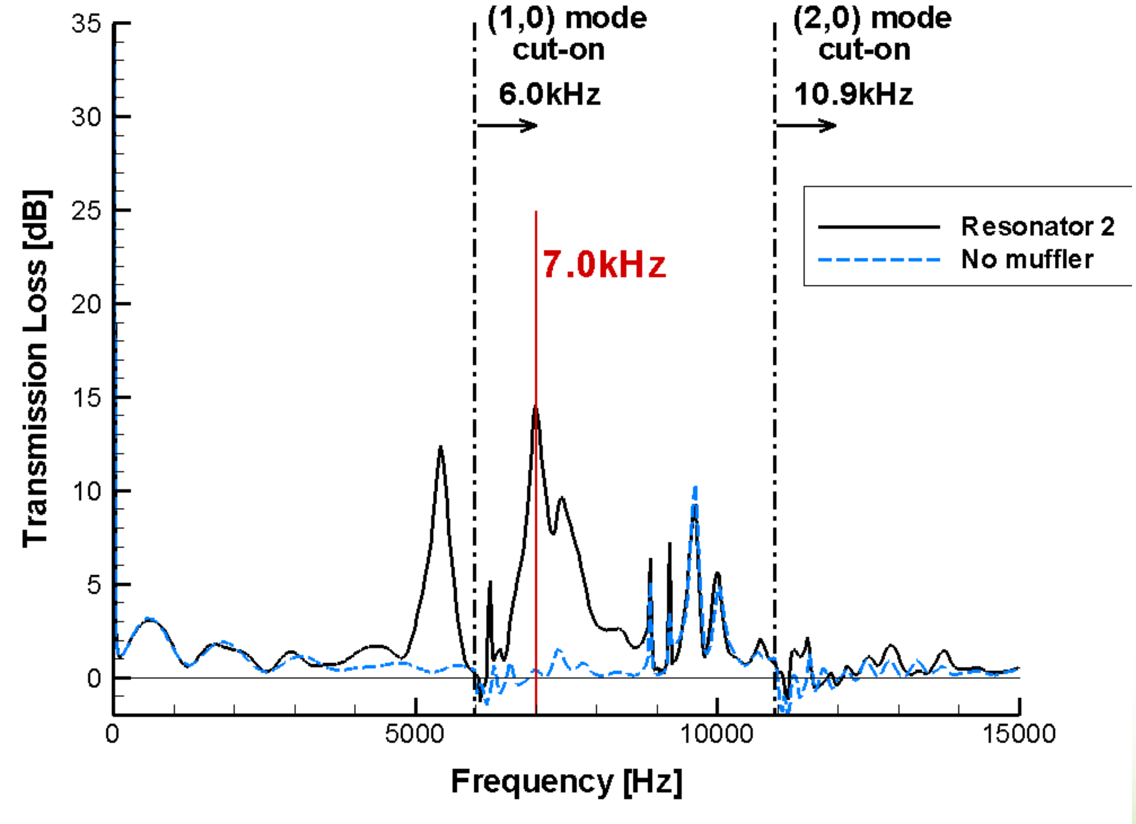

Application

❖ 13-Points DRP scheme (based on central difference)

$$\left(\frac{\partial f}{\partial x}\right)_i \simeq \frac{1}{\Delta x}(a_6 f_{i-6} + a_5 f_{i-5} + \ldots + a_1 f_{i-1} + a_1 f_{i+1} + \ldots + a_5 f_{i+5} + a_6 f_{i+6})$$

a_1 = 0.91595792650492, a_2=-0.3492225163622, a_3=0.14398145036906
a_4 =-0.0512369917290, a_5=0.01327318112590, a_6=-0.0018126562895

Governing equation (turbulent and incompressible channel flow)

$$\nabla \vec{U} = 0, \quad \frac{\partial U_i}{\partial t} + \nabla(U_i \vec{U}) = -\frac{\partial p}{\partial x_i} + \frac{1}{\mathrm{Re}} \Delta U_i$$

where U_i : the i-th velocity component
p : pressure

$$\frac{\partial^2 p}{\partial x_j \partial x_i} = -2\frac{\partial \overline{U}_i}{\partial x_j}\frac{\partial u_j}{\partial x_i} - \left(\frac{\partial u_i}{\partial x_j}\frac{\partial u_j}{\partial x_i} - \overline{\frac{\partial u_i}{\partial x_j}\frac{\partial u_j}{\partial x_i}}\right) = f(x_i, t) \quad \text{with solution} \quad p = -\frac{1}{4\pi}\int_V f(x_i, t)\,dV$$

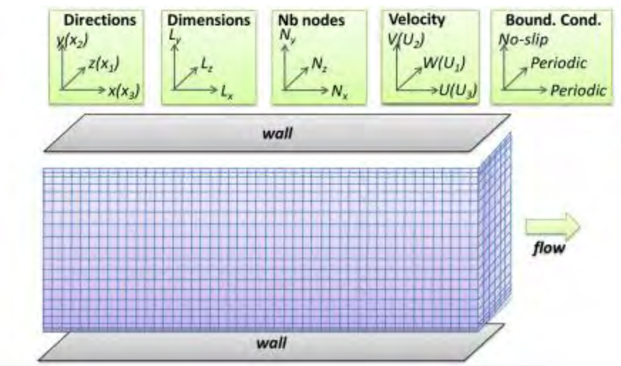

Fig. 4. Overview of computational domain and flow configuration

Grid	N_x x N_y x N_z	Δx^+	$\Delta y^+_{min}/\Delta y^+_{max}$	Δz^+
Coarse	128x64x64	17.7	1/11	11.8
Fine	128x128x128	17.7	0.45/5.6	5.9
Moser [23]	128x128x128	17.7	0.05/4.4	5.9

Table 4. Resolution and grid spacing for fine, coarse and Moser grids. The dimensions of computational domain are the same in the three cases (4πh x 2h x 4πh/3)

Application

✓ Results

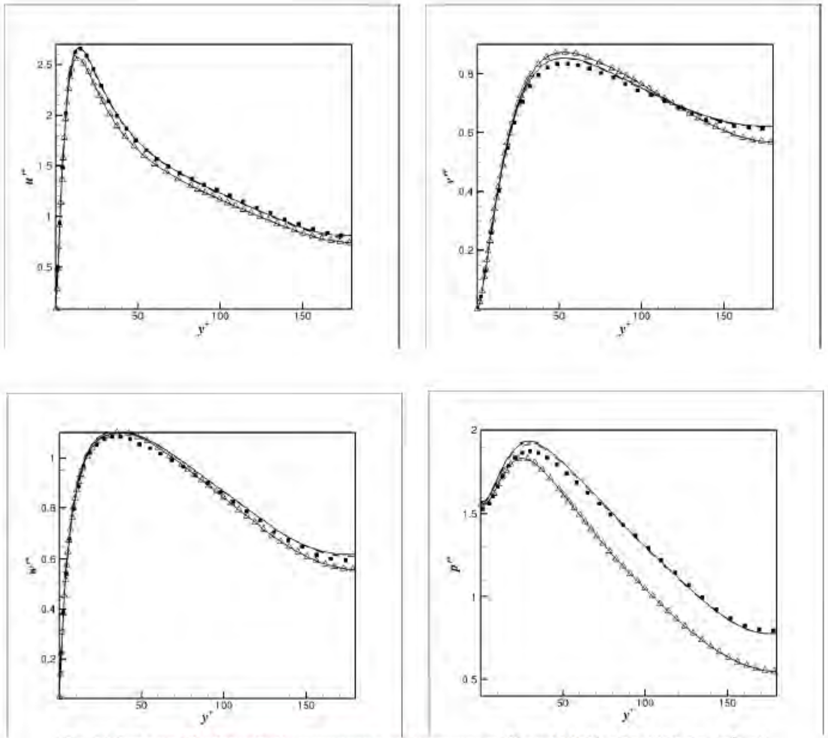

Fig. 14. R.m.s profiles for velocity components and pressure on fine grid (128x128x128). O2 (—△—), CS (dashed line), DRP(solid line) configurations and Moser [23] (■)

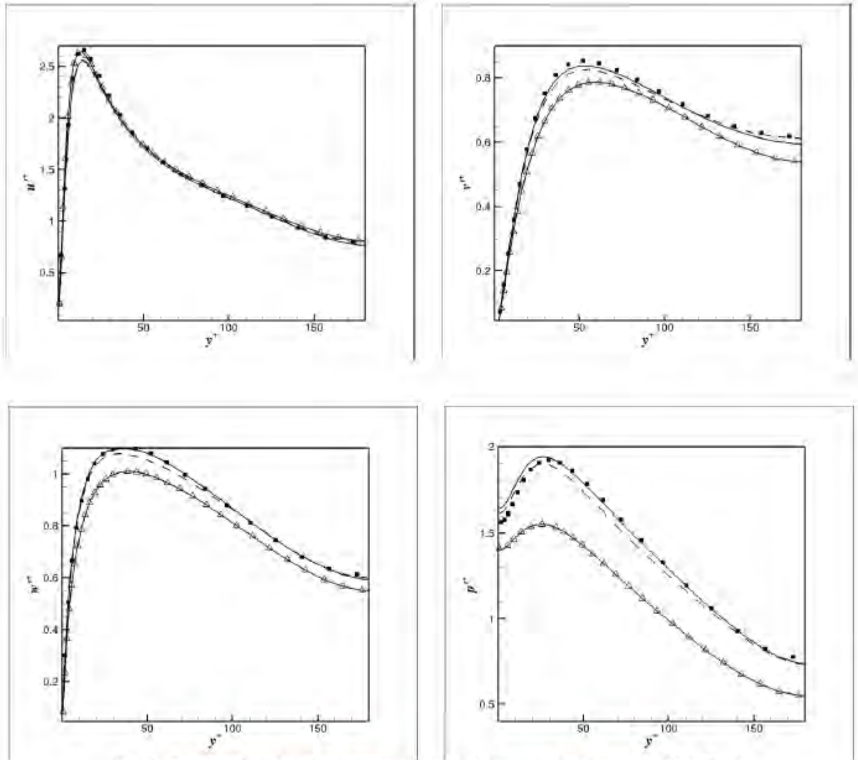

Fig. 16. R.m.s profiles for velocity components and pressure on coarse grid. O2 (—△—), CS(dashed line), DRP(solid line) configurations and CS on fine grid (■)

Application

❖ Flow Equations at the Polar Axis in Cylinder Coordinates Using Series Expansions

Most general expansion of any function can be written as

$$F(r,\theta)=\sum_{m=0}^{\infty}(f_m(r)\cos(m\theta)+g_m(r)\sin(m\theta))$$

where f_m and g_m are polynomial in r that have mth-order zeroes at r=0
If m is even, f_m and g_m are both symmetric around r=0.

$$F(r,\theta)=\sum_{m=0}^{\infty}(f_m(r)e^{im\theta})$$

$$=\sum_{m=0}^{\infty}c_n(m)r^n e^{im\theta}=r^m e^{im\theta}\sum_{m=0}^{\infty}c_n(m)\mathrm{r}^{n-m}=\omega^m\sum_{m=0}^{\infty}c_n(m)\mathrm{r}^{n-m}$$

$$u_x=\alpha_{00}^{(x)},$$

$$\frac{\partial u_x}{\partial r}=\alpha_{10}^{(x)}\cos(\theta)+\beta_{10}^{(x)}\sin(\theta),$$

$$\frac{\partial^2 u_x}{\partial r^2}=2\alpha_{01}^{(x)}+2\alpha_{20}^{(x)}\cos(2\theta)+2\beta_{20}^{(x)}\sin(2\theta),$$

$$u_r=A_{10}^{(r)}\cos(\theta)+B_{10}^{(r)}\sin(\theta),$$

$$\frac{\partial u_r}{\partial r}=A_{10}^{(r)}+A_{20}^{(r)}\cos(2\theta)+B_{20}^{(r)}\sin(2\theta),$$

$$\frac{\partial^2 u_r}{\partial r^2}=2A_{11}^{(r)}\cos(\theta)+2B_{11}^{(r)}\sin(\theta)+2A_{30}^{(r)}\cos(3\theta)+2B_{30}^{(r)}\sin(3\theta).$$

Application

$$\frac{\partial u_x}{\partial x}+\frac{\partial u_r}{\partial r}+\frac{1}{r}\left(u_r+\frac{\partial u_\theta}{\partial \theta}\right)=\frac{\partial \alpha_{00}^{(x)}}{\partial x}+2A_{01}^{(r)},$$

$$\frac{\partial \rho}{\partial t}=-\left(\frac{\partial \rho u_x}{\partial x}+\frac{1}{r}\frac{\partial r\rho u_r}{\partial r}+\frac{1}{r}\frac{\partial \rho u_\theta}{\partial \theta}\right)=-\left(\frac{\partial \alpha_{00}^{(\rho)}\alpha_{00}^{(x)}}{\partial x}+A_{10}^{(r)}\alpha_{10}^{(\rho)}+B_{10}^{(r)}\beta_{10}^{(\rho)}+2A_{01}^{(r)}\alpha_{00}^{(\rho)}\right)$$

$$\frac{\partial^2 u_x}{\partial x^2}+\frac{\partial^2 u_x}{\partial r^2}+\frac{1}{r}\frac{\partial u_x}{\partial r}+\frac{1}{r^2}\frac{\partial^2 u_x}{\partial \theta^2}=\frac{\partial^2 \alpha_{00}^{(x)}}{\partial x^2}+4\alpha_{01}^{(x)}.$$

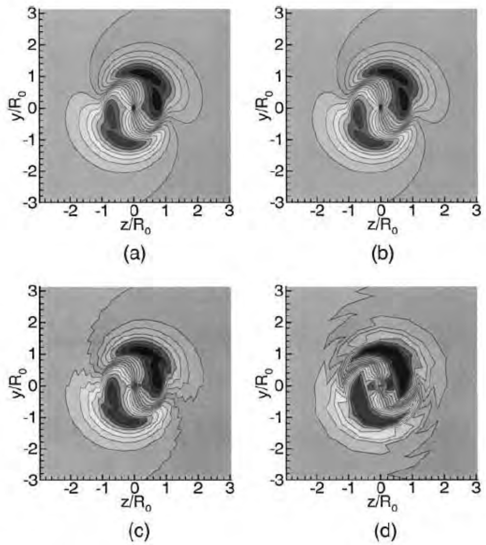

FIG. 1. Radial velocity contours in a plan situated at $x=5R_0$ from the inlet section of the inviscid forced jet at time $t=12R_0/U$. Radial velocity fields are shown with 15 equally spaced contours between $-0.0006U$ and $0.0006U$. (a) Theoretical solution via linear stability analysis; (b) fine-grid solution; (c) medium-grid solution; (d) coarse-grid solution.

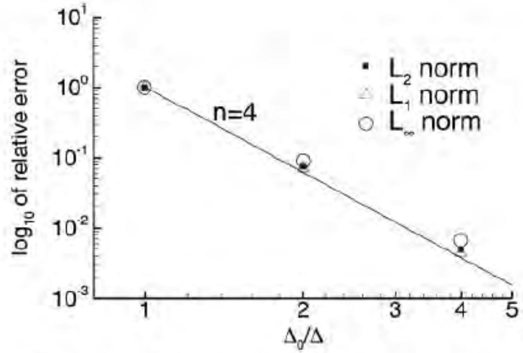

FIG. 2. Variation of error with mesh size for an inviscid test case.

$$e_\Delta^{(2)}=\sqrt{\frac{\sum_1^N (q_\Delta-q)^2}{N}},\quad e_\Delta^{(1)}=\frac{\sum_1^N |q_\Delta-q|}{N},\quad e_\Delta^{(\infty)}=\max|q_\Delta-q|$$

Application

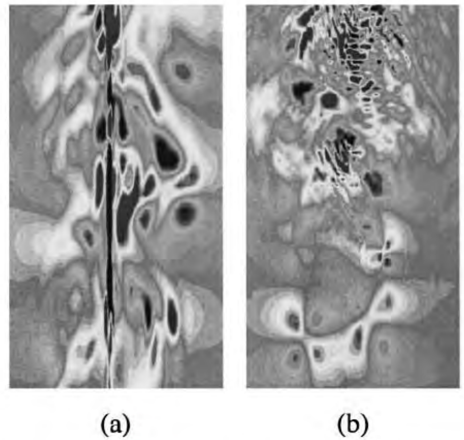

FIG. 5. Dilatation contours in an area situated after the end of the potential core for the turbulent jet. Dilatation fields are shown with 18 equally spaced contours between $-0.08U/R_0$ and $0.08U/R_0$. (a) Method of Mohseni and Colonius; (b) series expansions treatment.

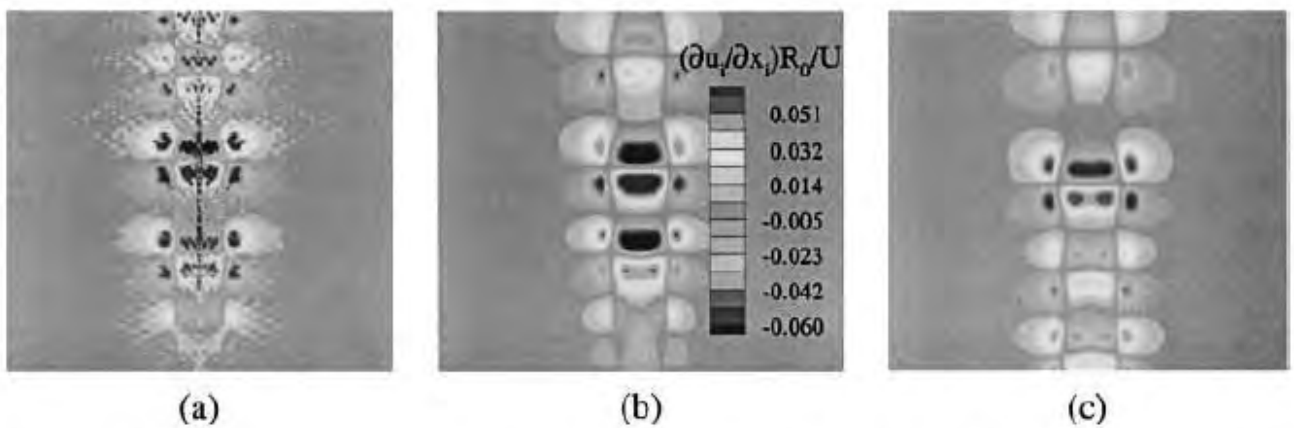

FIG. 4. Dilatation contours in the forced jet. (a) Cartesian coordinates; (b) method of Mohseni and Colonius; (c) series expansions treatment.

Application

❖ LES (Large Eddy Simulation) of compressible turbulent jets

$$f = \frac{\overline{\rho f}}{\overline{\rho}}$$

Where the bar denotes the standard the LES filtering and ρ the density

Governing equation (turbulent and incompressible channel flow)

$$\frac{\partial \overline{\rho}}{\partial t} + \frac{\partial}{\partial x_i}(\overline{\rho} u_i) = 0$$

$$\frac{\partial \overline{\rho} u_i}{\partial t} + \frac{\partial}{\partial x_i}(\overline{\rho} u_i u_j) = -\frac{\partial \overline{p}}{\partial x_i} + \frac{\partial}{\partial x_j}\sigma_{i,j} - \frac{\partial}{\partial x_j}\overline{\rho}(u_i u_j - u_i u_j) \qquad \sigma_{i,j} = \overline{\mu}\left(\frac{\partial u_i}{\partial x_j} + \frac{\partial u_j}{\partial x_i} - \frac{2}{3}\delta_{i,j}\frac{\partial u_k}{\partial x_k}\right)$$

$$\frac{\partial \overline{E}}{\partial t} + \frac{\partial}{\partial x_i}(u_i(\overline{E} + \overline{p})) = -\frac{\partial}{\partial x_i} q_i + \frac{\partial}{\partial x_j}(\sigma_{i,j} u_i) - \frac{\partial}{\partial x_i}(\overline{E u_i} - \overline{E} u_i + \overline{p u_i} - \overline{p} u_i) \qquad q_i = -\overline{\kappa}\frac{\partial T}{\partial x_i}$$

Table 1. Some parameters used in the simulations.

	I	II
Re	36,000	100,000
$N_x \times N_r \times N_\theta$	$192 \times 128 \times 64$	$320 \times 150 \times 96$
L_x	$45R_0$	$47.5R_0$
L_r	$8R_0$	$11R_0$
Δx_{max}	$0.42R_0$	$0.15R_0$
Δx_{min}	$0.14R_0$	$0.15R_0$
Δr_{max}	$0.1R_0$	$0.09R_0$
Δr_{min}	$0.03R_0$	$0.03R_0$

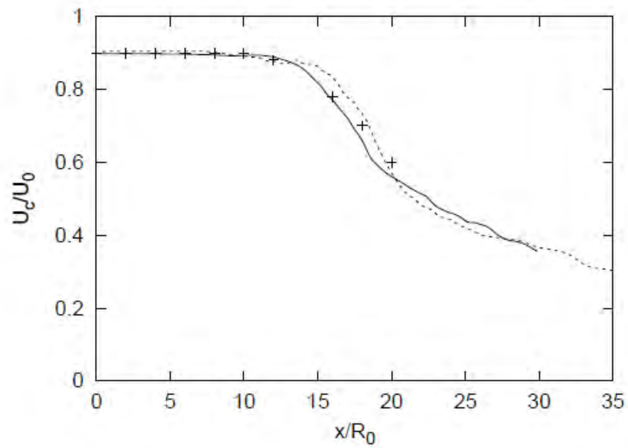

FIGURE 1. The mean centerline velocity as a function of the axial coordinate x, obtained from the LES, DNS (Freund 1999), and experiment (Stromberg *et al.* 1980). DNS 3600: ——— ; Stromberg *et al.* : + ; LES 36000: ---- .

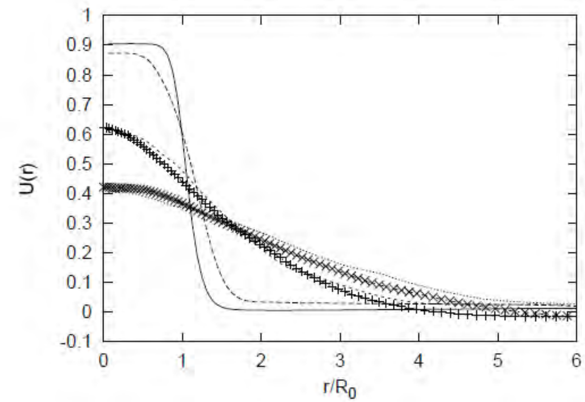

FIGURE 2. The mean velocity as a function of the radial coordinate at various different downstream positions. LES: $x = 3.2R_o$, ——— ; $x = 13.0R_o$, — — — ; $x = 19.5R_o$, ---- ; $x = 25.9R_o$, ········ . DNS: $x = 19.5R_o$, smallplus; $x = 25.9R_o$, × .

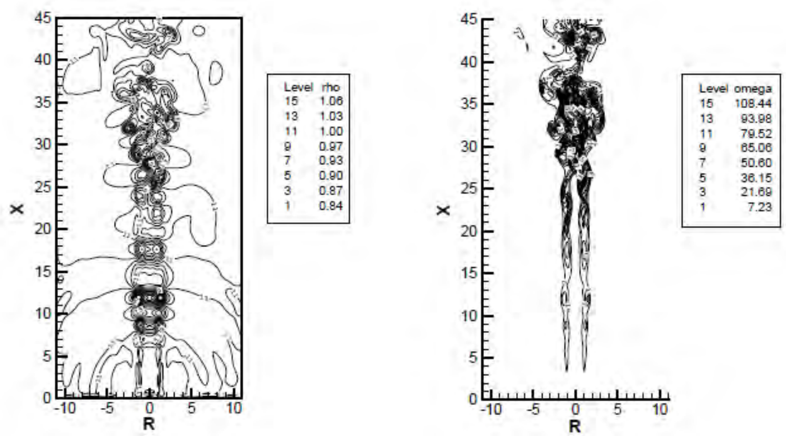

FIGURE 4. Left: Contour plot of the density; Right: Contour plot of the total vorticity multiplied by the axial coordinate $x|\omega|$.

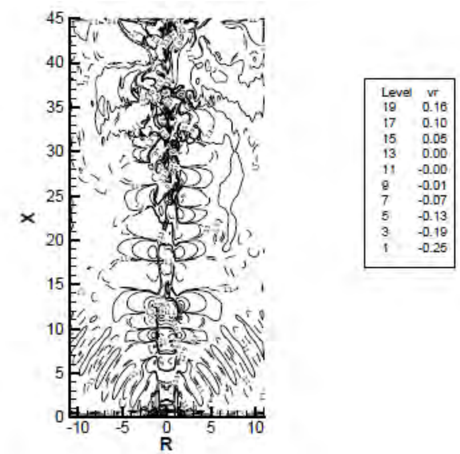

FIGURE 5. A contour plot of the dilatation $(\partial u_i/\partial x_i)$.

大學 (University)

格物 致知 正心 誠意

修身 齊家 治國 平天下

Material Property, Life,

Righteous Mind, Sincere Attitude

My Self, Family,

Country, Peaceful world

AeroAcoustics Lab

Thank You